

**Functional characterisation of the mesenchymal cell-derived  
extracellular matrix  
in myelodysplastic neoplasms**

Dissertation  
zur Erlangung des akademischen Grades  
Dr. rer. nat.

an der Medizinischen Fakultät  
der Universität Leipzig

eingereicht von:

Master of Science  
**Amanpreet Kaur Bains**

Geboren am 19.03.1996 in Hyderabad, India

angefertigt an der  
Medizinischen Fakultät, Universität Leipzig,  
Forschungslabor Hämatologie und Zelltherapie  
Arbeitsgruppe Platzbecker/ Cross

Betreuer: Prof. Dr. med. Uwe Platzbecker  
Ko-Betreuer: Dr. phil. habil. Michael Cross; Dr. rer. nat. Manja Wobus

Date awarded: 19.12.2023

## Content

Content.....	i
Abbreviations .....	iv
List of Figures.....	viii
List of Tables.....	x
1. Introduction .....	1
1.1. Haematopoietic system .....	1
1.2. Bone marrow microenvironment.....	2
1.2.1. Mesenchymal stromal cells .....	3
1.2.2. Extracellular matrix .....	4
1.2.2.1. Biophysical composition of ECM.....	5
1.2.2.2. Biochemical composition of ECM .....	5
1.3. Myelodysplastic neoplasms (MDS).....	11
1.3.1. Definition and classification .....	11
1.3.2. Current treatment options .....	12
1.3.3. MSCs in MDS .....	13
2. Aim .....	14
3. Materials and Methods.....	15
3.1. Patient cohort .....	15
3.2. Materials.....	17
3.2.1. Software and devices .....	17
3.2.2. Reagents .....	19
3.2.3. Antibodies .....	24
3.2.4. Primers.....	26
3.3. Cell culture .....	27
3.3.1. MSC isolation and cell culture .....	27
3.3.2. MSC passage, cryopreservation and thawing .....	27
3.3.3. Proliferation studies of MSCs .....	28
3.3.4. Analysis of osteogenic differentiation and Von kossa staining of MSCs.....	28
3.3.5. Analysis of adipogenic differentiation and Oil Red-O staining of MSCs .....	28
3.3.6. Generation of ECM from MSCs.....	29
3.3.7. Isolation, cryopreservation and thawing of CD34+ HSPC.....	30
3.3.8. Cell culture and proliferation of HSPCs on different ECM.....	31
3.3.9. CFU assay .....	32

---

3.3.10.	Cell surface marker detection by flow cytometry .....	32
3.3.11.	LMW-HA stimulation of MNCs .....	32
3.4.	Biophysical analysis .....	32
3.4.1.	Atomic force microscopy (AFM) .....	32
3.5.	Biochemical analysis .....	33
3.5.1.	Quantification of total collagen .....	33
3.5.2.	Quantification of sulphated GAGs by Blyscan assay .....	33
3.5.3.	Immunostaining .....	34
3.5.4.	Lectin staining .....	34
3.5.5.	Separation and visualization of ECM GAGs.....	35
3.5.6.	Quantification of HA in the ECM substrates .....	35
3.6.	Molecular biology .....	35
3.6.1.	Cell Lysis and RNA isolation .....	35
3.6.2.	Reverse transcription .....	36
3.6.3.	RT-qPCR analysis .....	37
3.6.4.	Next generation sequencing and analysis of mRNA .....	37
3.7.	Statistical analysis .....	38
4.	Results .....	39
4.1.	The biophysical and biochemical composition of MSC-derived ECM is altered in MDS.....	39
4.1.1.	MSC from healthy donor and MDS bone marrow have similar phenotypes .....	39
4.1.2.	The biophysical properties of bone marrow MSC-derived ECM differ between MDS patient and healthy donors.....	40
4.1.3.	Fibronectin deposition in the ECM is unchanged in MDS versus healthy donor derived MSC.....	41
4.1.4.	MDS MSCs deposit high levels of collagens .....	42
4.1.5.	MDS MSC-derived ECM has an altered GAG profile .....	43
4.1.6.	LR-MDS MSC derived ECM contains high levels of CS and HA .....	44
4.2.	MDS-associated changes in the ECM involve both transcriptional and post-transcriptional regulation .....	46
4.2.1.1.	mRNA levels of core ECM genes only partially reflect the level of the corresponding proteins in the ECM .....	46
4.2.1.2.	Transcriptomic analysis is indicative of ECM deregulation in HR-MDS .....	47
4.3.	MDS MSC-derived ECM modulates HSPC behaviour .....	49
4.3.1.	LMW-HA stimulates inflammatory markers gene expression in bone marrow MNCs .	49
4.3.2.	MDS ECM has a functional impact on the HSPCs behaviour .....	50
4.3.3.	MDS and healthy ECM have similar growth factor retention and presentation capacities... ..	53

---

4.4.	AZA therapy reverts MDS-associated changes in MSC-derived-ECM.....	55
4.4.1.	MSCs isolated from MDS patients before and after AZA treatment or HSCT have similar phenotypic properties.....	55
4.4.2.	Improved rigidity and structure of ECM after AZA treatment.....	56
4.4.3.	Improved deposition of collagens after AZA treatment.....	57
4.4.4.	AZA treatment does not improve the GAG profile of MDS MSCs .....	58
4.4.5.	AZA treatment improves ECM-mediated haematopoietic support .....	60
4.4.6.	<i>In vitro</i> AZA treatment does not change the phenotypic characteristics of MDS MSC-derived ECM .....	61
4.4.7.	AZA has direct and acute effects on ECM deposition by MSCs, as well as long-term effects that may be indirect .....	62
4.4.8.	Collagen incorporation into ECM is affected differentially by <i>in vivo</i> and <i>in vitro</i> AZA treatment.....	63
4.4.9.	<i>In vitro</i> AZA treatment partially alter haematopoietic behaviour of HSPCs on MDS MSC-derived ECM.....	64
5.	Discussion .....	66
5.1.	Phenotypic and transcriptional characteristics of MDS MSCs .....	66
5.2.	Biophysical alteration in MDS MSC-derived ECM .....	68
5.3.	MDS associated changes in the composition of MSC-derived ECM .....	69
5.3.1.	Alterations in collagens .....	69
5.3.2.	Alterations in GAGs .....	70
5.4.	Functional impact of MDS MSCs-derived ECM on healthy HSPCs.....	71
6.	Summary.....	74
7.	Zusammenfassung der Arbeit .....	77
8.	Bibliography .....	80
9.	Annexes .....	91
9.1.	Annex I .....	91
9.2.	Annex II .....	92
9.3.	Annex III .....	93
10.	Disclosure .....	94
11.	Curriculum Vitae .....	95
12.	Publications .....	97
13.	Acknowledgment .....	98

## Abbreviations

AFM	Atomic force microscopy
APC	Allophycocyanin
APC-Cy7	Allophycocyanin Cyanine <sup>®</sup> 7
ATG	Antithymocyte globulin
AZA	Azacytidine
BMME	Bone marrow microenvironment
bp	Base pairs
BSA	Bovine serum albumin
BV421	Brilliant Violet 421
CD	Cluster of differentiation
cDNA	Complementary deoxyribonucleic acid
CFU	Colony formation Unit
CFU-E	Colony formation Unit-erythroid
CFU-GM	Colony formation Unit-granulocyte and macrophage
CHST11	Carbohydrate sulfotransferase 11
CHSY1	Chondroitin sulphate synthase 1
CLP	Lymphoid progenitor
cm	Centimetre
CMP	Common myeloid progenitor
CO <sub>2</sub>	Carbon dioxide
COL1a1	Collagen I alpha 1
COL4a2	Collagen IV alpha 2
COL7a1	Collagen VII alpha 1
CS	Chondroitin sulphate
CSGALNACT1	Chondroitin sulphate N-acetylgalactosaminyltransferase 1
DDR	Discoidin domain receptor
DMEM	Dulbecco's modified eagle medium
DMSO	Dimethyl sulfoxide
DS	Dermatan sulphate
DSE	Dermatan sulphate epimerase
ECM	Extracellular matrix
EGF	Epidermal growth factor
ELISA	Enzyme-linked immunosorbent assay

---

EXT-1	Exostosin-1
FBS	Fetal bovine serum
Fc	Fragment crystallisable
FITC	Fluorescein iso-thiocyanate
FLT3-L	FMS-like tyrosine kinase 3 ligand
FN1	Fibronectin 1
G-CSF	Granulocyte colony-stimulating factor
GM-CSF	Granulocyte-macrophage colony-stimulating factor
GSEA	Gene set enrichment analysis
GvHD	Graft versus host disease
HA	Hyaluronic acid
HAS	Hyaluronic acid synthase
HBSS	Hanks' balanced salt solution
HCL	Hydrochloric acid
HMA	Hypomethylating agents
HR-MDS	High risk MDS
HS	Heparan sulphate
HSA	Human serum albumin
HSC	Haematopoietic stem cell
HSCT	Haematopoietic stem cell transplantation
HSPC	Haematopoietic stem and progenitor cell
HYAL-1	Hyaluronidase 1
IL18	Interleukin 18
IL1B	Interleukin 1 beta
IL3	Interleukin 3
IL6	Interleukin 6
ITGA2	Integrin alpha 2
ITGA2B1	Integrin alpha 2 beta 1
ITGAIb	Integrin alpha 2b
ITGAV	Integrin alpha V
ITGAVB3	Integrin alpha V beta 3
ITGB1	Integrin beta 1
ITGB3	Integrin beta 3
KS	Keratan sulphate
LAIR	Leukocyte associated immunoglobulin like receptor

---

LAM	Laminin
LOX	Lysyl oxidase
LOXL	Lysyl oxidase-like
LR-MDS	Low risk MDS
MDS	Myelodysplastic neoplasms
mg	Milligram
MgCl <sub>2</sub>	Magnesium chloride
MNC	Mono nuclear cells
mRNA	Messenger ribonucleic acid.
MSC	Mesenchymal stromal cells
Na <sub>2</sub> EDTA	Ethylenedinitrilotetraacetic acid disodium salt dihydrate
NaOH	Sodium hydroxide
NGS	Next generation sequencing
NH <sub>4</sub> OH	Ammonium hydroxide
NIH	National institute of health
NK	Natural killer cells
nm	Nano meters
nN	Nano newton
PBS	Phosphate buffer saline
PCA	Principal component analysis
PE	Phycoerythrin
PE-cy 7	Phycoerythrin cyanine®7
PerCP-Cy5.5	Phycoerythrin cyanine®5.5
PYCARD	PYD And CARD Domain Containing
RGD	Arginylglycylaspartic acid
RHAMM	Hyaluronan-mediated motility receptor
rpm	Revolutions per minute
RT	Room temperature
SCA-1	Spinocerebellar ataxia type 1
SCF	Stem cell factor
SD	Standard deviation
SDF-1	Stromal cell-derived factor 1
Seq	Sequencing
SMAD	Mothers against decapentaplegic
SPARC	Secreted protein acidic and rich in cysteine

TGFB	Transforming growth factor beta
TNC	Tenascin-C
V	Volts
w/v	Weight per volume
Wnt	Wingless/Integrated



## List of Figures

<b>Figure 1</b> Hierarchical differentiation of haematopoietic stem cells to mature blood cells.....	1
<b>Figure 2</b> Role of MSCs in the bone marrow and their interaction with HSPCs. ....	4
<b>Figure 3</b> Localization of different ECM components in the bone marrow and its interactions with HSPCs.....	10
<b>Figure 4</b> Model of clonal evolution, progression to MDS and its transformation to AML .....	12
<b>Figure 5</b> Schematic diagram of the ECM generation and work plan for characterisation of the ECM substrates .....	29
<b>Figure 6</b> Schematic diagram of the immunogenic sorting of CD34+ cells from leukapheresis samples and its subsequent culture on the ECM substrates. ....	31
<b>Figure 7</b> MSCs from healthy donor and MDS patient bone marrow have similar characteristics. ....	40
<b>Figure 8</b> The biophysical properties of the ECM derived from healthy donor vs MDS MSCs.....	41
<b>Figure 9</b> Fibronectin levels are unchanged in MDS vs healthy donor MSC-derived ECM. ....	42
<b>Figure 10</b> MDS-associated changes in the collagen content of MSC-derived ECM.....	43
<b>Figure 11</b> Disease stage specific changes in the GAG composition of MDS MSC-derived ECM. ....	44
<b>Figure 12</b> Disease stage specific changes in the HA and CS composition of MDS MSC-derived ECM. .	46
<b>Figure 13</b> Relative mRNA levels of core ECM proteins and GAG modifying enzymes in the MDS. ....	47
<b>Figure 14</b> MDS MSCs are transcriptionally different from healthy donor MSCs.....	49
<b>Figure 15</b> Low molecular weight HA stimulates pro-inflammatory gene expression in bone marrow MNCs. ....	50
<b>Figure 16</b> Neither proliferation nor surface marker expression of HSPCs are differentially affected by culture on ECM from healthy donor, LR- or HR-MDS MSCs.....	51
<b>Figure 17</b> HSPC expressing selected integrins or CD44 associate similarly to ECM from healthy donor, LR- and HR-MDS MSCs. ....	52
<b>Figure 18</b> Diminished support of healthy HSPCs on MDS MSC-derived ECM. ....	53
<b>Figure 19</b> MDS ECM does not differentially affect the growth factor presentation capability of the ECM. ....	54
<b>Figure 20</b> Phenotypic characteristics does not differ after AZA therapy and HSCT. ....	56
<b>Figure 21</b> Changes in the biophysical properties of the ECM from MDS MSCs isolated before and after AZA therapy and HSCT. ....	57
<b>Figure 22</b> Changes in the collagens in MDS MSC derived ECM post AZA therapy. ....	58
<b>Figure 23</b> GAG composition of MDS MSC-derived ECM does not change after AZA therapy or post HSCT. ....	59
<b>Figure 24</b> MDS ECM improves haematopoietic support post-AZA therapy and post-HSCT.....	60

---

<b>Figure 25</b> Phenotypic characteristics does not differ after <i>in vitro</i> and <i>in vivo</i> AZA therapy. ....	62
<b>Figure 26</b> <i>In vitro</i> AZA treatment has a tendency to revert the changes in the biophysical properties of the ECM from MDS MSCs. ....	63
<b>Figure 27</b> <i>In vivo</i> but not <i>in vitro</i> AZA treatment changes the collagen I and IV content of MDS MSC derived ECM. ....	64
<b>Figure 28</b> <i>In vitro</i> AZA treatment partially modulated the haematopoietic behaviour of MDS MSC-derived ECM. ....	65
<b>Figure 29</b> Gating strategy for flow cytometry analysis of MSCs. ....	91
<b>Figure 30</b> Gating strategy for flow cytometry analysis of HSPCs on different ECMs.....	92
<b>Figure 31</b> Analysis of specificity of lectin staining and CS staining after pre-treatment with heparinases-1 and chondroitinase ABC respectively. ....	93

## List of Tables

<b>Table 1</b> List of enzymes that play a role in GAG biosynthesis and degradation.....	8
<b>Table 2</b> Characteristics of patients and healthy donors .....	15
<b>Table 3</b> List of laboratory equipment used for the experimental work .....	17
<b>Table 4</b> List of software used for experimental work .....	18
<b>Table 5</b> List of chemicals and reagents used for the experimental work.....	19
<b>Table 6</b> List of reagents used in cell culture .....	20
<b>Table 7</b> List of cell culture and cryopreservation medium used in the experimental work .....	21
<b>Table 8</b> List of buffers and solutions used for the experimental work .....	23
<b>Table 9</b> List of commercial kits used for the experimental work .....	24
<b>Table 10</b> List of antibodies used for immunostaining. ....	24
<b>Table 11</b> List of lectins used for histochemical-lectin staining .....	25
<b>Table 12</b> List of antibodies used for flow cytometry .....	25
<b>Table 13</b> List of primers and their respective sequences used for RT-qPCR .....	26
<b>Table 14</b> Composition of standard reaction master mix for reverse transcription of RNA samples ....	36
<b>Table 15</b> Amplification program for reverse transcription of RNA samples .....	36
<b>Table 16</b> Amplification program for cDNA during RT-qPCR.....	37

# 1. Introduction

## 1.1. Haematopoietic system

Haematopoiesis is the process of production and differentiation of mature blood cells from haematopoietic stem cells (HSCs) in the bone marrow<sup>1,2</sup>. This maintains a balance of cells and soluble factors within the blood during the lifetime of an individual<sup>1,2</sup>. The HSCs are quiescent for most of their lifespan, but when activated can undergo either asymmetric division to maintain stem cell number while generating new progenitors, or symmetric divisions that generate either 2 stem cells or 2 progenitors<sup>3</sup>. Differentiation of HSCs to mature cell types is a multistep process, in which HSCs first give rise to multipotent progenitor cells, with a decreased capacity of self-renewal<sup>1,2</sup>. Subsequent steps of differentiation diminish self-renewal ability, while the proliferative activity tends to increase. The multipotent progenitors give rise to lineage-specific common myeloid progenitor (CMP) or lymphoid progenitor (CLP) cells. These cells have no true self-renewal potential and instead undergo proliferative differentiation into cells of the myeloid lineage such as megakaryocytes, monocytes, granulocytes and erythroid cells; or into cells of the lymphoid lineage such as B-, T-, natural killer (NK-) and dendritic cells, respectively (Figure 1)<sup>1,2</sup>.

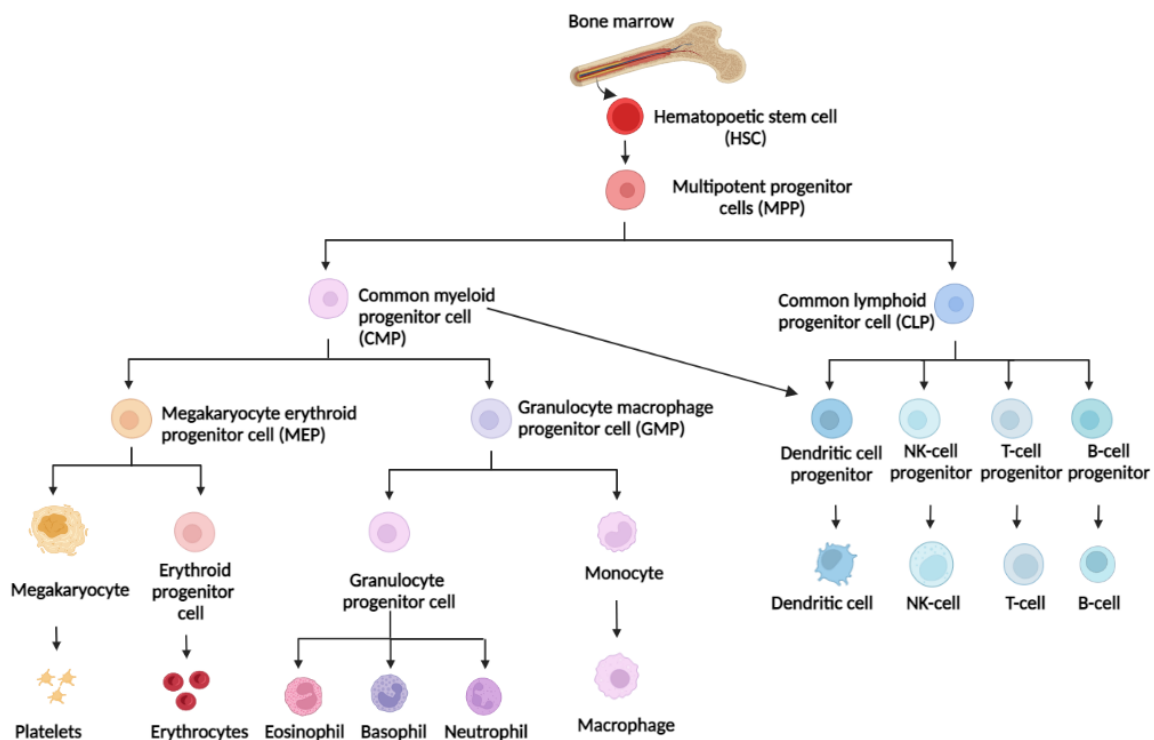


**Figure 1** Hierarchal differentiation of haematopoietic stem cells to mature blood cells. Created with BioRender.com<sup>4</sup>.

The self-renewal and differentiation of the HSCs to mature blood cells is tightly regulated by intrinsic and extrinsic process within the bone marrow<sup>1,2,5</sup>. Accordingly, disruption of the balance between self-renewal and differentiation can lead to a disease state. The risk of such disruptions increases with aging as mutations accumulate in the stem cell pool. While the majority of mutations has either no affect or is disadvantageous for the stem cell, some mutations can interfere with the balance between self-renewal and differentiation and result in outgrowth of the affected clone. Low-level, non-neoplastic over-representation of a mutated clone is known as clonal haematopoiesis (CH) and is now recognised to be a common phenomenon in the elderly<sup>6</sup>. However, the accumulation of more disruptive mutations, sometimes in addition to a pre-existing CH mutation, leads to more severe phenotypes, including myelodysplastic neoplasms (MDS) or acute myeloid leukaemia (AML)<sup>7-9</sup>. In all these cases, the changes intrinsic to the mutated haematopoietic clone are accompanied by changes in the bone marrow microenvironment (BMME) or “niche” with which it interacts, so that disease progression is determined by the properties of the niche as a whole, and not simply by those of the haematopoietic clone.

## **1.2. Bone marrow microenvironment**

The BMME forms a variety of different niches within the bone marrow. A bone marrow niche is a distinct anatomical location where haematopoiesis is supported by intricate signalling between the haematopoietic compartment and the other “stromal” cells that surround it. Communication takes place via cell-cell; cell-matrix interactions and by the paracrine release of soluble growth factors and cytokines<sup>10-12</sup>. haematopoietic bone marrow niches are further divided into endosteal (near the bone) and vascular (near blood vessels) niches<sup>12,13</sup>, which can involve either sinusoidal or arterial endothelia<sup>14</sup>. Each of these niches typically comprise a dynamic assembly of cellular components that includes mesenchymal stromal (MSCs), endothelial, osteogenic, adipogenic, neuronal, and haematopoietic cells as well as non-cellular components including extracellular matrix (ECM) and exosomes<sup>11-13</sup>. Although the essential role of bone marrow niches in maintaining the stem cell pool and regulatory haematopoiesis is widely accepted, it is far from completely characterised. This is partly because the complexity of cellular interactions takes place in a 3D environment of superimposed growth factor signalling, metabolic, and oxygen gradients<sup>11,13,14</sup>, all of which are likely to contribute to homeostasis. De-regulation in any of these niche characteristics could potentially disrupt normal haematopoietic, control mechanisms, and promote a disease phenotype<sup>10,15-20</sup>. A common starting point for characterisation of niche interactions has been to focus on mesenchymal stromal cells. These

cells are not only a major supportive component for normal haematopoiesis but also are involved in the evolution of clonal disorders such as MDS and AML<sup>10,18,19,21,22</sup>.

### 1.2.1. Mesenchymal stromal cells

From the analytical perspective, MSCs are generally described as a plastic-adherent subset of non-haematopoietic cells in the bone marrow with the ability of osteogenic, adipogenic and chondrogenic differentiation<sup>23</sup>. However, over the years there has been many discrepancies about the nomenclature and other tissue sources of these cells<sup>23–26</sup>. Therefore, in 2006, International Society for Cellular Therapy defined a minimal set of criteria for the MSCs<sup>23</sup>. They state MSCs i.e. multipotent mesenchymal stromal cells as plastic-adherent cells, which must express surface specific antigens like CD105, CD73 and CD90 and lack CD45, CD34, CD14 or CD11b, CD79a or CD19, and HLA class II<sup>23</sup>. Additionally, the cells must be able to differentiate into osteoblasts, adipocytes and chondroblasts *in vitro*<sup>23</sup>. However, the different differentiation pathways of the MSCs are not strictly separated. There seems to be a balance and plasticity among the differentiation pathways, which is governed by epigenetic mechanisms<sup>22</sup>. Different subsets of bone marrow MSCs express different markers like SCA-1, CD271, CD146, CD166, nestin, and platelet-derived growth factor- $\alpha$ <sup>22,23,27</sup>. Within the bone marrow, the MSCs provide indispensable cues for haematopoietic stem and progenitor cell (HSPC) homeostasis, mobilisation, and homing<sup>28</sup>.

MSCs comprise about 0.001 to 0.01 % of the bone marrow cells<sup>29</sup> that are mostly present in the perivascular area wrapped around the vessels<sup>10,20</sup>. They are involved in organization of the haematopoietic microenvironment via cell-cell contact, and matrix bound paracrine secretion of growth factors<sup>22,30,31</sup>. Modulation of HSC and HSPC development by MSCs has been attributed to the difference in the location of the MSCs and growth factors within the bone marrow<sup>10,14,22,32</sup>. The MSCs near the bone surface i.e. close to their differentiated counterparts, osteoblasts and near the arterioles are thought to promote HSC quiescence<sup>10,14,22,32</sup>. Moreover, the MSCs close to the sinusoidal niches are thought to be involved in HSPC maintenance and retention<sup>10,14,22</sup>. In addition, the HSPCs fate is also governed by cell-cell contact via presentation of notch ligands<sup>31,33,34</sup>. Furthermore, HSPC mobilization, cycling and differentiation is governed by paracrine signalling mediated by soluble growth factors like stem cell factor (SCF), Stromal cell-derived factor 1 (SDF-1), transforming growth factor beta (TGFB), activins, and various immunomodulatory cytokines<sup>22,35,36</sup>. Generally in the bone marrow, growth factors secreted by the MSCs and other stromal cells are bound to different ECM components, thereby maintaining a gradient of growth factor pool<sup>30,37–41</sup>. Interactions of MSCs with HSCs in the bone marrow are summarised in Figure 2.

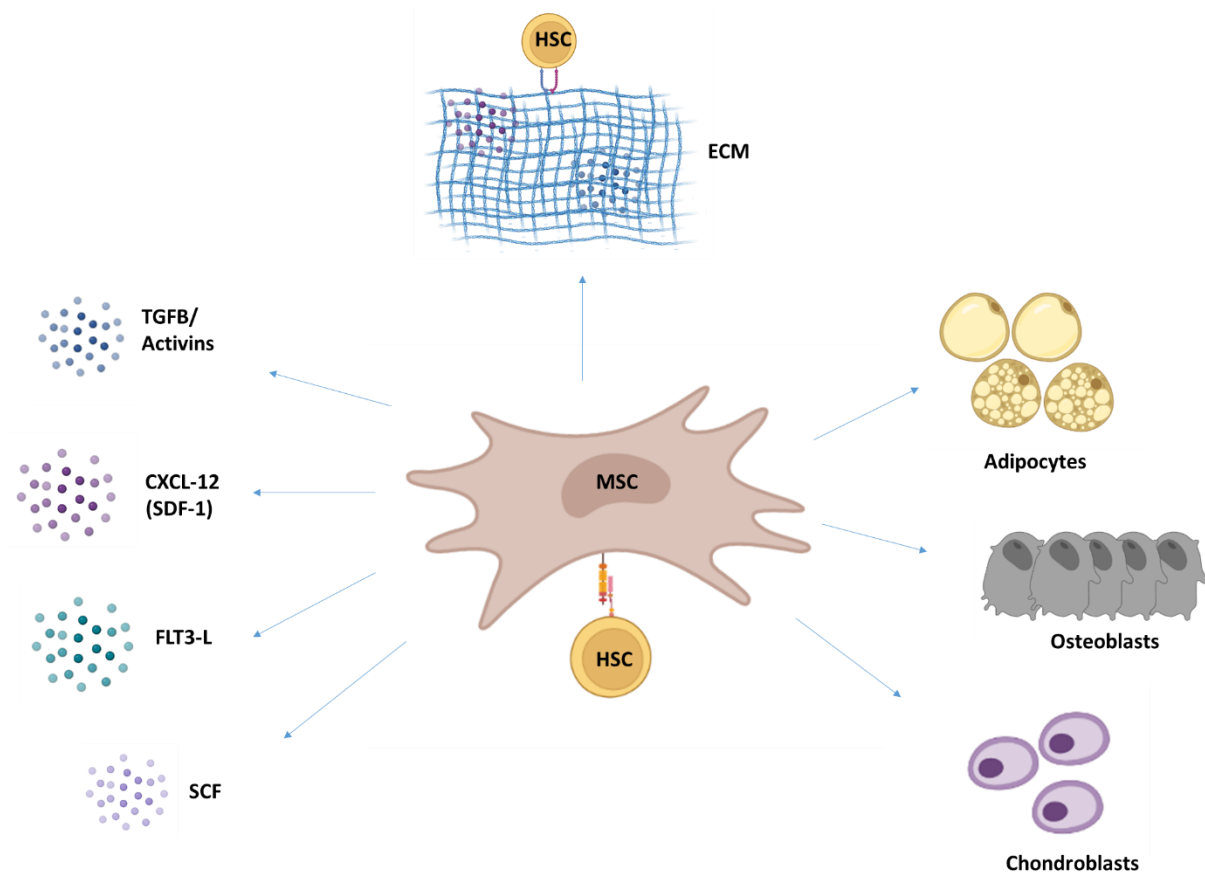


**Figure 2 Role of MSCs in the bone marrow and their interaction with HSPCs.** Differentiated counterparts of MSCs like osteoblasts modulate HSC behaviour via cell-cell interactions and production of cytokines like BMP-4. MSCs also govern HSC function through cell-cell interactions via presentation of various ligands. Paracrine signalling mediated via MSC-secreted soluble growth factors is involved in homing and migration of HSCs and HSPCs. These growth factors are presented to the HSCs in its active form via the MSC secreted ECM. The image was created with BioRender.com<sup>4</sup>.

### 1.2.2. Extracellular matrix

Extracellular matrix is three dimensional protein meshwork, that provides mechanical and biochemical supports to surrounding cells in the microenvironment<sup>42</sup>. It maintains stiffness, and hydration, and provides compartmentalization of growth factors. In the bone marrow, these ECM components are spatially localized and known to regulate various aspects of haematopoiesis including homing, migration, proliferation, and differentiation via biophysical and biochemical interactions<sup>30,42</sup>.

### 1.2.2.1. Biophysical composition of ECM

Structural support by ECM is very well understood. However, the biophysical regulation behind it is often overlooked. ECM regulates the behaviour of the surrounding cells via mechanical scaffolding, fibre orientation, and elasticity<sup>42-46</sup>. The cells recognise these topographical changes via cell adhesion molecules such as integrins that mediate a process of outside-in and inside-out signalling<sup>42-47</sup>. This modulates the intracellular actin cytoskeletal dynamics and ligand density, leading to changes in cell cycle, migration, and differentiation<sup>42-47</sup>. Similar to the spatial localization of the different cells in the niche, the biophysical cues are also spatially confined. The rigidity (young's modulus) of the ECM which can be measured by atomic force microscopy (AFM), is expressed as the stress required for the deformation of a given substrate. AFM analysis of the pig bone marrow, has revealed a stiffer matrix (> 30 kPa) near the endosteal surface, with softer matrix being present towards the vascular niche and adipose tissue (1-3 kPa), as well as in the area immediately surrounding cell membranes (< 1 kPa)<sup>47,48</sup>. Previous studies have shown that biophysical properties, pore size, and rigidity can directly influence HSPCs behaviour. Matrix with larger pore size and increased rigidity was shown to better support the proliferation of HSPCs and to maintain stemness<sup>46</sup>. Moreover, HSPCs cultured on fibronectin or collagen coated stiff substrates exhibited a certain polarized morphology compared to the round morphology that is seen on soft substrates and that is associated with fate specification<sup>43,47</sup>. Similarly, reduced expansion of Lin-SCA 1+ c-Kit+ (LSK) murine stem cells was observed when they were cultured on tropoelastin substrates with intact signalling domains but impaired elasticity<sup>49</sup>. Myosin II is thought to be an integral component in mechano-transduction of the HSPCs. In response to varied stiffness and polarized myosin II was observed in HSPCs cultured on stiffer matrix, in contrast to the non-polarized myosin II seen when cultured on softer matrix<sup>43,50</sup>. The polarized myosin II on stiffer matrix resulted in increased asymmetric division and higher CD34 marker expression on HSPCs<sup>50</sup>.

### 1.2.2.2. Biochemical composition of ECM

In addition to providing structural and biophysical support, ECM is also known to regulate cell proliferation and differentiation through the actions of its various biochemical components. ECM is composed of complex, dynamic spatially organised components including glycoproteins, collagens, and proteoglycans with their associated glycosaminoglycan (GAG) chains<sup>42</sup>. The matrix is a major extracellular reservoir of proteases and growth factors, which bind to the matrix components and are presented to the cells in the active form<sup>47,51,52</sup>. ECM composition undergoes constant remodelling during homeostasis and malignant haematopoiesis, suggesting that matrix composition and turnover may provide an opportunity to explore new options for disease monitoring markers or therapeutic targets<sup>42,53-55</sup>. The ECM-haematopoietic cell interactions are summarized in Figure 3.



### 1.2.2.2.1. Glycoproteins

Glycoproteins are a family of highly glycosylated, multifunctional proteins<sup>40</sup>. Various glycoproteins like fibronectin, secreted protein acidic and rich in cysteine (SPARC), tenascins and laminins are known to be involved in modulating haematopoietic behaviour in normal and stress haematopoiesis<sup>56–59</sup> (Figure 3). Fibronectin is predominantly present in bone marrow parenchyma, where it is involved in adhesion, migration and differentiation of HSPCs through arginylglycylaspartic acid (RGD)-mediated binding of integrins<sup>60–63</sup>. Increased fibronectin levels in MSCs of patients with pre-fibrotic myelofibrosis co-related with their reduced haemoglobin levels<sup>64</sup>. Moreover, various types of multiple myeloma cells showed increased adhesion to fibronectin<sup>65</sup>.

The glycoprotein tenascin-C (TNC) is known to interact with fibronectin via its epidermal growth factor (EGF)-domain which regulates growth and differentiation particularly in the lymphoid niche<sup>57,66,67</sup>. It is localized in the endosteal layer in between developing haematopoietic cells<sup>57,68,69</sup>. In contrast to a well-characterised anti-adhesive function, tenascin mediates specific adhesion to HSCs<sup>68,70</sup>. However, this adhesive property decreases in some multiple myeloma cells, even though TNC is found at high levels in the bone marrow of multiple myeloma marrow<sup>65</sup>.

SPARC, also known as osteonectin, is secreted by both osteoblast and endothelial cells and is known to support the development of erythroid progenitor cells<sup>71</sup>. Moreover, high levels of SPARC in HSCs are found during the its migration from the fetal liver<sup>56</sup>. Increased return of HSCs to quiescence after 5-florouravil treatment was seen in mice, which did not express SPARC<sup>56</sup>, indicating the role of SPARC in maintaining stem cell pool during stress haematopoiesis. Furthermore, decreased expression of SPARC was observed in the stromal cells of hypo-cellular aplastic anaemia patients<sup>17,72</sup>. While, increased SPARC expression was observed in MSCs from hyper-cellular bone marrow of LR-MDS patients<sup>17</sup>, indicating that SPARC may play a role in maintaining the overall cellularity of the marrow.

High molecular weight (HMW) ECM glycoproteins such as laminins are preferentially localized close to the vascular niche underlying the endothelial cells<sup>59,63</sup>. 15 different laminins are named based on the combination of consist of  $\alpha$ ,  $\beta$  and  $\gamma$  chains, encoded by 11 genes (five  $\alpha$ , three  $\beta$  and three  $\gamma$  isoforms)<sup>73</sup>. In the bone marrow,  $\alpha 4$  or  $\alpha 5$  are the major isoforms present in combination with a range of different  $\beta$  and  $\gamma$  chains<sup>30,40,59</sup>. Increased adhesion of multiple myeloma cell lines to the  $\alpha 4$  chain was observed in comparison to other ECM proteins like fibronectin and collagen I, while haematopoietic cell lines adhere to  $\alpha 4$  chain either poorly or not at all<sup>65,74,75</sup>. Genetic deletion of the  $\alpha 4$  chain in mice nonetheless led to a reduction in proliferation, migration and reconstitution ability of the HSPCs<sup>59</sup>, suggesting that the HSPC-laminin interaction is important for normal haematopoiesis. Increased adhesion of acute myeloid leukaemia cells to laminin was also associated with increased

monocytic differentiation both *in vivo* and *in vitro*<sup>76</sup>. The fact that HSPC adhesion to laminin increases myeloid differentiation<sup>43</sup>, suggests that laminin may play a particularly important role in niches supporting myelopoiesis.

#### 1.2.2.2.2. Glycosaminoglycans and proteoglycans

Proteoglycans consist of a core protein attached to a GAG side chains<sup>77,78</sup>. In addition to the protein core, the GAGs and the sulphation pattern greatly influence the proteoglycan function<sup>77,78</sup>. GAGs mainly consist of repeating units of hexosamine (N-acetyl-galactosamine or N-acetyl-glucosamine) and hexuronic acid (D-glucuronic or L-iduronic acid) or galactose sugars<sup>77,78</sup>. Based on the combination of the sugar chains there are 5 major GAGs: hyaluronic acid (HA), heparan sulphate (HS), chondroitin sulphate (CS), dermatan sulphate (DS) and keratan sulphate (KS)<sup>77,78</sup>. All the GAGs except HA undergo sulphation and are attached to a protein core<sup>77</sup>. Biosynthesis of the GAGs is a multi-step non-template driven enzymatic process (refer to Table 1 for a few enzymes involved in GAG synthesis and degradation)<sup>79</sup>. GAGs play a multifunctional role in the ECM by providing biophysical cues like stiffness and hydration to the ECM but also maintain and present morphogenic gradients<sup>80</sup>.

The role of HS proteoglycans (HSPG) has been extensively studied in comparison to other sulphated GAGs. HSPGs are known to bind several growth factors and cytokines including TGF $\beta$ , Granulocyte-macrophage colony-stimulating factor (GM-CSF), IL3, SDF-1, IL8, and fibroblast growth factor in the bone marrow to modulate homing and engraftment of the HSCs<sup>80,81</sup>. In addition to, maintaining growth factor gradients, HSPGs also modulate the proliferation and differentiation of HSPCs by modulation of WNT and RANK/RANKL/OPG pathways<sup>80,82-84</sup>. Accordingly, deficiency of exostosin-1 (EXT-1, a key enzyme of HS synthesis) in a mouse model lead to decreased engraftment of the HSCs in the bone marrow<sup>85</sup>.

CS is another sulphated GAG that is widely distributed throughout the BMME<sup>86</sup>. However, there is limited information about the role of CS in haematopoiesis. The CS proteoglycan, versican is known to interact with HA and to play a role in inflammation, T-cell migration and trafficking<sup>87,88</sup>. Increased proliferation of HSPCs was observed following ex-vivo exposure of CS<sup>89</sup>. Moreover, an increased LSK cell fraction in bone marrow and delayed short-term reconstitution in HSPCs, were observed in a CS-N-acetylgalactosaminyltransferase-1 (CSGALNACT1) knock out mouse model<sup>90</sup>, both of which indicate retardation of haematopoiesis.

HA, the only non-sulphated GAG, has diverse functions ranging from homing, engraftment and modulation of inflammation within the marrow via its interactions with its receptors CD44 and hyaluronan-mediated motility receptor (RHAMM)<sup>91-95</sup>. A triple knock out mouse model lacking all three

hyaluronan synthase (HAS) genes had decreased HSPC numbers in the bone marrow together with increased extra medullary haematopoiesis. Similar observations were made in the haematopoietic activity during chemical inhibition of HA in the *in vitro* long-term bone marrow cultures<sup>91</sup>. These observations are consistent with a role in regulating the stem cell pool by promoting the quiescence of HSCs<sup>96</sup>. Moreover HA plays a diverse roles in regulating inflammation in a manner that is strongly dependent on its molecular weight. HMW-HA is known to be anti-inflammatory, while low molecular weight (LMW) HA is known for being pro-inflammatory<sup>94,95,97</sup>. Increased levels both of HA and of its receptor CD44 have been reported in certain haematological disorders, including AML, chronic lymphocytic leukaemia, and multiple myeloma<sup>98-101</sup>. Finally, the fact that ligation of CD44 with LMW-HA reduced the drug-induced apoptosis in a myeloid cell line KG1, show that HA environments may modulate the drug response<sup>102</sup>.

**Table 1** List of enzymes that play a role in GAG biosynthesis and degradation.

Name	GAGs involved	Function
<b>GAG modifying enzymes</b>		
Hyaluronan synthase 1 (HAS1)	HA	HA synthesis <sup>103</sup>
Hyaluronan synthase 2 (HAS2)	HA	HA synthesis <sup>103</sup>
Hyaluronan synthase 3 (HAS3)	HA	HA synthesis <sup>103</sup>
Carbohydrate sulfotransferase 11 (CHST11)	CS	Catalyses the transfer of sulphate to position 4 of the N-acetyl-galactosamine residue of CS <sup>104</sup>
Chondroitin sulphate N-acetylgalactosaminyltransferase 1 (CSGALNACT1)	CS	Elongation CS chains by transfer of N-acetyl- galactosamine to the core tetra saccharide linker <sup>104</sup>
Chondroitin sulphate synthase 1 (CHSY1)	CS	Transfer glucuronic acid and N-acetyl-galactosamine to the CS chain <sup>104</sup>
Dermatan sulphate epimerase (DSE)	DS	Conversion of D-glucuronic acid to L-iduronic acid <sup>104</sup>

Exostosin 1 (EXT-1)	HS	Transfer glucuronic acid and N-acetyl-glucosamine HS chain <sup>105</sup>
<b>GAG degrading enzymes</b>		
Hyaluronidase 1 (HYAL-1)	HS	Degradation of HA <sup>105</sup>
Heparanase-1 (HPSE)	HS	Degradation of HS <sup>106</sup>

### 1.2.2.2.3. Collagens

Collagens are the most abundant ECM proteins consisting of  $\alpha$  chain triple helix with alternating triplet amino acid sequence comprising of glycine-X-Y with X often being proline and Y often being hydroxyproline<sup>107</sup>. The  $\alpha$  chains undergo glycosylation and hydroxylation in the endoplasmic reticulum followed by crosslinking by lysyl oxidase (LOX) and LOX-like (LOXL) enzymes before being secreted by the cells<sup>107</sup>. The 28 known collagens are sub-divided into different groups based on their structure and assembly. The major groups of collagens are fibril forming collagens (collagen I, II, III, V, XI, XXIV, XXVII), fibril associated collagens with interrupted triple helices (collagen IX, XII, XIV, XVI, and XIX to XXII), network forming collagens (collagen IV, VIII, and X), membrane bound collagens (collagen XIII, XVII, XXIII, XXV) and multiplexins (collagen XVIII)<sup>107</sup>. The cells interact with collagens through different cell surface receptors like Leukocyte associated immunoglobulin like receptor (LAIR), Discoidin domain receptor (DDR), integrins, and membrane bound proteoglycans<sup>108</sup>. Collagens do not only regulate the biophysical properties of the ECM but also provide biochemical support to the cells<sup>40,109,110</sup>.

In the bone marrow, the expression of collagens I, II, III, IV, V, VI, XI, XIV, XIV had been reported with collagen I and IV being the most abundant and well-studied<sup>40</sup>. Collagen I is found throughout the bone marrow while collagen IV is mainly located near the central marrow around sinusoids<sup>63,111</sup>. Cytokines and growth factors, particularly TGF $\beta$  are known to regulate collagen I synthesis<sup>112-114</sup>. Many erythroid and myeloid cells display strong attachment to collagen I and IV<sup>115</sup>. Moreover, HSPC culture on collagen I showed slightly diminished proliferation but an increase in colonies using colony forming unit (CFU) assay when compared to suspension cultures<sup>110,116</sup>. However, results are inconsistent, with other studies having reported increased proliferation of HSPCs cultured on collagen I-coated substrates<sup>43</sup>. Both platelets and megakaryocytes interact with collagen I via expression of the collagen receptor integrin  $\alpha$ 2  $\beta$ 1 (ITGA2B1), resulting in inhibition of pro-platelet formation at sinusoids. In contrast, binding between the same integrins and collagen IV has been reported to promote platelet formation<sup>117,118</sup>. Binding assays have also indicated displacement of collagen I by collagen IV

specifically at the sinusoids. This level of organisation that may help to prevent premature platelet release into the bone marrow cavity while subsequently promoting pro-platelet formation at the sinusoids<sup>118</sup>. Increased levels of bone marrow collagen IV have been found in patients with strongly reduced platelet counts<sup>111</sup>.

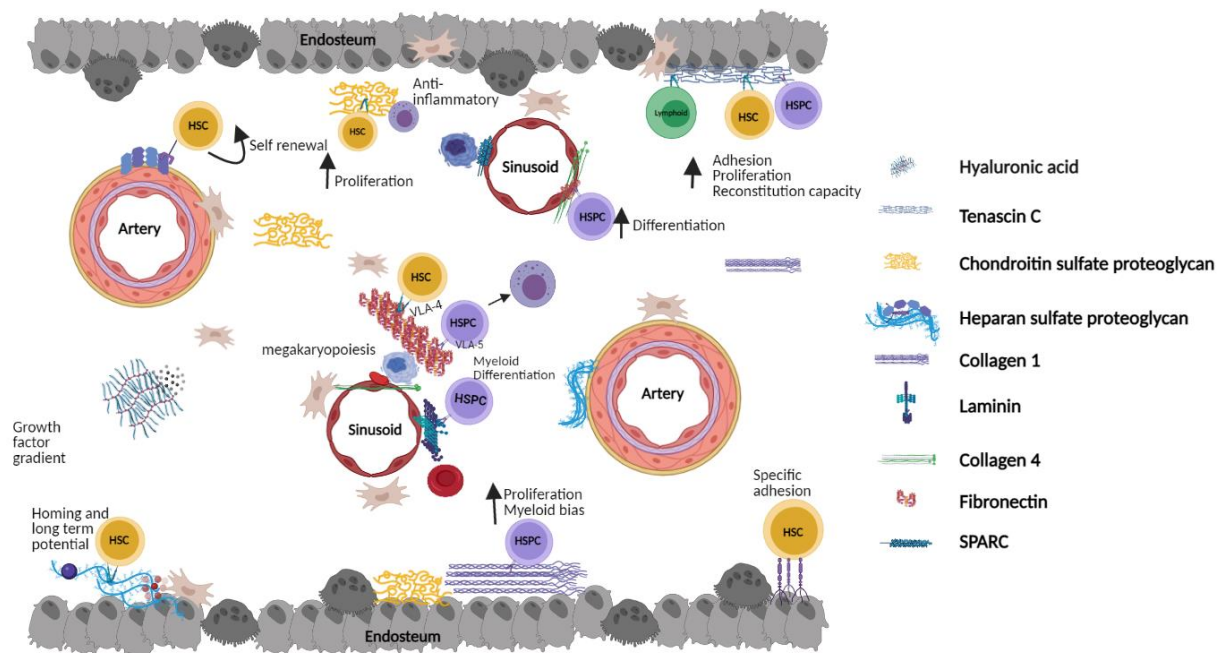


**Figure 3** Localization of different ECM components in the bone marrow and its interactions with HSPCs. Range of ECM proteins and GAGs are involved in controlling the proliferation, migration and differentiation of haematopoietic cells of all lineages in the bone marrow. HSC: haematopoietic stem cell, HSPC: haematopoietic stem and progenitor cell. The image created with BioRender.com<sup>4</sup> and was adapted from Zanetti & Krause.2020<sup>42</sup>.

Multiple myeloma cells also attach more strongly to collagen IV than to collagen I, indicating a potentially differential role of collagens in disease<sup>65</sup>. Attachment of leukemic cells to collagen I via ITGA2B1 inhibits doxorubicin-induced apoptosis in acute T-cell lymphoblastic leukaemia and in AML<sup>119,120</sup>. Furthermore, recent studies have shown that either targeting the ECM via LOX and LOXL enzymes or by blocking HSPC-integrin alpha5 beta1 (ITGAVB1) interactions in haematological malignancies like myeloproliferative neoplasms and AML can improve the therapeutic response<sup>54,121</sup>.

Although collagens I and IV are the most prevalent in bone marrow, there is clear evidence that other collagens also play key roles. The levels of collagen VII have also been reported to be diminished in the bone marrow of multiple myeloma patients<sup>53</sup>. A degradation product of collagen XVII, endostatin, is known to increase the bone marrow vascularity in AML patients and is associated with favourable outcome<sup>122,123</sup>.

Collectively, the results to date indicate a strong role of biophysical as well as biochemical properties of the ECM in modulating HSPC behaviour as well as in improving the therapeutic response in haematological disorders. This suggests that a better understating of the bone marrow ECM in homeostasis and in diseases like MDS and AML may provide novel therapeutic targets in otherwise hard to treat haematological malignancies.

### **1.3. Myelodysplastic neoplasms (MDS)**

#### **1.3.1. Definition and classification**

MDS are heterogeneous neoplasms of myeloid lineages. They are considered disorders of the elderly with a median onset age of 70 years at an incident of 75 per 100,000 compared to 4-5 per 100,000 in the younger population<sup>124</sup>. MDS are characterised by ineffective haematopoiesis and peripheral blood cytopenia in one or more haematopoiesis lineages. Single or multiple driver gene mutations and chromosomal abnormalities in the HSC or HSPC compartment lead to MDS<sup>124–126</sup>. These somatic gene mutations account for the dysregulation of epigenetic, DNA repair, cohesion complex, and spliceosome pathways. The International prognostic scoring system (IPSS) was developed in 1997, revised (IPSS-R) in 2016 and updated in 2022 (IPSS-M) to classify MDS into low risk (LR-), intermediate (Int-) and high risk (HR-) groups<sup>127,128</sup>. This classification is based on the number of dysplastic lineages, cytogenetic and genetic abnormalities, presence or absence of ring sideroblasts (abnormal deposition of iron in the mitochondria of erythroid precursors), and percentage of blasts in the bone marrow and peripheral blood<sup>127,128</sup>.

One third of the MDS cases progress to AML<sup>129</sup>. The progression of MDS to AML is a multistep process (Figure 4). The early stages (LR- and Int- MDS) are characterised by accumulation of somatic clonal mutations in combination with a myelosuppressive environment. This eventually leads to hyper methylation and hence downregulation of tumour suppressor genes, leading to an immune evading environment in the later stages (HR-MDS)<sup>125</sup>. Moreover, the interaction of the haematopoietic compartment with its microenvironment has become increasingly evident in disease pathogenesis and progression<sup>10,22</sup>. BMME especially MSCs and their differentiated counterparts like osteoblasts have been known to harbour genetic abnormalities, providing fitness advantage to the clonal progenitor and aiding in disease initiation and progression<sup>17,21,130</sup>.

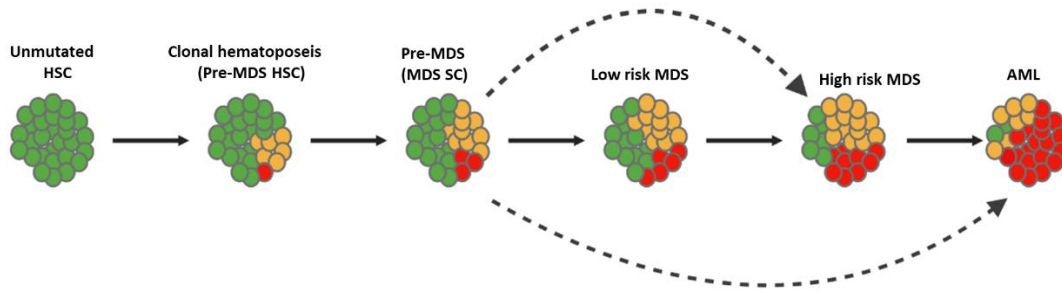


**Figure 4 Model of clonal evolution, progression to MDS and its transformation to AML.** Clonal cells (orange) within the healthy HSPC compartment (green) gain additional driver mutations (red) which are the basis of pre-MDS and eventually lead to a systematic progression from LR-MDS to HR-MDS and to AML. In few cases, the driver clones can directly transform to either HR-MDS or AML as represented by the dotted lines. The image was created with BioRender.com<sup>4</sup> and was adapted from Chen.et al.2018<sup>7</sup>.

### 1.3.2. Current treatment options

The current treatment strategies for MDS patients are based on the IPSS-R with the major focus to improve the quality of life while delaying disease progression<sup>125,131</sup>. The median survival of LR-MDS is 5 to 8 years after the initial diagnosis, therefore the treatment aims to improve cytopenia especially anaemia using erythrocyte transfusion and erythroid stimulating and maturing agents like erythropoietin or darbepoietin alfa<sup>125</sup>. Lenalidomide, an immunomodulatory drug is also used to improve the erythroid counts in transfusion dependent LR-MDS patients<sup>125,131,132</sup>. Activin receptor ligand traps luspatercept and sotatercept have been shown effective in treating late stage erythropoiesis defects in LR-MDS patients with SF3B1 mutations or ring sideroblasts<sup>132</sup>. Immunosuppressive agents antithymocyte globulin (ATG, either horse or rabbit), with or without addition of cyclosporine is recommended in hypoplastic MDS<sup>131,132</sup>. However, the response to the treatments is only short-lived and the disease develops towards HR-MDS and AML, with increasingly severe symptoms and a very poor prognosis.

With the median survival time of less than 12 months for HR-MDS, the treatment aims to delay disease progression to AML<sup>125</sup>. The first line of therapy for HR-MDS is intensive chemotherapy using hypomethylating agents (HMA) like azacytidine (AZA) and decitabine, with only AZA being currently approved in Europe<sup>131</sup>. However, the response rate to AZA is low with a complete or partial remission in 40-50 % of the patients<sup>131</sup>. AZA followed by allogeneic haematopoietic stem cell transplantation (HSCT) for the patients with blast count less than 10 % have been tested to reduce the risk of relapse after transplantation<sup>125,131,132</sup>. HSCT is potentially curative but is rarely an option in elderly and frail patients.

Due to the challenges related to treatment of MDS, there is an unmet need for new and effective therapies to slow or stop disease progression at the stage of LR-MDS and improve the response to therapies in HR-MDS. Recent studies have revealed the role of bone marrow inflammation and pyroptosis of progenitor cells in driving clonal progression in MDS<sup>33,133</sup>. Based on this, a number of anti-inflammatory drugs are already entering clinical trials<sup>134</sup>. In addition, the role of BMME, specially mesenchymal signalling in modulating and predicting therapeutic response has been increasingly investigated<sup>54</sup>.

### 1.3.3. MSCs in MDS

Mesenchymal cells and their differentiated counterparts have long been implicated in MDS pathogenesis<sup>15,17,21,22</sup>. However, contradicting results regarding the cell surface marker expression and differentiation potential of MDS MSC have been reported<sup>17-19,27,135</sup>. A number of studies observed increased adipogenic differentiation of MDS MSCs, while other studies found no changes in their differentiation profile<sup>18,19,135,136</sup>. Deregulated SDF-1, SCF,  $\beta$ -catenin, Notch and Wnt signalling are also observed in MDS MSCs<sup>16,34,112,137-141</sup>. Furthermore, the mesenchymal compartment harbours certain cytogenetic, genetic and epigenetic aberrations which are different from the ones observed in the haematopoietic compartment<sup>16,137,142,143</sup>. Indeed, MSCs are thought to contribute to the inflammatory and immune microenvironment of the bone marrow and to contribute to the expansion of the clonal progenitors, thus promoting the development and progress of the disease<sup>17,137,144,145</sup>. MDS MSCs exhibit reduced support of healthy donor-derived HSPCs *in vitro* where they increase apoptosis and suppress differentiation without affecting the proliferation<sup>15,135</sup>.

Similar findings were observed in mouse models, where MDS MSCs support long-term engraftment and expansion of MDS HSPCs<sup>17</sup>. Moreover, increased myeloid differentiation was observed in MDS HSPCs when compared to healthy donor-derived HSPCs when engrafted alongside MDS MSCs in mice<sup>17</sup>. The impact of MDS MSCs on HSPCs behaviour was reversed by direct treatment of MDS MSCs with current treatment options like AZA, luspatercept and lenalidomide<sup>15,112,135</sup>. Interestingly, transcriptomic analysis of human MDS MSCs with or without AZA treatment showed dysregulation in pathways related to inflammation and ECM synthesis and remodelling<sup>17,135</sup>. Currently, the role of inflammation in MDS is receiving much attention, however, the role of MSC-derived ECM MDS has still been largely underexplored.



## 2. Aim

The involvement of the BMME especially MSC-HSPCs signalling in MDS progression and therapeutic response is indisputable<sup>17,54,112</sup>. BMME provides a supportive milieu for haematopoiesis and may be targeted by clinically available drugs such as AZA<sup>135</sup>. However, pathological changes in the composition of the ECM and the involvement of the ECM in the response to therapy is poorly explored. Therefore, this study was carried out with the aim of characterising the MDS MSC-derived ECM (both LR- and HR-MDS) in comparison to that from healthy age matched donors in terms of composition, biophysical properties and functional haematopoietic support. This study also aims to evaluate the impact of *in vivo* and *in vitro* AZA therapy on MDS MSC-derived ECM.

These analyses will help uncover disease-specific properties of the ECM contributing to the pathogenesis of MDS. This will also allow a better understanding of the changes in the microenvironment and its response to current therapies, with the ultimate aim of identifying new therapeutic targets that may be used to develop novel interventions for the treatment of MDS.

### 3. Materials and Methods

#### 3.1. Patient cohort

MSCs from MDS patients ( $n = 10$ ) inclusive of LR-MDS including Int-MDS ( $n = 5$ ) and HR-MDS ( $n = 5$ ) based on IPSS-R classification and controls from haematologically healthy donors who underwent hip replacement surgery ( $n = 7$ ) were collected after informed written consent. The control and MDS cohorts were age matched with a median age of  $66.8 \pm 2.5$  years for the LR-MDS group,  $63.4 \pm 5.5$  years for the HR-MDS group, and  $65 \pm 2.8$  years for the controls. To investigate the impact of treatment, MSCs from MDS patients at time point of diagnosis ( $n = 7$ ), after receiving 3-4 cycles of AZA therapy ( $n = 7$ ) and post-HSCT ( $n = 3$ ) were collected with median age of  $65 \pm 4.6$  years,  $65 \pm 4$  years, and  $71 \pm 4.7$  years respectively. The MDS patient and healthy donor characteristics are summarized in Table 2.

**Table 2** Characteristics of patients and healthy donors

No.	Sex	Age	Diagnosis	IPSS	IPSS-R	Sample type	Time point
1	M	59	MDS	High	High	MSC	Diagnosis
2	M	62	MDS	Int-2	High	MSC	Diagnosis
3	M	62	MDS	High	Very high	MSC	Diagnosis
4	M	61	MDS	High	Very high	MSC	Diagnosis
5	M	73	MDS	Int -2	High	MSC	Diagnosis
6	M	69	MDS	Int-1	Low	MSC	Diagnosis
7	F	66	MDS	Int-1	Int	MSC	Diagnosis
8	M	63	MDS	Low	Low	MSC	Diagnosis
9	M	67	MDS	Int-1	Int	MSC	Diagnosis
10	M	69	MDS	Int-2	Int	MSC	Diagnosis
11	F	70	MDS	Int-2	Int	MSC	Diagnosis
12	F	62	MDS	High	Very high	MSC	Diagnosis
13	M	69	MDS	Int -1	Int	MSC	Diagnosis
14	M	70	MDS	Int-2	Int	MSC	Diagnosis

15	M	59	MDS	Int-2	Int	MSC	Diagnosis
16	M	61	MDS	High	Very high	MSC	Diagnosis
17	F	65	MDS	High	High	MSC	Diagnosis
18	F	71	MDS	-	-	MSC	AZA 4 cycles
19	F	62	MDS	-	-	MSC	AZA 4 cycles
20	M	69	MDS	-	-	MSC	AZA 3 cycles
21	M	70	MDS	-	-	MSC	AZA 4 cycles
22	M	60	MDS	-	-	MSC	AZA 4 cycles
23	M	62	MDS	-	-	MSC	AZA 4 cycles
24	F	65	MDS	-	-	MSC	AZA 4 cycles
25	F	73	MDS	-	-	MSC	Post-HSCT
26	F	64	MDS	-	-	MSC	Post-HSCT
27	M	71	MDS	-	-	MSC	Post-HSCT
28	M	64	-	-	-	MSC	
29	F	65	-	-	-	MSC	
30	M	68	-	-	-	MSC	
31	M	61	-	-	-	MSC	
32	F	68	-	-	-	MSC	
33	M	62	-	-	-	MSC	
34	F	67	-	-	-	MSC	
35	M	64	-	-	-	MNC	
36	M	68	-	-	-	MNC	
37	F	62	-	-	-	MNC	

## 3.2. Materials

### 3.2.1. Software and devices

**Table 3** List of laboratory equipment used for the experimental work

<b>Tool</b>	<b>Company</b>
550 EVL Autoclave	Tuttnauer
Analytical balance AX4202	Sartorius
Bioanalyzer	Agilent
Biotek 800™ TS Absorbance Reader	Biotek
Bright field microscope primover	Zeiss
Centrifuge 5424R	Eppendorf
Constant climate chamber KBF-S 240: Hot air oven	Binder
DNA Engine Thermal cycler	Bio-Rad
EPSON Perfection V750 Pro Scanner	Epson
FACSVerse flow cytometer	BD Biosciences
Fluorescence microscope	Keyence
Fresco -17 Centrifuge	Thermo Fisher
Hera cell 150i CO2 Incubator	Thermo Fisher
Heraeus Mega centrifuge	Thermo Fisher
Inverted Phase Contrast Microscope	Leica
KS 4000 i control Incubator	IKA
MACS MS columns	Miltenyi Biotech
MACS Pre-Separation Filter	Miltenyi Biotech
MilliQ water purification system	Millipore
Mr. Frosty™ Freezing Container	Thermo Fisher Scientific
Nano drop one	Thermo Fisher
Nano wizard 2	JPK instruments

Neubauer haemocytometer	Paul Marienfeld
Real-time PCR system 7500	Applied biosystems
Scanlaf Mars Laminar flow cabinet	Labogene
Serological pipettes	Sarstedt
Shaker	Edmund Bühler
Tissue culture dish (6-well and 24-well)	Techno Plastic Products
Tissue culture flasks (T75 and T25)	Sarstedt
Vortex Genie 2	Scientific industries
V-shaped cantilever (NPN-TR-TL-Au)	Bruker
Water bath	Lauda

**Table 4** List of software used for experimental work

<b>Software Name</b>	<b>Company</b>
7500 System software	Applied biosystems
BioRender	Y Combinator
BZ-800 analyser	Keyence
Citavi 6	Swiss Academic Software GmbH
EPSON Scan2 Version 6.4.94.0	Epson
FlowJo 10.8.1	LLC
Graph pad Prism 8.0.1	Dotmatics
ImageJ	NIH
JPK data processing 7.1.18	Bruker
Microsoft office	Microsoft

### 3.2.2. Reagents

**Table 5** List of chemicals and reagents used for the experimental work

Reagent	Company
Acetic acid	Merck
Bovine chondroitin sulphate-A	Sigma-Aldrich
Bovine serum Albumin (BSA)	CalBiochem
Chondroitinase ABC	Sigma-Aldrich
Chondroitin sulphate-A/C	Innovent e.V.
Citrate phosphate dextrose	Sigma-Aldrich
Cysteine hydrochloric acid	Sigma-Aldrich
EDTA Disodium salt	Sigma-Aldrich
Ethanol	Merck
Fluor mount-G Mounting Medium	Thermo Scientific
Heparinase I from Flavobacterium heparinum	Sigma-Aldrich
High molecular-weight hyaluronan	Innovent e.V.
Human serum albumin (HSA)	CSL Behring
Hyaluronan (10kda)	Lifecore Biomedical
Hyaluronan molecular weight ladders	Amsbio
Low molecular-weight hyaluronan	Innovent e.V.
Magnesium chloride (MgCl <sub>2</sub> )	Sigma-Aldrich
M-Bond-610 Adhesive	ME systems
Oil red O	Sigma-Aldrich
Pancoll human, Density: 1.077 g/ml	PAN-biotech
Papain from papaya latex	Sigma-Aldrich
Paraformaldehyde	Laborchemie Apolda GmbH
Pepsin from porcine gastric mucosa	Sigma-Aldrich
Porcine heparin	Sigma-Aldrich

Pyrogallol	Merck
RNAase inhibitor	Applied biosystems
Shark chondroitin sulphate-C	Sigma-Aldrich
Silica beads (Ø10 mm)	Kisker Biotech GmbH
Silver nitrate	Sigma-Aldrich
Sodium acetate	Sigma-Aldrich
Sodium phosphate dibasic	Sigma-Aldrich
Sodium phosphate monobasic	Sigma-Aldrich
Sodium thiosulfate	Merck
B-Mercaptoethanol	Sigma-Aldrich
Stains-all stain	Sigma-Aldrich
Tris hydrochloric acid	Sigma-Aldrich
Tris-acetate	Sigma-Aldrich
Triton-X 100	Carl Roth

**Table 6** List of reagents used in cell culture

Reagent/medium	Company
3-Isobutyl-1-methylxanthine (IBMX)	Sigma-Aldrich
5-Azacytidine (AZA)	Sigma-Aldrich
Ammonia solution	Merck
Ascorbic acid	Sigma-Aldrich
Cell Genix GMP SCGM	Cell Genix
Citrate-phosphate-dextrose solution	Sigma-Aldrich
CTS TrypLE select enzyme	Gibco
Dexamethasone	Sigma-Aldrich
Dimethyl sulfoxide (DMSO)	Sigma-Aldrich
DMEM Glutamax low glucose	Gibco

DNase-1	Sigma Aldrich
Fetal bovine Serum (FBS)	PAN-Biotech
Fibronectin human plasma 0,1 % solution	Sigma-Aldrich
FMS-like tyrosine kinase 3 ligand (FLT3-L)	Peprtech
HBSS, Calcium, Magnesium,	Gibco
Indomethacin	Sigma-Aldrich
Insulin (human)	Sigma-Aldrich
Interleukin 3 (IL-3)	Peprtech
MethoCult™ H4434 Classic	Stem cell technologies
Phosphate buffer saline (PBS)	Gibco
Stem cell factor (SCF)	Peprtech
Trypan blue	Gibco
β-Glycerophosphate	Sigma-Aldrich

**Table 7** List of cell culture and cryopreservation medium used in the experimental work

Medium	Component	Final Concentration
<b>MSC medium</b>	Dulbecco's modified Eagle's medium low glucose	1 X
	FBS	10%
<b>Osteogenic medium</b>	Dulbecco's modified Eagle's medium low glucose	1 X
	FBS	10%
	β-Glycerophosphate	20 mM
	Ascorbic acid	50 μM
	Dexamethasone	0.1 μM



<b>Adipogenic medium</b>		
	Dulbecco's modified Eagle's medium low glucose	1 X
	FBS	10%
	IBMX	500 $\mu$ M
	Indomethacin	100 mM
	Insulin	1 mg/ml
	Dexamethasone	1 $\mu$ M
<b>MSC cryopreservation medium</b>		
	HSA	2%
	DMSO	10%
	PBS	
<b>HSPC medium</b>		
	Cell Genix GMP SCGM	1 X
	FBS	2.50%
	SCF	2.5 ng/ml
	FLT-3L	2.5 ng/ml
	IL-3	2.5 ng/ml
<b>HSPC cryopreservation medium</b>		
	Cell Genix GMP SCGM	1 X
	FBS	50%
	DMSO	50%

**Table 8** List of buffers and solutions used for the experimental work

Buffer/solution	Chemical reagent	Final Concentration
<b>Pepsin buffer</b>		
	Acetic acid	0.5M
	Pepsin	0.1 mg/ml
<b>Sodium phosphate buffer (0.2M)</b>		
	Sodium acetate	0.1 M
	Na <sub>2</sub> EDTA	0.01 M
	Cysteine HCL	0.005 M
	PBS	
<b>Papain extraction reagent</b>		
	Sodium phosphate buffer	0.2 M
	Papain	0.1mg/ml
	ddH <sub>2</sub> O	
<b>TAE buffer</b>		
	Tris-acetate	0.04 M
	Na-EDTA	1 mM
	ddH <sub>2</sub> O	
<b>Stains-all reagent</b>		
	Stains-all stain	5 mg
	Ethanol	50%
<b>RLT buffer</b>		
	RLT	1ml
	B-Mercaptoethanol	10 µl

<b>Wash buffer</b>	BSA	0.50%
	Citrate phosphate dextrose	0.60%
	MgCl <sub>2</sub>	1 mM
	PBS	
<b>DNase buffer</b>		
	Wash buffer	1 X
	DNase I	10 µg/ml

**Table 9** List of commercial kits used for the experimental work

<b>Kit name</b>	<b>Company</b>
RNeasy Micro Kit	Qiagen
QuantiTect SYBR Green PCR Kit	Qiagen
High-Capacity cDNA Reverse Transcription Kit	Applied biosystems
Sircol™ - Soluble Collagen assay kit	Biocolor Life science assays
Blyscan™ - sulphated Glycosaminoglycan (sGAG) assay kit	Biocolor Life science assays
CD34 Micro Bead Kit, human	Miltenyi Biotech
Hyaluronan ELISA kit	R&D Systems

### 3.2.3. Antibodies

**Table 10** List of antibodies used for immunostaining.

<b>Antibody</b>	<b>Company</b>	<b>CatLog number</b>
Chondroitin Sulphate monoclonal antibody Cs56 Antibody produced in mouse	Sigma	C8035-100UL
Donkey anti goat Alexa Fluor plus 594	Invitrogen	A32758
Goat anti-Mouse IgG (H+L), Super clonal™ Recombinant Secondary Antibody, Alexa Fluor™ 488	Invitrogen	A28175

Goat Anti-Rabbit IgG H&L (Alexa Fluor® 594) pre-adsorbed	Abcam	ab150088
Goat Anti-Type IV Collagen-UNLB	Southern Biotech	SBA-1340-01
Mouse anti-Vinculin Monoclonal Antibody (VLN01)	Invitrogen	MA5-11690
Rabbit polyclonal anti-Collagen I antibody	Abcam	ab34710
Rabbit polyclonal anti-Fibronectin	Rockland	600-401-117

**Table 11** List of lectins used for histochemical-lectin staining

Lectins	Company	CatLog number
Lectin peanut agglutinin Alexa Fluor™ 488 Conjugate	Invitrogen	L21409
Lectin wheat germ agglutinin, Alexa Fluor™ 594 Conjugate	Invitrogen	W11262

**Table 12** List of antibodies used for flow cytometry

Antibody	Fluorophore	Company	Product number	Dilution	cell type
CD90	FITC	BD	561969	1:100	MSC
CD73	PE	BD	550257	1:50	MSC
CD105	APC	BD	562408	1:100	MSC
CD166	PE	BD	559263	1:50	MSC
PECD146	APC	Miltenyi Biotech	130-120-771	1:125	MSC
CD44	FITC	BD	560977	1:50	MSC/HSPC
CD34	APC	BD	345804	1:500	HSPC
CD117	APC Cy7	Bio legend	313227	1:100	HSPC
CD38	PerCP-Cy5.5	Bio legend	303522	1:50	HSPC
CD41	BV-421	Bio legend	303730	1:1000	HSPC
CD51	PE-cy 7	Bio legend	327915	1:100	HSPC
CD61	FITC	BD	347407	1:25	HSPC
CD29	PE-cy 7	Bio legend	303026	1:1000	HSPC

### 3.2.4. Primers

All the primer oligos were synthesised by Invitrogen, Germany. 100 µM primer stocks were prepared by re-suspending the oligos in nuclease free water and stored at -20 °C until further use.

**Table 13** List of primers and their respective sequences used for RT-qPCR

Target	Forward primer (5' -3')	Reverse Primer(5' -3')
Hyaluronan synthase 1 (hHAS1)	CGGAGATTCGGTGGACTACG	CCCAGGAGTCCAGAGGGTTA
Hyaluronan synthase 2 (hHAS2)	GTCGAGTTTACTTCCCGCCA	ATCACACCACCCAGGAGGAT
Hyaluronan synthase 3 (hHAS3)	GGTCATGTACACGGCCTTCA	CCAGGACTCGAAGCATCTCG
Carbohydrate sulfotransferase 11 (hCHST11)	ATGCGGAGGAATCCCTTT	GCAGGACAGCAGTGTGTTGAG
Chondroitin sulphate N-acetylgalactosaminyltransferase 1 (hCSGALNACT1)	CATGGCCAACACGCTTATCA	CTGAAGTTGGCAGCTTTGGAAG
Chondroitin sulphate synthase 1 (hCHSY1)	GCACGACCACTACTTGGACA	TCGCTGCTGTTCAAACCTCCT
Collagen I alpha 1 (hCOL1a1)	AGGCTGGTGTGATGGGATT	TCCAGCCTCTCCATCTTTGC
Collagen IV alpha 2 (hCOL4a2)	AGCCTGGATTGGTCGGTTT	AAGTCCTCTGTTGCCTTGCT
Collagen VII alpha 2 (hCOL7a1)	CCTTGCTGGAGACCTGGTG	CTCCTGGGTCACCCTTGAAA
Dermatan sulphate epimerase (hDSE)	GGAAACAACCTGGGTGCCTTG	GACCTCATCCAAGGAGCATC
Exostosin 1 (hEXT-1)	TGCCTGTCGTCGTCATTGAA	AGGCGAAATCCACCTCTGTT
Fibronectin (hFN1)	GGACATGCATTGCCTACTCG	TGGCATTGGTCGACGGGA
hIL18	TGCAGTCTACACAGCTTCGG	ACTGGTTCAGCAGCCATCTT
hIL1b	TGATGGCTTATTACAGTGGCA	GGTGGTCGGAGATTTCGTAGC
hIL6	TGGCAGAAAACAACCTGAACC	CCAGTGATGATTTTCACCAGGC
hNLRP3	CAAGCAAGATGCGGAAGCTC	GTCCTCCACCAGGTAGGACT
hS100A9	CGGCTTTGACAGAGTGCAAG	GCCCCAGCTTCACAGAGTAT
hSPARC	GAGGGCCTGGATCTTCTTTCT	TAGCTCCCACAGATACCTCAG
hU6	AACGCTTCACGAATTTGCGT	CTCGCTTCGGCAGCACA
Hyaluronidase 1 (hHYAL-1)	ACACGACAAACCACTTTCTGC	GCCCCAGTGTAGTGTCCATA

Tenascin-C (hTNC)	AACCAAAACCACACTCACAGGT CT	GGCTGGTCTCTGCAGTTTCA
-------------------	------------------------------	----------------------

### 3.3. Cell culture

#### 3.3.1. MSC isolation and cell culture

MSCs were isolated from the bone marrow aspirates as described by Oswald et al., 2004; Hempel et al., 2016<sup>116,146</sup>. Briefly, 5-7 ml of bone marrow aspirates were diluted at the ratio of 1:2 in 1 X PBS. The diluted aspirate was carefully layered over pancoll solution with the density of 1.077 g/ml (PAN-Biotech, Germany) at a ratio of 1:3 of pancoll and centrifuged at room temperature (RT) and 1400 rpm without break (acceleration: 9 and deceleration: 0). Mononuclear cells (MNCs) at the interface of the ficoll were aspirated and washed with 1 X PBS. MNCs were cultured in T25 culture flasks at the density of 1-3 x 10<sup>6</sup> in MSC medium (refer Table 7). Non-adherent cells were removed the next day via PBS wash. The medium was changed every 2-3 days until cells reached confluence. MSCs were selected for their plastic adherent property and characterised according to the criteria of the International Society for Cellular Therapy<sup>23</sup>. The cells were then cryopreserved at passage 0 or passage 1. The cells for the subsequent experiments were expanded in DMEM-low glucose (Gibco, Germany) with 10 % fetal bovine serum (FBS, PAN-Biotech, Germany) at 37 °C with 5 % CO<sub>2</sub> in a cell culture incubator. To investigate the impact of AZA treatment, the cells were cultured in MSC medium containing 10 µM AZA (Sigma, Germany).

#### 3.3.2. MSC passage, cryopreservation and thawing

MSCs at 90-100 % confluence were recovered via trypsination. When most cells detached from the plastic surface, the trypsin reaction was stopped by adding MSC medium and centrifuged at RT and 1200 rpm for 10 minutes. The pellet was re-suspended and cells were counted using a Neubauer haemocytometer and 4 % trypan blue solution (Gibco, Germany) using the formula:

$$\text{Cell count (x 10}^4 \text{ cell per ml)} = \left( \frac{\text{sum of cells counted in all squares}}{\text{number of squared counted}} \right) \times \text{dilution factor}$$

The cells were replated at a density of 1500-2000 cells/cm<sup>2</sup> or cryopreserved at a density of 1-5 x 10<sup>5</sup> cells/ml in MSC cryopreservation medium (refer Table 7) and stored in liquid nitrogen. When needed, one vial of cells was thawed in a 37 °C water bath for 2-3 minutes and diluted dropwise with MSC medium, followed by a PBS wash and plated into a T-25 flask.

### 3.3.3. Proliferation studies of MSCs

The proliferation of MSCs was observed by culturing them in a culture flask seeded at a density of 1500-2000 cells/cm<sup>2</sup> up to four passages. The cells were subcultured after they reached confluence. At the end of each passage, the viable cells were counted as described in 3.3.2. Expansion factor (referred as population doubling), absolute cell number, and fold change within one passage was calculated as follows:

***Expansion factor***

$$= \text{Total cell number at confluence} / \text{starting cell number at same passage}$$

***Absolute cell number***

$$= \text{Expansion factor} \times \text{total number of cells at end of previous passage}$$

$$\text{Fold change} = \log_{10} (\text{Absolute cell number at a given passage} \\ / \text{starting cell number at the first passage})$$

### 3.3.4. Analysis of osteogenic differentiation and Von kossa staining of MSCs

MSCs from MDS patients and healthy donors were analysed for their ability to differentiate into osteoblasts. The cells were seeded at a density of 1 x 10<sup>3</sup> cells per cm<sup>2</sup> and cultured at 37 °C with 5 % CO<sub>2</sub>. After 24 hours, the medium was replaced by MSC medium supplemented with 10 μM AZA (Sigma). After 3-4 days, the medium was replaced with osteogenic medium (refer Table 7). The cells were cultured for 21 days with medium change every 2-3 days. The calcium deposition was observed using Von kossa staining. Briefly, the medium was discarded and the cell layer was washed with PBS, and fixed with 4 % paraformaldehyde (Sigma, Germany). The monolayer was stained with 2 % (w/v) of silver nitrate (Sigma, Germany) for 15-30 minutes. 2 mg/ml Pyrogallol (Merck, Germany) was used as a developer and fixed using 300 mM of sodium thiosulfate (Merck) at RT. 12 images per sample were taken using a Keyence BZ-X810 microscope. Calcium deposition was quantified using ImageJ (NIH). Each Image for a given sample was scored based on the percentage of area stained and subsequently the mean score for each sample was calculated.

### 3.3.5. Analysis of adipogenic differentiation and Oil Red-O staining of MSCs

MSCs from MDS patients and healthy donors were analysed for their adipogenic differentiation potential after treatment with AZA. The cells were seeded and cultured for 3-4 days with or without AZA as described in 3.3.4. After 3-4 days, the medium was replaced with an adipogenic medium (refer Table 7) and cultured for 14 to 21 days. Oil droplets were stained using Oil Red-O staining. Briefly, the

medium was discarded and washed with PBS, and fixed with 4 % paraformaldehyde. The monolayer was stained with 2 mg/ml of Oil Red-O (Sigma, Germany) in ethanol (Merck, Germany) for 15 minutes at RT. The monolayer was washed with PBS three times and 12 images per sample were taken using a Keyence BZ-X810 microscope and quantified by ImageJ (NIH). Each image for a given sample was scored based on the percentage of cells stained and subsequently the mean score for each sample was calculated.

### 3.3.6. Generation of ECM from MSCs

MSCs were used in the second to fourth passage for all experiments. To yield cell-free ECM substrates, MSCs were seeded on poly-octadecene-alt-maleic anhydride (POMA) and 5  $\mu\text{g}/\text{cm}^2$  fibronectin (Sigma, Germany) coated glass cover slides as described previously<sup>147</sup>. Dr. Valentina Magno from the Leibniz Institute of Polymer Research Dresden, TU Dresden, Dresden, Germany, provided the POMA coated cover slides of diameter 32 mm and 13 mm for 6 well and 24 well plates, respectively. The MSCs were cultured for 10 days at 37 °C with 5 % CO<sub>2</sub> in the MSC medium. Medium change was performed every 2-3 days. For *in vitro* AZA treatment condition, after 24 hours of seeding, 10  $\mu\text{M}$  AZA was added to MSC medium. This was used for every subsequent medium change. Decellularization was performed on day 10 using an aqueous solution of 20 mM NH<sub>4</sub>OH (Merck, Germany), and DNA residues were removed by incubating the samples with DNase I (Merck, Germany) as indicated in Figure 5. Samples were washed in PBS and stored in Hank's balanced salt solution (HBSS) with calcium and magnesium (Merck, Germany) at 4 °C until further use for no more than a month.

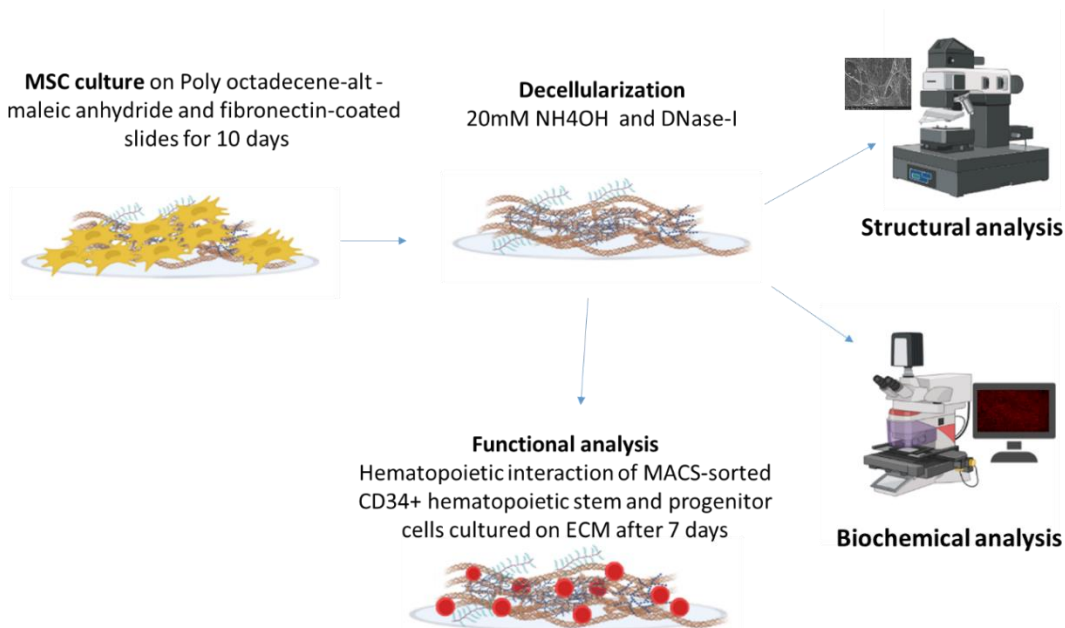


**Figure 5 Schematic diagram of the ECM generation and work plan for characterisation of the ECM substrates.** The image was created with BioRender.com<sup>4</sup>.



### 3.3.7. Isolation, cryopreservation and thawing of CD34+ HSPC.

HSPCs were isolated from granulocyte colony-stimulating factor (G-CSF)-mobilized peripheral blood (leukapheresis) from healthy donors, collected at the Bone marrow transplantation centre of the Carl Gustav Carus University Hospital, TU Dresden. Informed written consent was given by the donors and the study was approved by the local ethics committee (ethical approval no. EK 307082018). The cells were purified by immunogenic sorting using CD34 Microbeads Kit Ultrapure (Miltenyi Biotech, Germany) following the manufacturer's instructions (Figure 6). Briefly, a small volume of the leukapheresis preparations (1-2 ml) was diluted in 8-10 ml PBS and centrifuged at RT and 300 x g for 10 minutes. The pellet, with up to  $2 \times 10^8$  cells, was re-suspended in 300  $\mu$ l of DNase buffer (refer Table 8). The cells were incubated at 4 °C for 30 minutes with 100  $\mu$ l of human FcR blocking reagent to avoid unspecific binding of the beads to the Fc receptors and 100 $\mu$ l of anti-human CD34 microbeads for binding of anti-CD34 antibodies coupled to 50 nm sized magnetic beads to the CD34 antigen receptor. The samples were washed with DNase buffer and then separated by passing it through the MACS column attached to a magnetic platform. The cells in the MACS column were washed three times with 1 ml wash buffer (refer Table 8). After the removal of the MACS column from the magnetic field, the CD34+ cells were flushed out with wash buffer. The cells were washed with 1 X PBS and counted in a similar manner as in 3.3.2. The cells were cryopreserved in aliquots of  $1-4 \times 10^5$  cells/ml in HSPC cryopreservation medium (refer Table 7) until further use. The cells were thawed at 37 °C water bath for 2-3 minutes and diluted dropwise to HSPC medium (refer Table 7) and incubated at 37 °C for 30 minutes (to avoid clumps) followed by a PBS wash. The purity of isolated HSPCs was analysed by CD45, CD34, and CD38 marker expression using flow cytometry. The cells with >95 % purity for CD34 expression were used for further experiments.

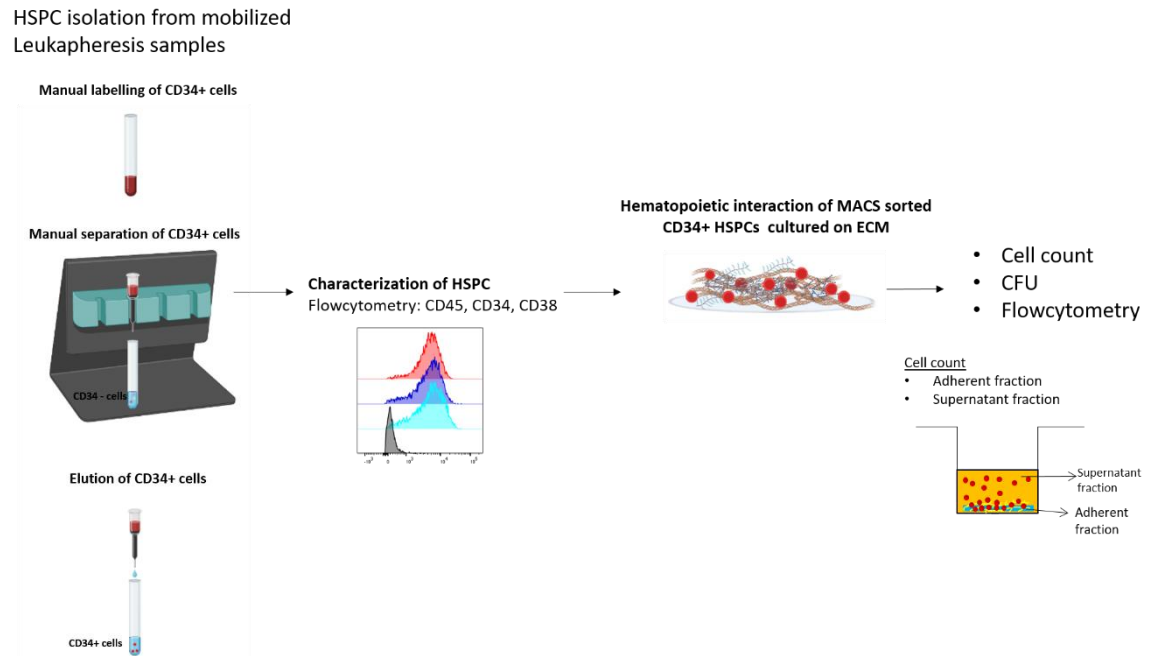


**Figure 6** Schematic diagram of the immunogenic sorting of CD34+ cells from leukapheresis samples and its subsequent culture on the ECM substrates. After 7 days of culture, the HSPCs in the supernatant fraction were counted and subjected to CFU assay and flow cytometry analysis. The image was created with BioRender.com<sup>4</sup>.

### 3.3.8. Cell culture and proliferation of HSPCs on different ECM

Isolated HSPCs from 3-4 donor samples were thawed and pooled for each experiment. Cells were counted in a similar manner as in 3.3.2 and seeded on different ECM with a density of  $1 \times 10^4$  cells per  $\text{cm}^2$  in HSPC medium as mentioned in 3.3.7. The cells were cultured at  $37^\circ\text{C}$  with  $5\% \text{CO}_2$  for 7 days without medium change. After 7 days, the cells in the supernatant and adherent layers were counted. For the supernatant fractions, the cells in the medium that were not attached to the ECM were used (refer to Figure 6). For the adherent fraction, the cells attached to the ECM were recovered by PBS washed and mechanical disruption of the ECM using a pipette. The cells recovered from different fractions were centrifuged at 1200 rpm for 5 mins. The pellet was re-suspended in  $100 \mu\text{l}$  of PBS and counted. Each fraction was analysed for cell surface markers using flow cytometry.  $10 \mu\text{l}$  of cell suspension from each fraction for a sample was pooled and counted for CFU assay.

To investigate the growth factor presentation of the ECM substrates. Different ECM substrates were pre-incubated overnight in HSPC medium with or without growth factors at  $37^\circ\text{C}$  with  $5\% \text{CO}_2$ . On the next day, the ECM was washed once with PBS and seeded with HSPCs with a density of  $1 \times 10^4$  cells per  $\text{cm}^2$  in HSPC medium without growth factors. As controls, ECM substrates with overnight pre-incubation with HSPC medium without FBS and growth factors were used. Furthermore, for the controls HSPCs were cultured in either HSPC medium with or without growth factors containing

medium on the ECM without pre-incubation. The cells were incubated at 37 °C with 5 % CO<sub>2</sub> for 7 days without medium change. The cells were processed as mentioned above for CFU assay.

### **3.3.9. CFU assay**

CFU assays were carried out using CD34+ HSPCs harvested after 7 days of culture on different ECM samples, 300 cells were plated in MethoCult™ H4434 Classic (Stem cell technologies, Germany). Colonies were counted after 2 weeks and classified into CFU-Granulocyte, erythroid, macrophage and megakaryocyte (CFU-GEMM), CFU-granulocyte and macrophage (CFU-GM), and CFU-erythroid (CFU-E) based on presence or absence of hemoglobinized cells.

### **3.3.10. Cell surface marker detection by flow cytometry**

MSCs and HSPCs were analysed for different cell surface markers using flow cytometry. The harvested cells were washed with PBS before staining. All the antibody cocktails (refer to Table 12) were diluted in 2 % BSA/PBS solution to avoid unspecific binding of antibodies to the Fc receptor. 50 µl of antibody cocktail was added to the cells and incubated at RT for 15 minutes in the dark. The cells are washed with 2 % BSA/PBS solution and re-suspended in 100 µl of 2 % BSA/PBS and stored at 4 °C until measured using FACS verse flow cytometer (BD biosciences). The data was analysed using FlowJo 10.8.1 (LLC) software.

### **3.3.11. LMW-HA stimulation of MNCs**

Healthy bone marrow MNCs were isolated as mentioned in 3.3.1. MNCs (5x10<sup>6</sup> cells/ml) were stimulated with 10 µg/ml of LMW-HA of size 10-20 kDa (Life core Biomedical, USA) for 24 hours in HSPC medium. Unstimulated cells were used as a control. mRNA was isolated using an RNeasy micro kit (Qiagen, Germany). The mRNA expression of different inflammatory genes relevant to MDS such as *hIL6*, *hIL1B*, *hIL18*, *hNLRP3*, *hPYCARD*, and *hS100A9* (refer Table 13 for the primer sequences) was analysed by real time semi-quantitative PCR (RT-qPCR).

## **3.4. Biophysical analysis**

### **3.4.1. Atomic force microscopy (AFM)**

AFM measurements were performed using Nano Wizard 2 AFM (JPK instruments) mounted on an inverted optical microscope (Leica, Germany). Young's modulus was measured using 200 µm long, V-shaped cantilever (NPN-TR-TL-Au, Bruker) with a nominal spring constant of 80 mN/m. The cantilevers were modified with silica beads (Ø10 nm, Kisker Biotech GmbH, Germany). Briefly, the

beads were attached to the cantilevers using M-Bond-610 Adhesive (ME systems, Germany) and cured overnight at 85 °C. The cantilevers were then stored at RT until further use. Each cantilever was calibrated using thermal noise spectrum and Lorentz function (JPK SPM software). Force-distance curves were acquired in closed loop, constant height mode using 3 nN contact force and 5  $\mu\text{m s}^{-1}$  approach/retract velocity. Each data set was generated by probing a minimum of 45 different spots on each sample. The data processing software provided by the AFM manufacturer (JPK Instruments) was used to extract the elastic modulus from approach force-distance curves.

### **3.5. Biochemical analysis**

#### **3.5.1. Quantification of total collagen**

Total collagens in the different ECMs were quantified using Sircol assay (Biocolors, UK) according to manufacturer's instructions. Briefly, the ECMs were subjected to pepsin treatment (refer Table 8 for the pepsin solution) at 4 °C overnight to release the terminal non-helical collagen telopeptides into the solution. The collagens in the solution were concentrated at 4 °C overnight by first neutralising the pepsin solution using neutralization buffer containing NaOH in Tris HCL solution followed by addition of concentration reagent containing polyethylene glycol in Tris HCL at a pH of 7.6. Later, the collagen pellet was obtained by centrifugation at 12,000 rpm and 4 °C for 10 minutes. The centrifuged pellet was incubated in Sircol dye reagent containing Sirius red in Picric acid for 30 minutes on a shaker to aid the formation of collagen-dye complex. This complex was precipitated by centrifugation at 12,000 rpm, RT, for 10 minutes. The collagen pellet was washed with ice-cold acid salt wash containing acetic acid and NaCl. The bound dye was released using alkali reagent containing 0.5 M NaOH. The released dye solution was measured at the absorbance of 540 nm using a Biotek 800™ TS Absorbance Reader (Biotek, Germany). Sample concentration was obtained from a collagen standard curve generated from a collagen Type I solution provided by the manufacturer.

#### **3.5.2. Quantification of sulphated GAGs by Blyscan assay**

The sulphated GAGs (sGAGs) in the ECM substrates was measured using a blyscan assay kit (Biocolors, UK). Briefly, sGAGs were extracted using papain extraction reagent (refer Table 8) at 65 °C for 3 hours to release the GAGs into the supernatant. Blyscan reagent containing 1, 9-dimethyl-methylene blue was added to 100  $\mu\text{l}$  of the sample and was incubated at RT for 30 minutes, to allow the formation of the sGAG-dye-complex. The complex was pelleted, and the dye was eluted by adding a sodium salt of an anionic surfactant. The eluted dye was measured spectrophotometrically at 660 nm in duplicates using Biotek 800™ TS Absorbance Reader. Total sGAG content was later calculated using a calibration curve of the known concentration of sGAGs supplied by the manufacturer.

### 3.5.3. Immunostaining

Rabbit anti-human Collagen I antibody (Abcam, Germany), and a rabbit anti human fibronectin antibody (Rockland) together with goat anti-rabbit Alexa Fluor™ 594 (Abcam, Germany) secondary antibody were used to detect collagen I and fibronectin respectively. Goat anti-human collagen IV antibody (Southern Biotech, Germany) together with donkey anti-goat Alexa Fluor™ 594 (Invitrogen, Germany) was used to detect collagen IV. Mouse anti-human CS antibody (Sigma-Aldrich, Germany) together with goat anti-mouse Alexa Fluor™ 488 (Thermo-Fisher, Germany) secondary antibody was used to detect CS deposition. Briefly, The ECM substrates were fixed in 4 % paraformaldehyde (Sigma) for 15 minutes and blocked using 2 % BSA/PBS (Merck) for 1 hour at RT. The substrates were incubated with the aforementioned primary antibodies overnight at 4 °C followed by two PBS washes. Later the ECMs were incubated with the respective secondary antibodies for 1 hour at RT. The stained substrates were mounted using fluorescence mounting medium and stored in the dark until imaging. The substrates were imaged using a Keyence BZ-X810 microscope and fluorescence intensity was measured using ImageJ (NIH).

HSPCs on different ECMs were stained using mouse anti-human vinculin antibody (Invitrogen, Germany), goat anti-mouse Alexa Fluor™ 488 secondary antibody, and DAPI. The cells were fixed in 4 % paraformaldehyde (Sigma) for 15 minutes, permeabilized using PBS containing 0.1 % Triton X 100 for 15 minutes, and blocked using 2 % BSA/PBS (Merck) for 1 hour at RT. The cells were then incubated with primary antibody overnight at 4 °C followed by incubation with the secondary antibody and DAPI for 1 hour at RT. The stained substrates were mounted using fluorescence mounting medium and stored in the dark until imaging.

### 3.5.4. Lectin staining

Lectin peanut agglutinin Alexa Fluor™ 488 Conjugate (Invitrogen, Germany), and Lectin wheat germ agglutinin, Alexa Fluor™ 594 Conjugate (Invitrogen, Germany) were used to stain N-acetyl-galactosamine GAGs and N-acetyl-glucosamine GAGs respectively. The ECM substrates were fixed in 4 % paraformaldehyde (Sigma) for 15 minutes and blocked using 2 % BSA/PBS (Merck) for 1 hour at RT. The substrates were incubated with lectins conjugated with fluorophores for 1 hour at RT. The stained substrates were mounted using fluorescence mounting medium and stored in dark until imaging. The substrates were imaged using a Keyence BZ-X810 microscope and fluorescence intensity was measured using ImageJ (NIH).

### 3.5.5. Separation and visualization of ECM GAGs

Cells were cultivated on POMA-fibronectin-coated glass cover slides in 6-well plates for three weeks prior to decellularization with 20 mM ammonia and DNase I treatment as described in 3.3.6. Separation and visualization of ECM GAGs was performed by Dr. Sandra Rother and Dr Toni Radanovic from Centre for Molecular Signalling, Saarland University School of Medicine, Saarland, Germany. GAGs in the different ECM were extracted as described previously<sup>148</sup>. 5 µl hyaluronan molecular weight ladders (Amsbio) and 3-6 µg of commercially available GAGs: Low- and high-molecular-weight (LMW-HA, HMW-HA) and CS-A/C mixture (Innovent e.V., Germany), porcine heparin, bovine CS-A and CS-C shark (all from Sigma-Aldrich, Germany) were used as controls. Before the sample run, the agarose gel was pre-run for 6 hours at 80 V in the TAE buffer (refer Table 8). The gel run, separating the ECM GAGs was performed at 100 V for 3 hours. The GAGs were stained overnight with “Stains-all” reagent in the dark. The gel was washed with water before de-staining by exposing it to light until the background staining is reduced. The gel was imaged using an EPSON Perfection V750 Pro scanner and analysed by EPSON Scan2 Version 6.4.94.0 software (Both from Epson, Germany).

### 3.5.6. Quantification of HA in the ECM substrates

Cells were cultivated on POMA-fibronectin-coated glass cover slides described in 3.5.5. Quantification of HA in the ECM substrates was performed by Dr. Sandra Rother and Dr. Toni Radanovic from Centre for Molecular Signalling, Saarland University School of Medicine, Saarland, Germany. The dried ECMs were enzymatically degraded by overnight incubation with papain (1 mg/ml) in PBS at 60 °C. The amounts of hyaluronan in the cell-derived ECMs were quantified by sandwich enzyme-linked immunosorbent assay (ELISA) following the manufacturer’s instructions (R&D Systems).

## 3.6. Molecular biology

### 3.6.1. Cell Lysis and RNA isolation

Total RNA was isolated from MSCs after 10 days of culture on a plastic culture dish as well as from 24 hours stimulated MNCs using RNeasy micro Kit (Qiagen, Germany) according to the manufacturer’s instructions. Briefly, the cells on the plastic culture dish were lysed using an RLT buffer supplemented with B-Mercaptoethanol. The lysate was homogenized using a QIA shredder spin column (Qiagen, Germany) by centrifugation at full speed for 2 minutes. RNA was precipitated by adding equal volumes of 70 % ethanol. The RNA was precipitated using an RNeasy MinElute® spin column centrifuged at 11,000 rpm, for 30 seconds at RT followed by a DNase I treatment (Sigma Aldrich) for 15 minutes at RT to degrade any DNA present on the column. The DNA-free column containing RNA was washed and

precipitated once again using RPE buffer and 80 % ethanol. The RNA was eluted in RNase-free water by centrifugation at 11,000 rpm, for 1 minute. The total RNA concentration is measured using Nano drop one (Thermo Fisher Scientific, Germany).

### 3.6.2. Reverse transcription

mRNA was reverse transcribed to cDNA using the High-Capacity cDNA Reverse Transcription Kit (Applied Bio systems, Germany) according to the manufacturer's instructions. For each reverse transcription reaction, 1 µg of total purified RNA was used. A 2 X master mix was prepared (Table 14) and 1 µg of RNA was added to get a final concentration of 1 X master mix. The samples were then mixed adequately and the reaction was set up in accordance with the manufacturer's instructions (Table 15).

**Table 14** Composition of standard reaction master mix for reverse transcription of RNA samples

Component	Volume
H2O, PCR grade	3.2 µl
RT Buffer	2.0 µl
dNTP Mix (100mM)	0.8 µl
RT Random Primers	2.0 µl
RNase Inhibitor	1.0 µl
MultiScribe Reverse Transcriptase	1.0 µl
Volume per tube	10.0 µl
DNase free RNA (1 µg)	10.0 µl
total Volume	20.0 µl

**Table 15** Amplification program for reverse transcription of RNA samples

Temperature	Time (minutes)
25 °C	10:00
37 °C	120:00
85 °C	05:00
4 °C	HOLD

### 3.6.3. RT-qPCR analysis

Relative expression of specific transcripts was analysed by RT-qPCR using QuantiTect SYBR Green PCR Kit (Qiagen, Germany) according to the manufacturer's instructions (refer Table 16 for amplification program information) on Real-time PCR system 7500 (Agilent Bio systems). For each reaction 10  $\mu$ M working concentration of forward and reverse primers were used.

**Table 16** Amplification program for cDNA during RT-qPCR

	Temperature	Time			
<b>Stage 1</b>	95 °C	15 minutes			
<b>Stage 2</b>	95 °C	15 seconds			
	60 °C	30 seconds	45x	Data collection	
	72 °C	30 seconds			
<b>Stage 3</b>	95°C	15 minutes			
	60 °C	30 minutes		Data collection	
	95 °C	15 minutes			

The staining dye intercalates with the double stranded cDNA resulting in the DNA-SYBR green complex, which is detected by the laser at 494 nm. This signal is directly proportional to the amount of dsDNA i.e. the amplified transcripts. CT ( $\Delta\Delta$ CT) method was used to quantify the relative expression to the control. Briefly, a CT value is calculated based on a minimum signal above a threshold. The CT values were normalized against U6 snRNA as the "housekeeping gene". Relative expression to the control was calculated as

$$\Delta CT = CT \text{ target gene} - CT \text{ housekeeper gene}$$

$$\Delta\Delta CT = \Delta CT_{\text{sample}} - \Delta CT_{\text{Control}}$$

### 3.6.4. Next generation sequencing and analysis of mRNA

Dr Knut Krohn at the Core unit DNA Technologies, Sächsischer Inkubator für klinische Translation (SIKT), Leipzig, Germany performed the next generation sequencing of mRNA. The mRNA from different MSCs was sequenced using transposon-based RNA-Seq with NEB depletion. Sequencing of 2 x 150 bp was performed with a NovaSeq sequencer (Illumina) according to the instructions of the manufacturer. De-multiplexing of raw reads, adapter trimming, and quality filtering were done as



described previously<sup>149</sup>. Reads were mapped against the human reference genome (hg38) using HISAT2<sup>150</sup>. Stringtie and the R package Ballgown were employed to calculate differential expression<sup>151</sup>. Expression data were normalized using the DESeq2 R Bioconductor package<sup>152</sup>.

Nora Grieb at Department of Haematology and Cell Therapy, Faculty of Medicine, University of Leipzig, Leipzig, Germany performed the further analysis of the expression data. All the mRNA transcripts differentially regulated between the healthy and MDS MSCs with a p-value below 0.1 were used for further analysis. Gene set enrichment analysis (GSEA) was the differentially regulated targets was analysed by R Bioconductor cluster profiler<sup>153</sup>. Go enrichment analysis was performed using gseGo and visualized by dotplot function.

### **3.7. Statistical analysis**

Statistical analysis was performed using Graph Pad Prism software version 8.01. (Graph Pad Software). Data is presented as mean  $\pm$  standard deviation (SD). For relative quantification measurements, one sample t-test and unpaired t-test were performed. For multiple group comparisons, ANOVA followed by Tukey' or Sidak's posthoc test was performed. A p-value of less than 0.05 was regarded as being statistically significant with \*p< 0.05, \*\*p< 0.01, \*\*\*p< 0.001, \*\*\*\*p< 0.0001. Statistical analysis for GSEA analysis was performed using Fisher exact test with elimination algorithm and p-adjust values were calculated using Benjamini-Hochberg corrections, p-adjust value of less than 0.1 was regarded as significant.

## 4. Results

### 4.1. The biophysical and biochemical composition of MSC-derived ECM is altered in MDS

#### 4.1.1. MSC from healthy donor and MDS bone marrow have similar phenotypes

Bone marrow MSCs from healthy donors, LR- and HR-MDS MSCs were analysed for their proliferation in culture, cell surface markers and potential for adipogenic and osteogenic differentiation. Structurally, the MSCs from all the groups had comparable fibroid morphologies. However, the HR-MDS MSCs generated a more disordered monolayer structure evident under bright field microscopy (Figure 7A). Trypan blue counting revealed no significant differences in the proliferation rate and doubling time between MSC groups (Figure 7B, C). Moreover, the expression of MSC surface markers such as CD73, CD90, CD105, CD44, CD166 and CD146 (see annex I for the gating strategy) was comparable between healthy and MDS MSCs (Figure 7D).

The adipogenic and osteogenic differentiation potential of MSCs showed a high degree of inter-individual variability (Figure 7E, F), with a tendency for individual samples to be biased towards one or the other lineage and a marked adipogenic differentiation in some of the LR-MDS samples that did not, however, reach significance (Figure 7E).

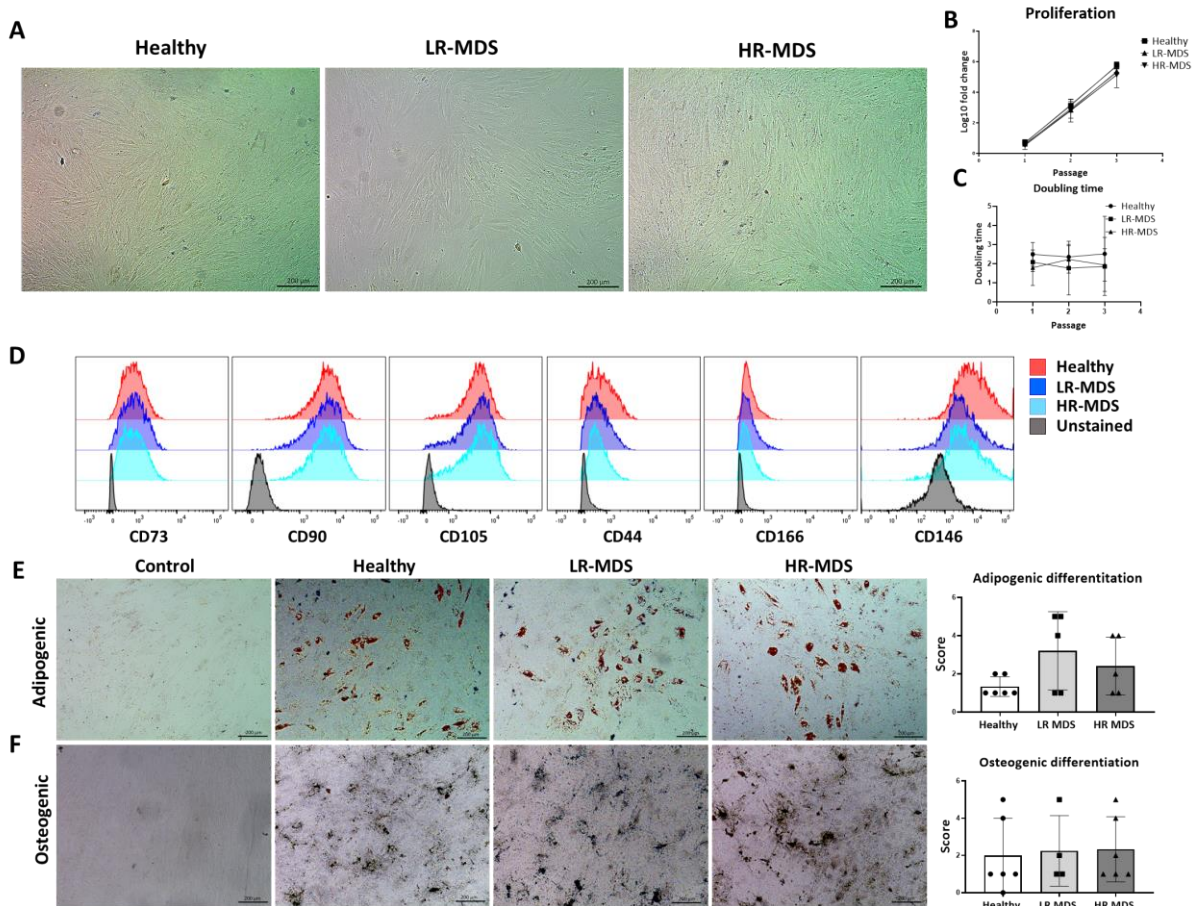


**Figure 7 MSCs from healthy donor and MDS patient bone marrow have similar characteristics.** A) Representative bright field images of MSC morphology from healthy donor, LR- and HR-MDS patients in culture. B) Cell counts represented as log<sub>10</sub> fold change from the starting number and C) Doubling time of MSCs determined by trypan-blue staining at indicated passages. Values represent mean  $\pm$  SD of  $n = 6$  for healthy donor MSCs and  $n = 5$  for each LR- and HR-MDS MSCs. D) Flow cytometry analysis of MSC surface markers before the start of ECM generation. E, F) Left: Representative images of the staining of MSCs with Oil Red O and Van kossa stains for adipogenic and osteogenic differentiation respectively. Right: Quantification of the differentiation staining of the MSCs using ImageJ. Bars represent mean  $\pm$  SD in triplicate of  $n = 6$  for healthy donor MSCs and  $n = 5$  for each LR- and HR-MDS MSCs.

#### 4.1.2. The biophysical properties of bone marrow MSC-derived ECM differ between MDS patient and healthy donors

The biophysical properties of the *in vitro* generated ECMs produced by healthy donor and MDS patient MSCs were analysed with regard to structure, deposition pattern and rigidity. Both LR- and HR-MDS MSCs deposited an ECM that appeared in bright field microscopy to be more dense and compact than that of healthy donor MSCs (Figure 8A). The rigidity (young's modulus) of ECM from each source was analysed using atomic force microscopy by Dr Jens Friedrichs at the Leibniz Institute of Polymer Research Dresden, Germany. This revealed a progressive reduction in rigidity from nearly 2 kPa in healthy donor to 1.3 kPa in LR-MDS to under 1 kPa in HR-MDS-MSC derived ECM (Figure 8B).

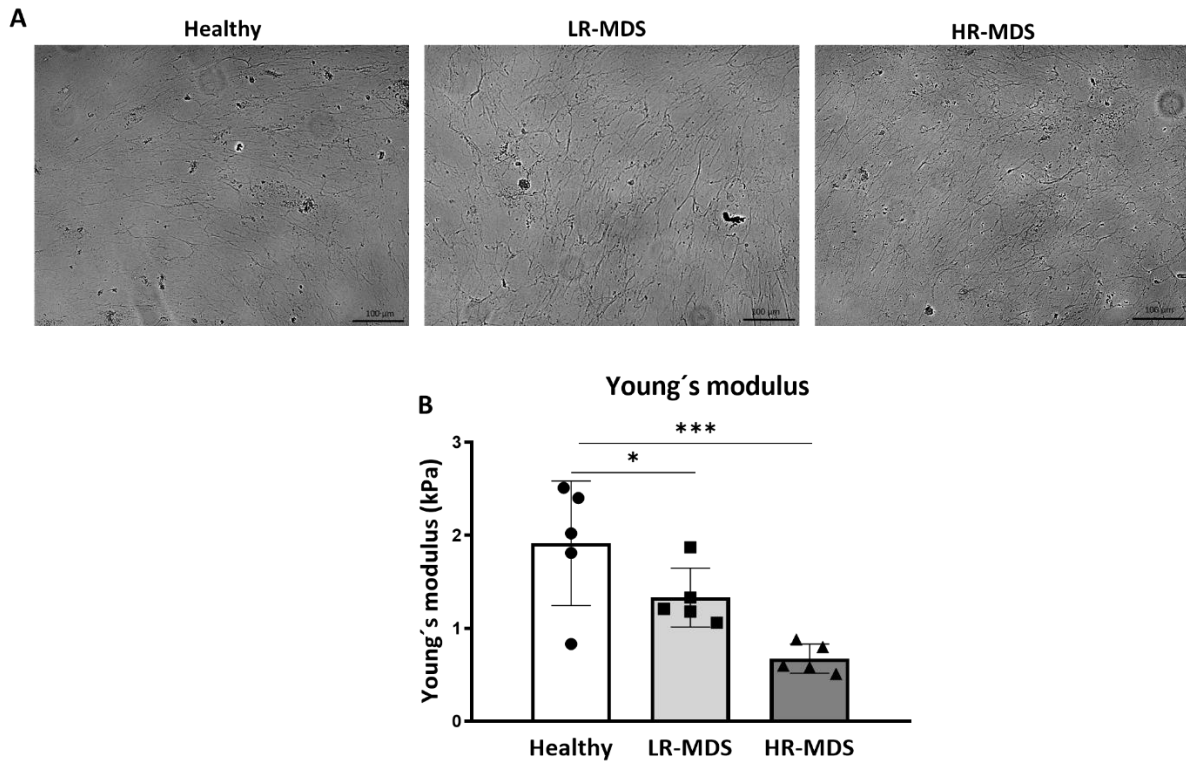


**Figure 8** The biophysical properties of the ECM derived from healthy donor vs MDS MSCs. A) Representative phase contrast images of the ECM from healthy donor, LR- and HR-MDS MSCs. B) Elastic modulus measurements of the ECM from healthy donor, LR- and HR-MDS MSC analysed by AFM. Bars represent mean  $\pm$  SD in duplicates for  $n = 5$  samples per group. \* $p < 0.05$ , \*\*\* $p < 0.001$ .

#### 4.1.3. Fibronectin deposition in the ECM is unchanged in MDS versus healthy donor derived MSC

As a first step towards biochemical analysis of the matrices, fibronectin deposition was detected immunohistochemically using a rabbit polyclonal anti human antibody. The fibrous fibronectin deposited by the MSCs could be clearly distinguished from that originally used to coat the POMA slides, which appears as a diffuse and relatively uniform layer below the ECM. Densitometry revealed no significant difference in the overall levels of fibronectin deposited by healthy donor, LR- and HR-MDS MSCs (Figure 9). However, the pattern of deposition was altered, being more dense and compact in the matrices from MDS MSCs (Figure 9), consistent with the bright field observations of the ECM shown above (Figure 8).

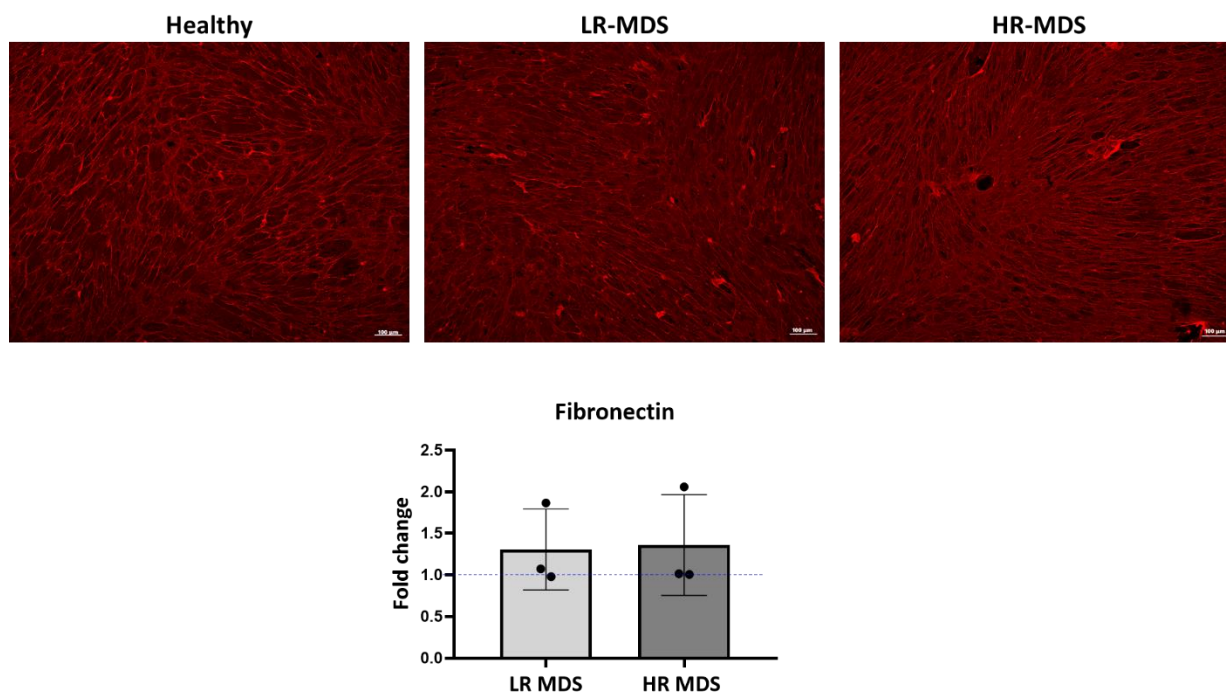


**Figure 9 Fibronectin levels are unchanged in MDS vs healthy donor MSC-derived ECM.** Top: Representative images of ECM samples immunostained for fibronectin. Bottom: Semi-quantitative analysis of relative fluorescence intensity in the immunofluorescence images by ImageJ analysis. Bars represent mean  $\pm$  SD of  $n = 3$  MDS samples, each measured in an independent experiment and expressed as fold change relative to the accompanying healthy MSC ECM control, shown by the dotted line with the ordinate value of 1.

#### 4.1.4. MDS MSCs deposit high levels of collagens

Total collagen content in the MSC-derived ECM from each source was quantified by the Sirius red binding (Sircol) assay. MDS MSCs were found to deposit higher levels of collagens when compared to healthy donor MSCs (Figure 10A). The collagen content of the ECM increased progressively from  $0.08 \mu\text{g}/\text{cm}^2$  in healthy donor to  $0.11 \mu\text{g}/\text{cm}^2$  in LR-MDS and to  $0.16 \mu\text{g}/\text{cm}^2$  in HR-MDS derived samples, in which the difference to healthy donor levels reached significance (Figure 10A). Two of the most abundant collagens: collagen I and IV were semi-quantified using an immunostaining approach. This showed MDS MSCs (both LR-and HR-MDS) to deposit around twice the amount of collagen I than healthy donor MSCs, consistent with the increase in total collagens described above (Figure 10B). Moreover, MDS MSCs also deposited significantly higher amounts of collagen IV (Figure 10C), the levels in ECM from LR-MDS and HR-MDS MSC being 3 fold higher and 2 fold higher respectively than in ECM produced by healthy donor MSCs. Indeed, both collagens I and IV were most prominent in LR-MDS derived ECM and somewhat lower in that from HR-MDS (Figure 10B, C), suggesting that the higher overall collagen content of ECM from HR-MDS is probably due to an increase in other collagens in the ECM. More accurate quantification by dot blot analysis was attempted but was unfortunately unsuccessful due to the low amounts of protein available.

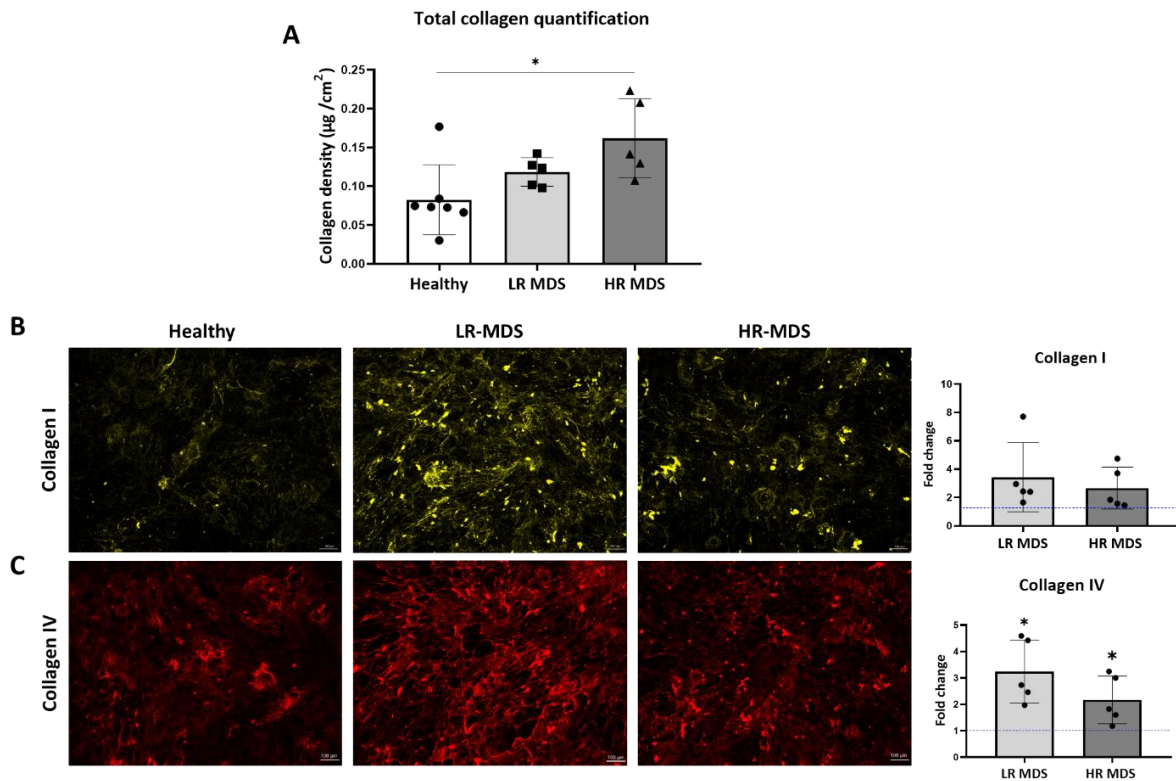


**Figure 10 MDS-associated changes in the collagen content of MSC-derived ECM.** A) Total collagen quantification of the ECM from healthy donor, LR-MDS and HR-MDS MSC. Bars represent mean  $\pm$  SD of  $n = 7$  healthy donor MSCs and  $n = 5$  for each of the LR- and HR-MDS MSC samples. B, C) Left: Representative images of collagen I (yellow) and collagen IV (red) immunostaining respectively. Right: Bars represent mean  $\pm$  SD of  $n = 5$  for each LR- and HR-MDS MSC samples, each measured in an independent experiment and expressed as fold change relative to the accompanying healthy MSC ECM control, shown by the dotted line with the ordinate value of 1. An asterisk above the bar indicates significant differences to the control:  $*p < 0.05$ .

#### 4.1.5. MDS MSC-derived ECM has an altered GAG profile

GAGs commonly constitute a major component of the ECM and were assessed first using the Blyscan assay that stains all the sulphated GAGs. This revealed no marked difference between the ECM produced by MSCs from MDS and those from healthy donor marrow (Figure 11A), although there was a slight tendency towards higher levels in LR-MDS. In order to analyse the content of individual GAGs at higher resolution, fluorophore-conjugated lectins specific for either N-acetyl-glucosamine and sialic acid (wheat germ agglutinin) or N-acetyl-galactosamine and terminal  $\beta$ -galactose (peanut agglutinin) groups were used. N-acetyl-glucosamine residues are present in HA, HS and KS, while N-acetyl-galactosamine or terminal  $\beta$ -galactose is found in CS, DS and KS. The specificity of lectin binding was confirmed by pre-digestion of GAGs with heparinase and chondroitinase ABC (Annex III).

Wheat Germ agglutinin staining identified an accumulation of N-acetyl-glucosamine groups in MDS MSCs-derived ECM, with a significant two-fold increase in LR-MDS MSC-derived ECM over that of healthy donor MSC-derived ECM (Figure 11B). This increase was specific for LR-MDS, since MSCs from

HR-MDS deposited levels of these GAGs similar to those from healthy donors (Figure 11B). Peanut agglutinin staining also revealed disease stage specific changes in N-acetyl-galactosamine containing GAGs content between the MDS subtypes. Here, too, LR-MDS MSCs deposited two-fold higher amounts of N-acetyl-galactosamine containing GAGs when compared to the healthy donor MSCs. However, HR-MDS MSCs deposited far lower amounts of these GAGs compared to both healthy donor and LR-MDS MSCs (Figure 11C).

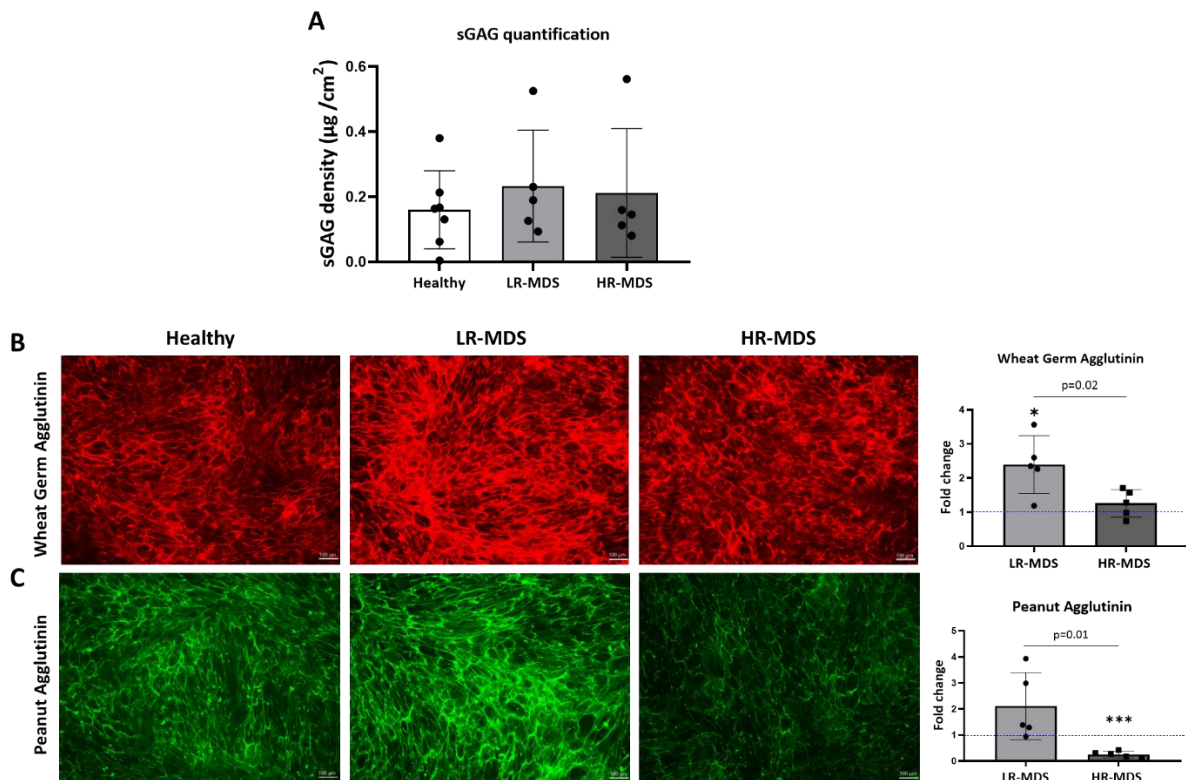


**Figure 11 Disease stage specific changes in the GAG composition of MDS MSC-derived ECM.** A) Quantification of sulphated GAGs of ECM from healthy donor, LR-MDS and HR-MDS MSC using Blyscan assay. Bars represent mean  $\pm$  SD of  $n = 7$  healthy donor MSCs and  $n = 5$  for each of the LR- and HR-MDS MSC samples. B,C) Left: Representative images from the lectin staining using Wheat germ agglutinin (red) which binds to N-acetyl-glucosamine GAGs (HA, HS and KS) and sialic acid and peanut agglutinin (green) binds to N-acetyl-galactosamine and terminal  $\beta$ -galactose containing GAGs (CS, DS and KS) from each sample group. Right: Semi-quantitative analysis of relative fluorescence intensity in the immunofluorescence images by ImageJ. Bars represent mean  $\pm$  SD of  $n = 5$  for each of the LR- and HR-MDS MSC samples, each measured in an independent experiment and expressed as fold change relative to the accompanying healthy MSC ECM control, shown by the dotted line with the ordinate value of 1. An asterisk above the bar indicates significant differences to the control: \* $p < 0.05$ , \*\*\* $p < 0.001$ . Differences between the two MDS groups are shown by the  $p$ -value above the respective bars.

#### 4.1.6. LR-MDS MSC derived ECM contains high levels of CS and HA

The changes indicated by peanut agglutinin staining were analysed further by specific immunostaining with an antibody to CS. Consistent with the peanut agglutinin staining, the CS content of MSC-derived ECM was around 2 fold higher in LR-MDS than in healthy donor samples, while the CS content of

HR-MDS MSC derived ECM was 3-7 lower compared to either healthy or LR-MDS respectively (Figure 12B). This was further confirmed by gel electrophoresis and stains all staining, which showed reduces intensity of CS-A/C in ECM from HR-MDS when compared that from LR-MDS MSC (Figure 12C, D). However, since the levels of CS-A/C in both healthy and HR-MDS samples were below the reliable detection limit of the gel electrophoresis/stains all assay, no quantitative comparison was possible.

To follow up the differences in GAGs stained by wheat germ agglutinin reported above, an ELISA assay was used to detect HA in the various ECM preparations. Here, too, the specific antibody-mediated detection supported the results of agglutinin staining, with significantly 2-3 times higher levels of HA in ECM from both LR- and HR-MDS MSCs compared to that from healthy donor MSCs (Figure 12A). Although the HA levels in HR-MDS ECM were somewhat lower than those in LR-MDS ECM, this difference was small compared to the significant difference in the amounts of wheat germ agglutinin staining (Figure 11B), suggesting that the latter may reflect significant differences in the expression of HS or KS.

The levels of HS present in the ECM samples proved to be too low for detection in the gel electrophoresis-stains all assay. However, HA was detectable in all samples tested (Figure 12C, D), with the highest concentrations in LR-MDS as previously seen using the ELISA assay. The electrophoretic separation of ECM proteins revealed a wide size distribution of HA ranging generally from 110 kDa to 1510 kDa (Figure 12C), although a relatively large amount of LMW-HA with a molecular weight of less than 20 kDa was detected in one of the LR-MDS donor MSC-derived ECM (Figure 12D).



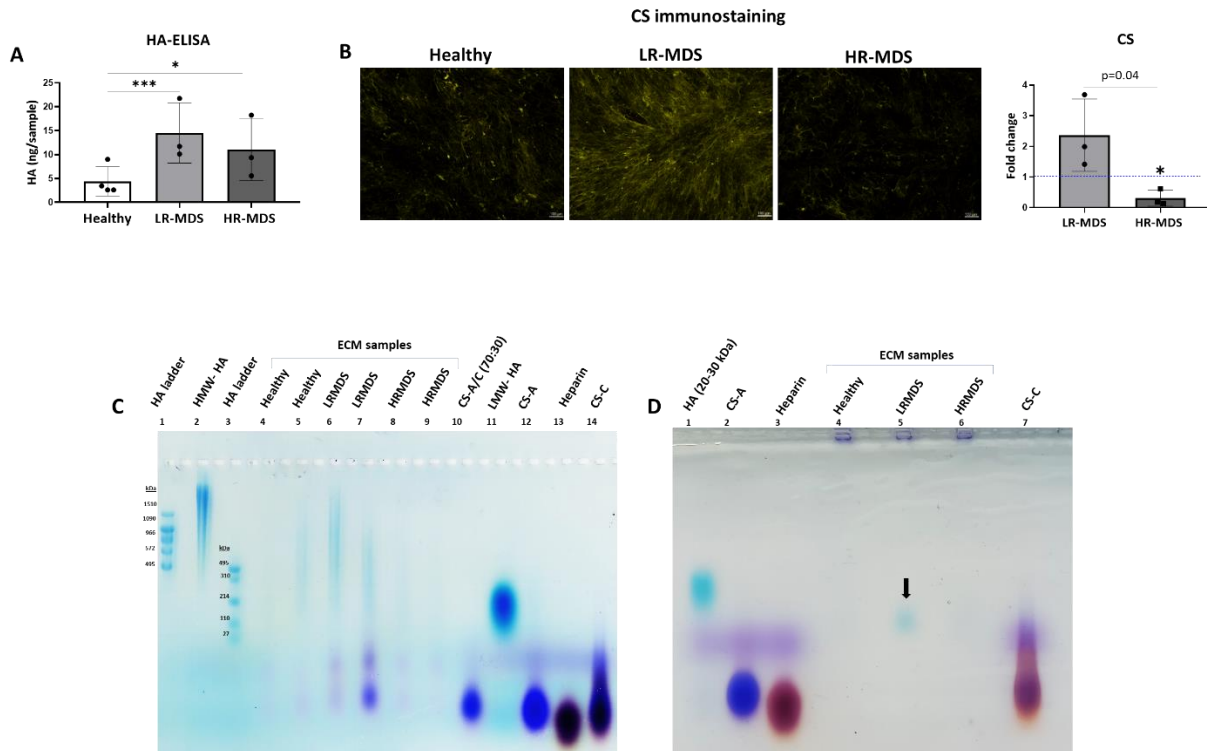


**Figure 12 Disease stage specific changes in the HA and CS composition of MDS MSC-derived ECM.** A) Total HA quantification of the ECM from healthy donor, LR-MDS and HR-MDS MSC using ELISA. Bars represent mean  $\pm$  SD in triplicate for  $n = 4$  for healthy donor MSC-derived ECM and  $n = 3$  for each of the LR- and HR-MDS MSC samples. B) Left: Representative images of CS immunostaining of ECM from healthy donor, LR-MDS and HR-MDS MSC. Right: Semi-quantitative analysis of relative fluorescence intensity in the immunofluorescence images by ImageJ. Bars represent mean  $\pm$  SD of  $n = 3$  for each of the LR- and HR-MDS MSC samples, each measured in an independent experiment and expressed as fold change relative to the accompanying healthy MSC ECM control, shown by the dotted line with the ordinate value of 1. An asterisk above the bar indicates significant differences to the control: \* $p < 0.05$ , \*\*\* $p < 0.001$ . Differences between the two MDS groups are shown by the  $p$ -value above the respective bars. C, D) Gel images of stains all gel staining to characterise the GAGs in the ECM samples from healthy donor, LR-MDS and HR-MDS MSC. The arrow indicates the HA detected in the sample. HA: Hyaluronic acid, HMW-HA: High molecular weight-hyaluronic acid, CS-A/C: Chondroitin sulphate-A/C.

## 4.2. MDS-associated changes in the ECM involve both transcriptional and post-transcriptional regulation

### 4.2.1.1. mRNA levels of core ECM genes only partially reflect the level of the corresponding proteins in the ECM

Having identified differences in the protein composition between ECM samples derived from healthy donors, LR-MDS and HR-MDS patient MSCs, a targeted RT-qPCR approach was used to investigate the expression of a range of ECM-related genes like *COL1a1*, *COL4a2*, *COL7a*, *TNC*, *SPARC* and *FN1* and GAG modifying enzymes like *HAS1*, *HAS2*, *HAS3*, *HYAL-1*, *CSGALNACT1*, *CHYS-11*, *CHST-1*, *DSE-1* and *EXT-1* (refer Table 1 for the enzyme function) in the MSCs. Although there was a high degree of inter-patient variability, each of the 3 collagen genes tested (*COL1a1*, *COL4a2* and *COL7a1*) tended to

be expressed at higher level in the LR-MDS than in either healthy donor or HR-MDS (Figure 13). This reflects the overall pattern of collagen I and IV protein expression noted above, consistent with transcriptional activation of collagen gene expression in LR-MDS. However, HR-MDS MSCs express levels of collagen I and IV mRNA that are comparable to those of healthy donor MSCs, despite the higher collagen content of the HR-MDS ECM shown above (Figure 13). This implies a post-transcriptional level of collagen I and IV in HR-MDS that may affect either translation or protein turnover.

The GAG modifying enzymes also showed a variable pattern of expression, but there was a tendency for high expression of *HAS1* (hyaluronic acid synthase 1), particularly in LR-MDS MSCs, that is in line with the increase in HA in the ECM deposited by these cells (Figure 13).

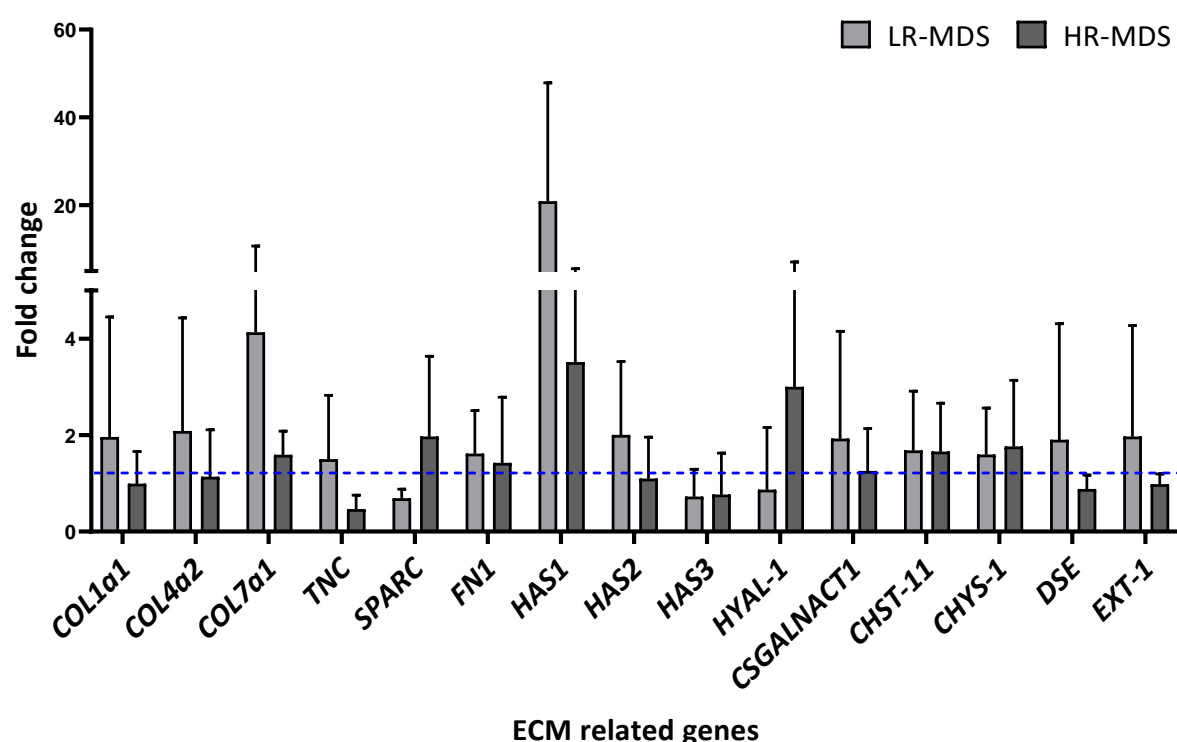
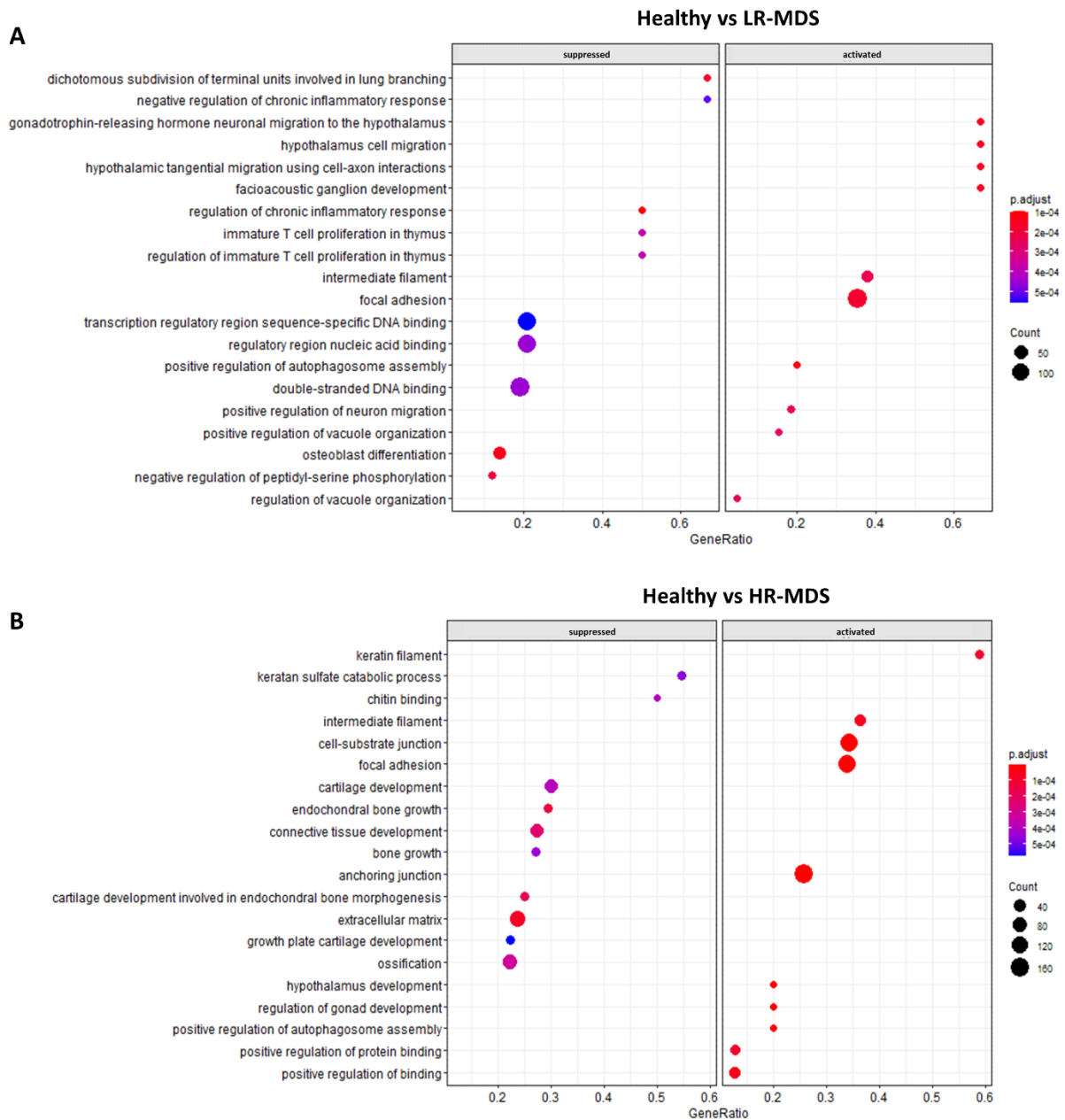


**Figure 13** Relative mRNA levels of core ECM proteins and GAG modifying enzymes in the MDS. Gene expression of a range of ECM proteins and GAG modifying enzymes of LR- and HR-MDS MSCs analysed by RT-qPCR. Bars represent mean  $\pm$  SD for  $n = 4-5$  MDS samples expressed as fold change relative to the healthy MSC sample, shown as the dotted line at ordinate value of 1.

#### 4.2.1.2. Transcriptomic analysis is indicative of ECM deregulation in HR-MDS

Moreover, LR- and HR-MDS MSCs were further analysed at the transcriptomic level using next generation sequencing of the mRNA. A total of  $12 \times 10^6$  reads per sample were detected after pre-processing and mapping to the human genome comprising of 22447 transcripts. GSEA analysis revealed activation of pathways involved in inflammation, cell migration, adhesion and organization,

with suppression of pathways related to nucleic acid binding and osteoblast differentiation in LR-MDS MSCs when compared to healthy donor MSCs (Figure 14A). Similar to LR-MDS MSCs, pathways involved in cell migration and adhesion were also activated in HR-MDS MSCs (Figure 14B). Interestingly, contradictory to the protein levels, pathways related to KS catabolism, ECM, and connective tissue development were suppressed in HR-MDS MSCs in comparison to healthy donor MSCs (Figure 14B). This suggests that transcriptomic analysis is indicative of ECM deregulation in HR-MDS but does not reflect the differences observed at the protein level. This may be due to collection of mRNA at the end of ECM generation experiments causing a feedback inhibition or stabilization of the mRNA of ECM genes in MDS MSCs. Furthermore, it was also indicative of increased inflammation in LR-MDS marrow which might conceal the changes related to the ECM.



### 4.3. MDS MSC-derived ECM modulates HSPC behaviour

#### 4.3.1. LMW-HA stimulates inflammatory markers gene expression in bone marrow MNCs

The detection of LMW-HA in LR-MDS MSC-derived ECM (Figure 12D) suggests a possible link between alterations in the ECM and the inflammatory state known to be a feature of LR-MDS<sup>125</sup>. Since, LMW-HA has been reported to promote inflammation<sup>94</sup>. To test directly the pro-inflammatory effects of LMW-HA on the BMME, bone marrow MNCs were stimulated with LMW-HA for 24 hours and

expression of a range of inflammatory genes like *IL1b*, *IL18*, *NLRP3*, *IL6* and *S100A9* were analysed. There was indeed a consistent trend towards higher expression of all inflammatory genes tested, 24 hours after exposure to LMW-HA (Figure 15). Only, in the case of *IL-6*, the increase was significant (Figure 15). These results demonstrate that specific changes in the composition of the MSC-derived ECM in LR-MDS bone marrow could contribute to the inflammatory environment that is thought to drive evolution of the disease.

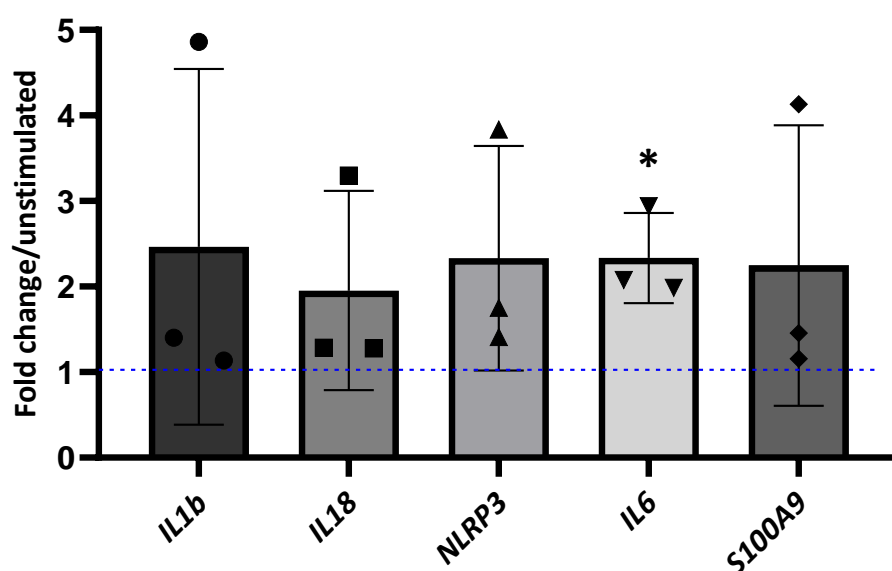


**Figure 15** Low molecular weight HA stimulates pro-inflammatory gene expression in bone marrow MNCs. The relative mRNA expression of pro-inflammation genes *IL1b*, *IL18*, *NLRP3*, *IL6* and *S100A9* measured via RT-qPCR analysis after stimulation by LMW-HA. Bars represent mean  $\pm$  SD for  $n = 3$  expressed as fold change relative to the unstimulated MNCs, shown as the dotted line at ordinate value of 1. An asterisk above the bar indicates significant differences to the unstimulated control. \* $p < 0.05$ .

#### 4.3.2. MDS ECM has a functional impact on the HSPCs behaviour

To further investigate the functional impact of the MDS ECM on HSPCs, CD34<sup>+</sup> HSPCs from both healthy donor and MDS patient bone marrow were cultured for 7 days on decellularized ECM derived from healthy, LR- and HR-MDS MSC. The cells were then assessed in terms of number, surface makers, colony formation ability, and cell morphology. HSPCs derived from MDS patient marrow showed little or no proliferation on any of the ECM tested (data not shown). Moreover, no colony forming cells were present after 1 week (data not shown), limiting the comparison to the effects of healthy and MDS ECM on HSPCs from healthy donors. These HSPCs proliferated similarly on ECM from all sources, although there tended to be fewer cells adhering to the MDS MSC-derived ECM (both LR- and HR-MDS) than to the healthy donor derived ECM (Figure 16A). There was no change in the overall percentage of early

progenitor cells (assessed as CD34+ and/or CD117+) at the end of the 7 day culture period on the different ECMs (Figure 16B, C, D). Progenitor cells expressing CD34 were consistently enriched in the ECM adherent fractions (Figure 16B).

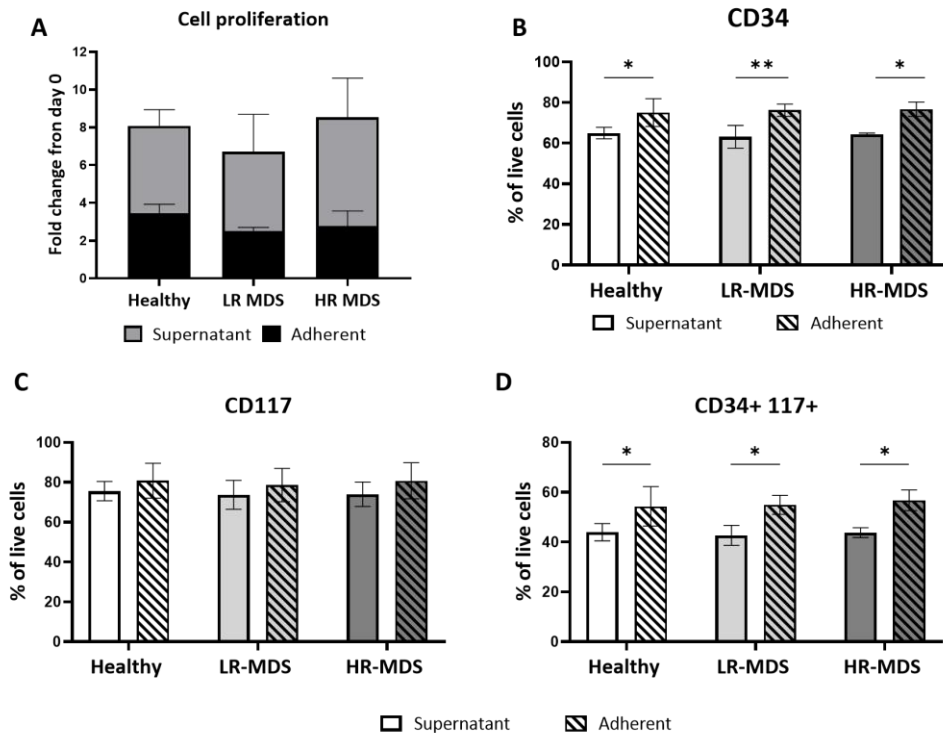


**Figure 16 Neither proliferation nor surface marker expression of HSPCs are differentially affected by culture on ECM from healthy donor, LR- or HR-MDS MSCs.** A) Proliferation of HSPCs on different ECM as determined using trypan blue. The supernatant fraction denotes the cells in aspirated medium whereas the adherent fraction denotes the cells in contact with the ECM. The cell numbers are expressed as fold change over day 0. B, C, D) Surface marker expression of CD34, and/or CD117 on the live HSPCs in the supernatant and adherent fraction of ECM from healthy donor, LR- and HR-MDS MSCs. Bars represent mean  $\pm$  SD for  $n = 4$ . An asterisk above the bar indicates significant differences to the control: \* $p < 0.05$ , \*\* $p < 0.01$ .

As potential determinants of the interaction of HSPC and matrix, the expression of a range of integrin proteins such as CD41 (ITGA11b), CD51 (ITGAV), CD61 (ITGB3) and CD29 (ITGB1) and of the HA receptor CD44 was investigated by flow cytometry (Figure 17). For gating strategy refer to annex II. No change in the integrins and CD44 expression was observed after culture on different ECMs (Figure 17). Each of the integrins tested was expressed at a higher level on the ECM-adherent cell population than on the supernatant cell population. This differential distribution of integrin-expressing cells reached significance for both CD41 and CD61 in the case of ECM from HR-MDS (Figure 17A, C). However, the distribution of CD51 and CD29/CD44 expressing cells between ECM and supernatant did not differ between the ECM derived from healthy donor MSCs and those from MDS patient MSCs.

There was a significant increase in the expression of CD41 in the adherent fraction of the ECM when compared to the supernatant fraction (Figure 17A). The expression of CD51 and CD61 remained higher

than that of the supernatant fraction (Figure 17A, B, C, E, and F). CD29 was expressed by all cells regardless of their adherent or supernatant fractions of the ECM in all the samples (Figure 17F). No difference in the expression of CD44 was observed on HSPCs cultured on different ECM nor in the adherent or supernatant fractions (Figure 17D).

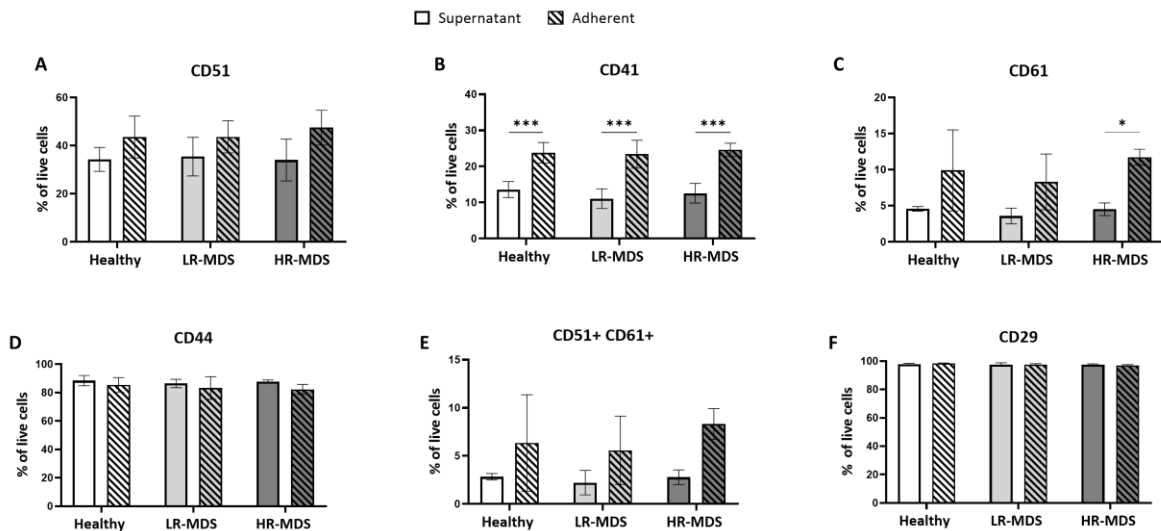


**Figure 17 HSPC expressing selected integrins or CD44 associate similarly to ECM from healthy donor, LR- and HR-MDS MSCs.** A) CD51, B) CD41, C) CD61, D) CD44, E) CD51 and CD61, and F) CD29 surface marker expression on live HSPCs cultured on ECM from healthy donor, LR- and HR-MDS MSCs as analysed by flow cytometry. Bars represent mean  $\pm$  SD for  $n = 4$ . An asterisk above the bar indicates significant differences to the control: \* $p < 0.05$ , \*\* $p < 0.01$ .

Although the analysis of selected adhesion receptors revealed no quantitative difference between HSPC binding to ECM from healthy donor- or MDS patient-MSCs. Immunostaining of the ECM-associated HSPCs for vinculin to examine cell shape showed that HSPC interacting with MDS-derived ECM lose their polarity (Figure 18A). While HSPCs interacting with ECM from healthy donors maintained their typical polarity (Figure 18A). Therefore, there might be a qualitative difference in binding that may potentially affect HSPC behaviour.

The ability of the ECM to maintain the functional haematopoietic potential of HSPCs was assessed by transferring the cells produced after 7 days of culture on ECM into colony assays. Interestingly, the HSPCs cultured on MDS MSC-derived ECM (both LR- and HR-MDS) had a diminished capacity to form CFU-GM (granulocyte and macrophage colonies) and CFU-E (erythroid colonies) when compared to HSPCs cultured on healthy donor MSC-derived ECM (Figure 18B). This loss of potential was more marked for ECM of LR-MDS than HR-MDS (Figure 18B).

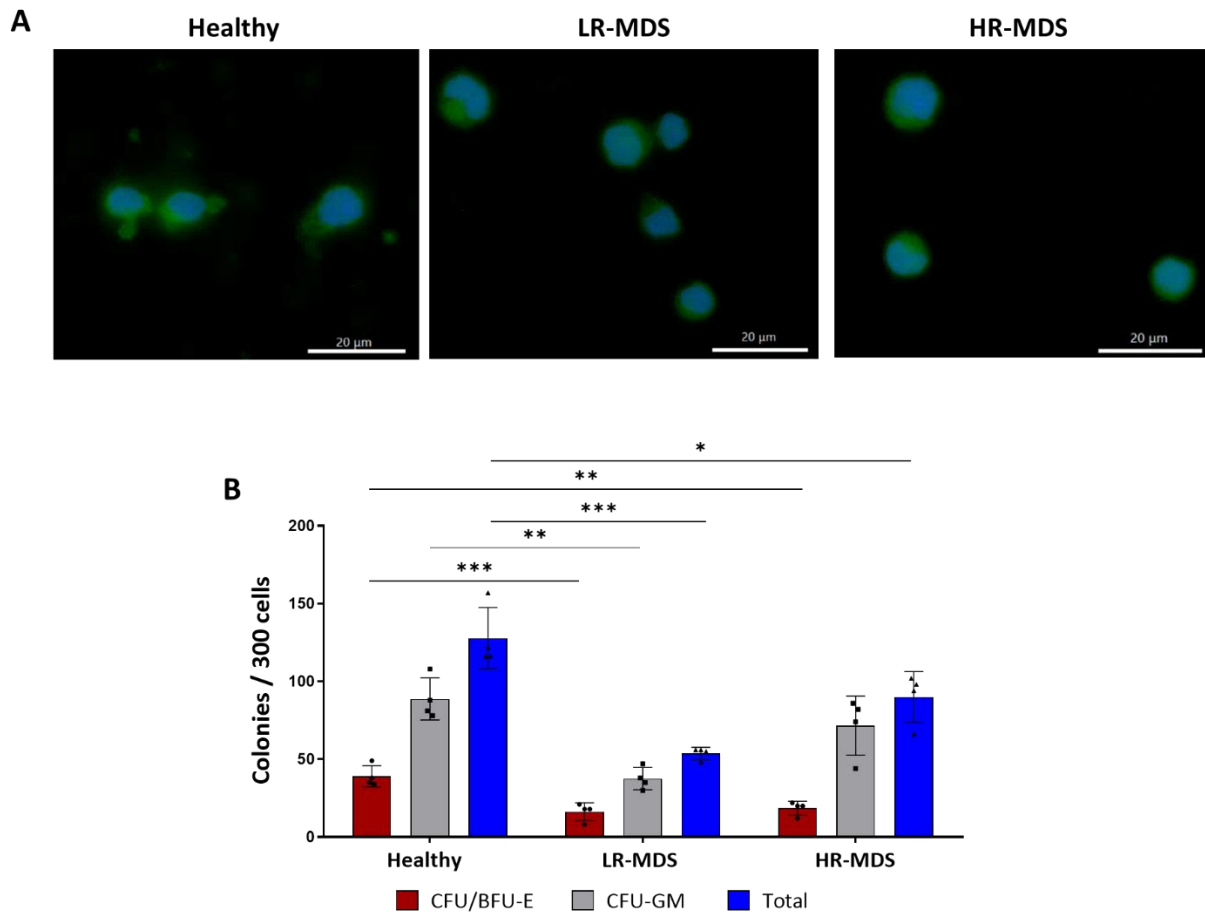


**Figure 18 Diminished support of healthy HSPCs on MDS MSC-derived ECM.** A) Representative images from the immunostaining of HSPCs on ECM substrates using anti-vinculin (green) and DAPI (blue). B) CFU assay after culturing of HSPCs on ECM from healthy donor, LR- and HR-MDS MSCs for 7 days. Bars represent mean  $\pm$  SD for  $n = 4$  samples per group. \* $p < 0.05$ , \*\*\* $p < 0.001$ , \*\*\*\* $p < 0.0001$ .

#### 4.3.3. MDS and healthy ECM have similar growth factor retention and presentation capacities

ECM is known to maintain growth factor gradients and to present ligands to target cells in an active form<sup>51</sup>. It was therefore of interest to test whether the differences between healthy donor and MDS-derived ECM in terms of haematopoietic support are associated with altered growth factor binding. The HSPCs were cultured for 7 days on the different ECMs that had been pre-incubated in medium containing FBS with or without the HSPC growth factors; SCF, IL-3 and FTL-3-L. After 7 days, the haematopoietic potential of the cultured cells was assessed by colony assay. Increased colony formation ability was observed on all ECMs that had been pre-incubated with growth factors when compared to the ECMs that have been pre-incubated with FBS (Figure 19), verifying the expected growth factor retention/presentation capacity of the matrices. However, there was high variability in colony formation ability of matrix-cultured HSPCs and no consistent differences between the matrices



from HD, LR-MDS or HR-MDS MSCs (Figure 19), indicating that growth factor presentation ability of the ECM is not the decisive factor in modulating the HSPC behaviour on MDS MSCs derived ECM.

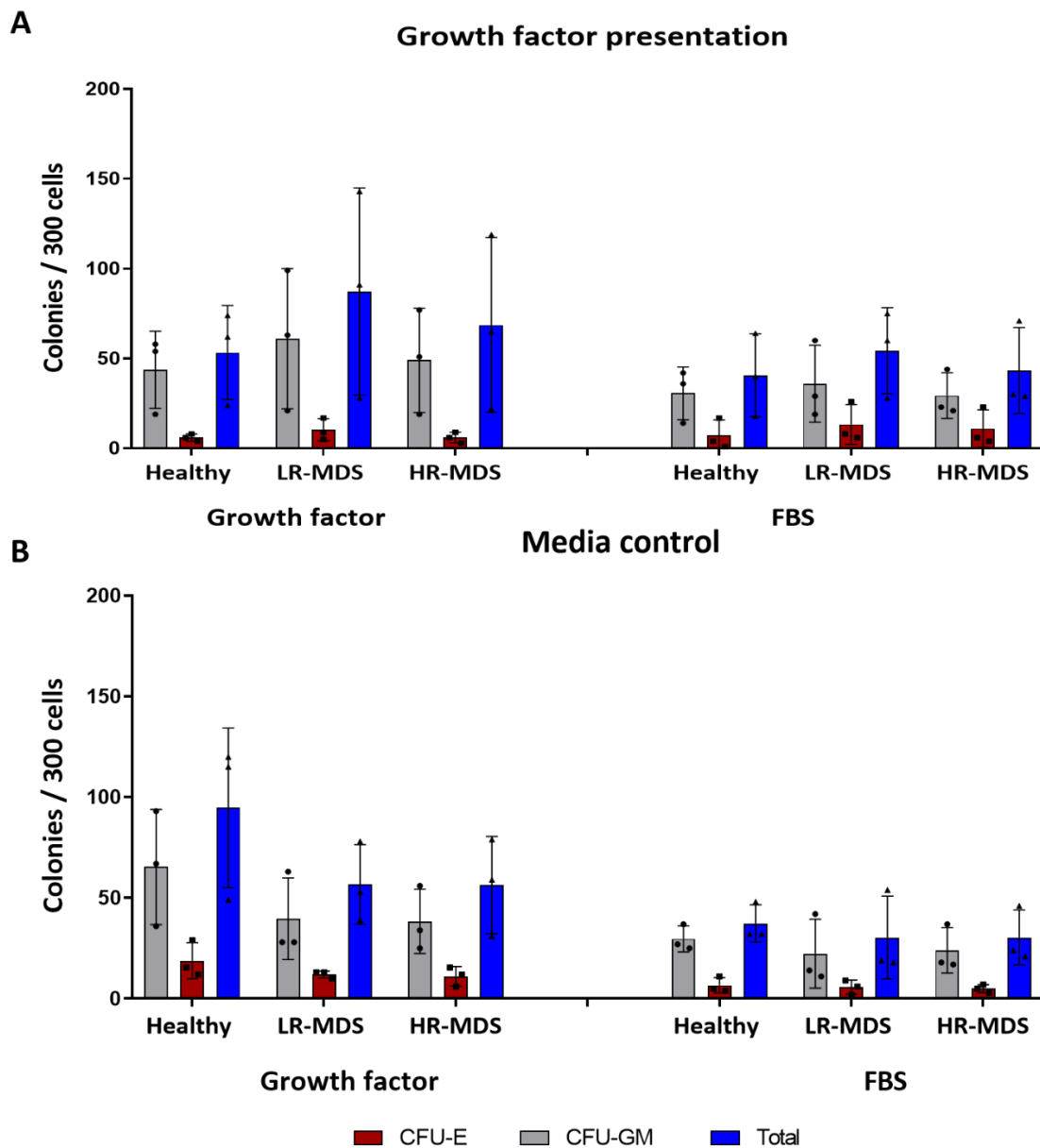


**Figure 19 MDS ECM does not differentially affect the growth factor presentation capability of the ECM.** CFU assay of HSPCs cultured on ECM from healthy donor, LR- and HR-MDS MSCs after 7 days. Above: Prior to the HSPC culture the ECM were pre-incubated with either growth factors or FBS. Below: Control cultures in which HSPCs were cultured in either growth factor or FBS containing medium on the ECM without any prior preincubation. Bars represent mean  $\pm$  SD for  $n = 3$  samples per group.

## 4.4. AZA therapy reverts MDS-associated changes in MSC-derived-ECM

### 4.4.1. MSCs isolated from MDS patients before and after AZA treatment or HSCT have similar phenotypic properties

The therapy with the HMA, AZA is commonly used to treat MDS, particularly in the later high-risk stages of disease, and has been used as a conditioning (clearing) treatment before allogeneic HSCT<sup>125,131,132</sup>. However, it is not clear to what extent the beneficial effects are achieved by action on the haematopoietic clone itself or whether effects on the stromal cells that establish the haematopoietic niche can also contribute to the response.

To investigate the effects of *in vivo* AZA therapy and HSCT on the BMME, MSCs were isolated from HR-MDS patients at diagnosis, following 3-4 cycles of AZA therapy and following a subsequent HSCT. Cultured MSCs were evaluated in terms of their proliferation, cell surface markers and both adipogenic and osteogenic differentiation potential. Bright field microscopy of the MSCs revealed no morphological differences between the different MSC groups (Figure 20A). Structurally, the MSCs from all the groups displayed a similar fibroid, disorganised morphology (Figure 20A) similar to that of the HR-MDS MSCs presented in 4.1.1. There was no significant difference in the proliferation and doubling time of the MSCs, although the MSCs derived from patients post-HSCT tended to maintain proliferative activity for longer (Figure 20B, C). There was no difference in the classical MSC surface markers CD73, CD90, CD105, CD44, CD166 and CD146 among the different groups of MSCs (Figure 20D). There was also no significant difference between the samples in terms of osteogenic or adipogenic differentiation capacity (Figure 20E, F). Although the MSCs isolated post-HSCT showed a non-significant ( $p=0.84$ ) trend towards adipogenic rather than osteogenic differentiation (Figure 20E, F).

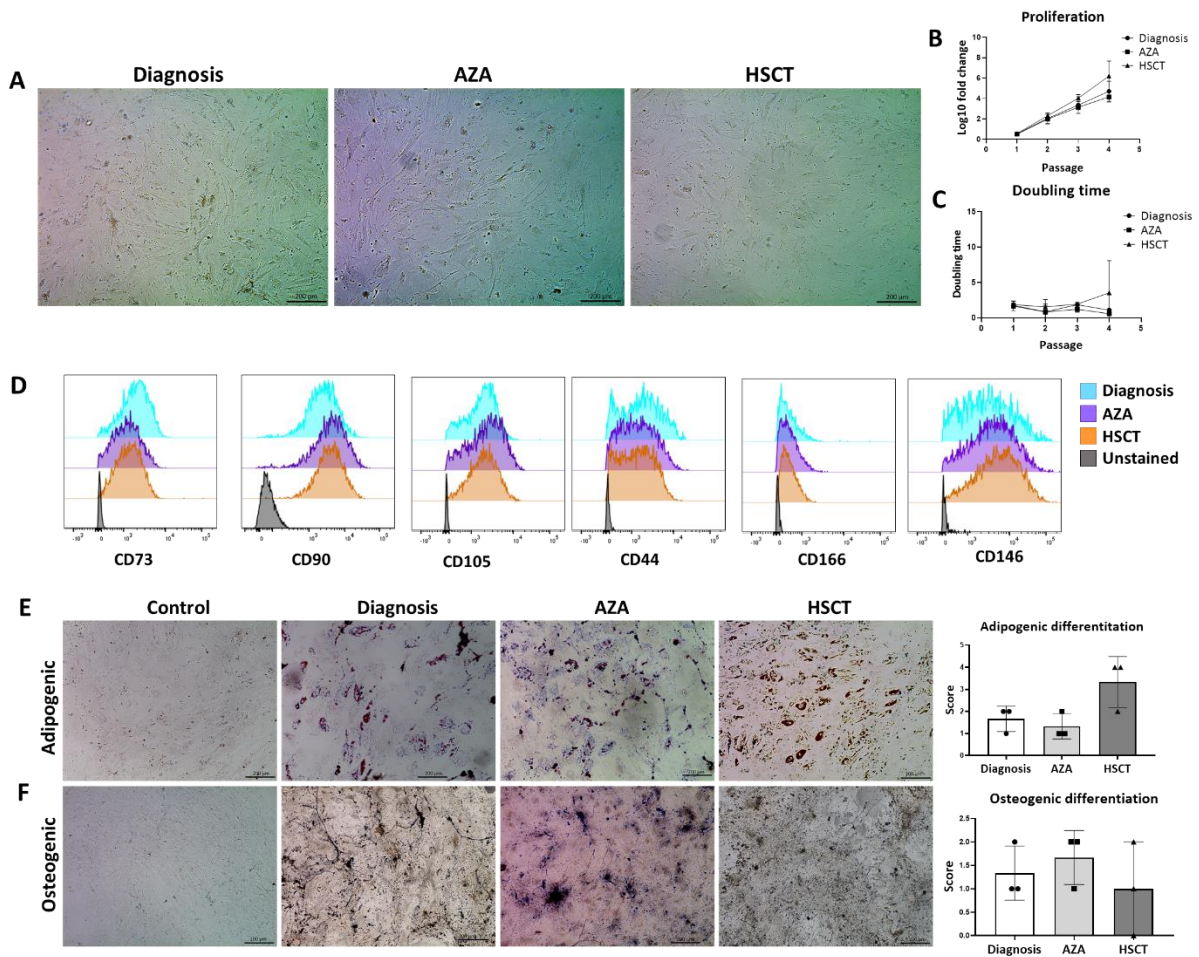


**Figure 20 Phenotypic characteristics does not differ after AZA therapy and HSCT.** A) Representative bright field images of MSC morphology from MDS patients at diagnosis, and after receiving AZA therapy and post-HSCT. B) Cell counts represented as log<sub>10</sub> fold change from the starting number and C) Doubling time of different MSCs determined by trypan-blue staining at indicated passages. Values represent mean ± SD of n = 3 for each group. D) Flow cytometry analysis of MSC surface markers before the start of generation of the ECM. E, F) Right: Representative images of the staining of MSCs with Oil Red O and Van kossa stains for adipogenic and osteogenic differentiation respectively. Left: Scoring of the differentiation potential of the MSCs using ImageJ. Bars represent mean ± SD in triplicate of n = 3 for each group.

#### 4.4.2. Improved rigidity and structure of ECM after AZA treatment

As reported above, MDS-derived ECM has a higher density and a lower rigidity than that derived from healthy donors (Figure 8). These effects are reversed following AZA treatment of the patients, with a decrease in density revealed by bright field imaging (Figure 21A) and significantly increased the rigidity to almost 2 kPa as measured by AFM (Figure 21B). Measurements were performed at the Soft Matter Physics Division, Peter Debye Institute for Soft Matter Physics, University of Leipzig, Leipzig, Germany. The physical properties of the ECM made by MSCs from AZA treated patients were therefore similar to those of ECM deposited by healthy donor MSCs (refer to 4.1.2), indicating a restoration of the biophysical properties. However, ECM from MSCs isolated from the same patients post HSCT displayed an intermediate stiffness of 1.3 kPa, indicating a partial reversion to the pre-treatment phenotype

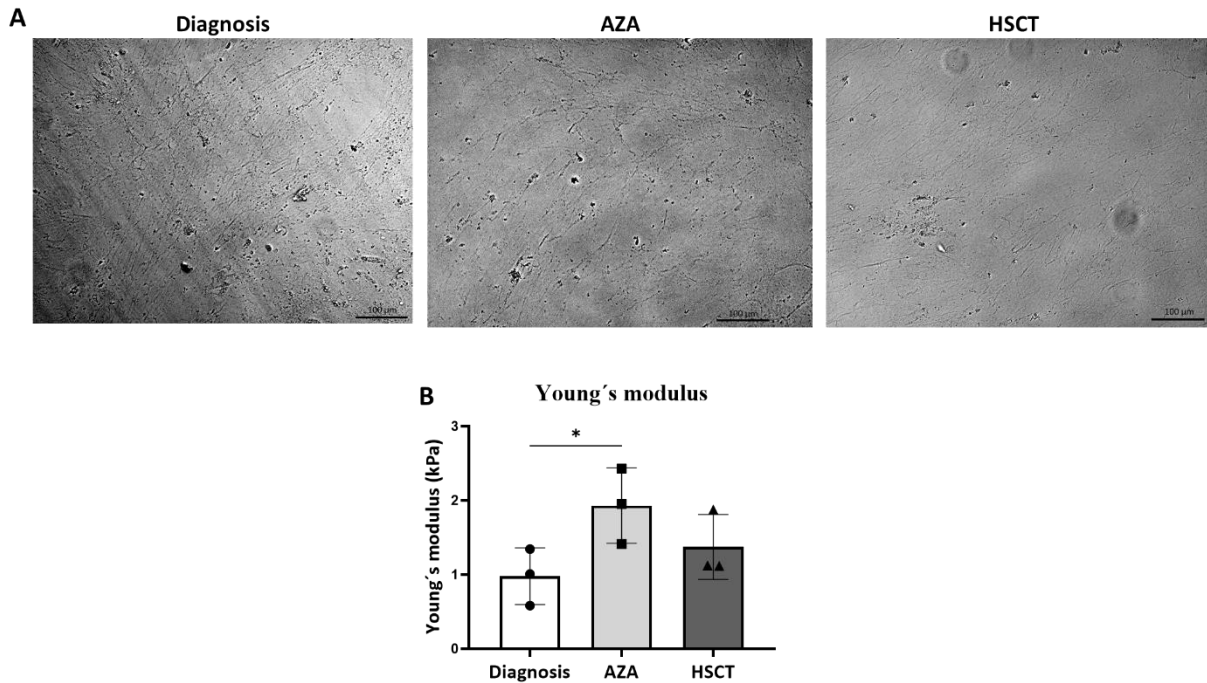


**Figure 21** Changes in the biophysical properties of the ECM from MDS MSCs isolated before and after AZA therapy and HSCT. A) Representative phase contrast images of ECM from MDS MSCs of patients at diagnosis, after receiving AZA therapy and post-HSCT. B) Elastic modulus measurements of the ECM from MDS MSCs of patients at diagnosis, and after receiving AZA therapy and post-HSCT as analysed by AFM. Bars represent mean  $\pm$  SD in duplicates for  $n = 3$  samples per group. \* $p < 0.05$ .

#### 4.4.3. Improved deposition of collagens after AZA treatment

The effects of AZA and HSCT therapy on the increased collagen deposition observed in MDS MSC-derived ECM were assessed by sircol assay and immunohistochemistry of ECM and by gene expression analysis of the cultured MSCs. Total collagen content of ECM from MSCs isolated post-AZA therapy was reduced to  $0.07 \mu\text{g}/\text{cm}^2$  (Figure 22A) to more closely resemble the situation in healthy donors, while HSCT was followed by a partial reversal of this effect, resulting in levels intermediate ( $0.12 \mu\text{g}/\text{cm}^2$ ) between healthy donor ( $0.08 \mu\text{g}/\text{cm}^2$ ) and untreated MDS patient ( $0.14 \mu\text{g}/\text{cm}^2$ ) marrow (Figure 22A). Although the variation in collagen mRNA; *COL1a1*, *COL4a2* and *COL7a1* was high, in contrast to the overall protein levels (Figure 22A), the general trend towards increased rather than decreased mRNA expression following therapy (Figure 22B). Specific immune histochemical analysis using antibodies to collagens I and IV confirmed that the levels of these collagen proteins in the ECM were almost reduced to half, while the corresponding mRNAs were higher in the treated MSCs relative to the untreated condition (Figure 22C, D).

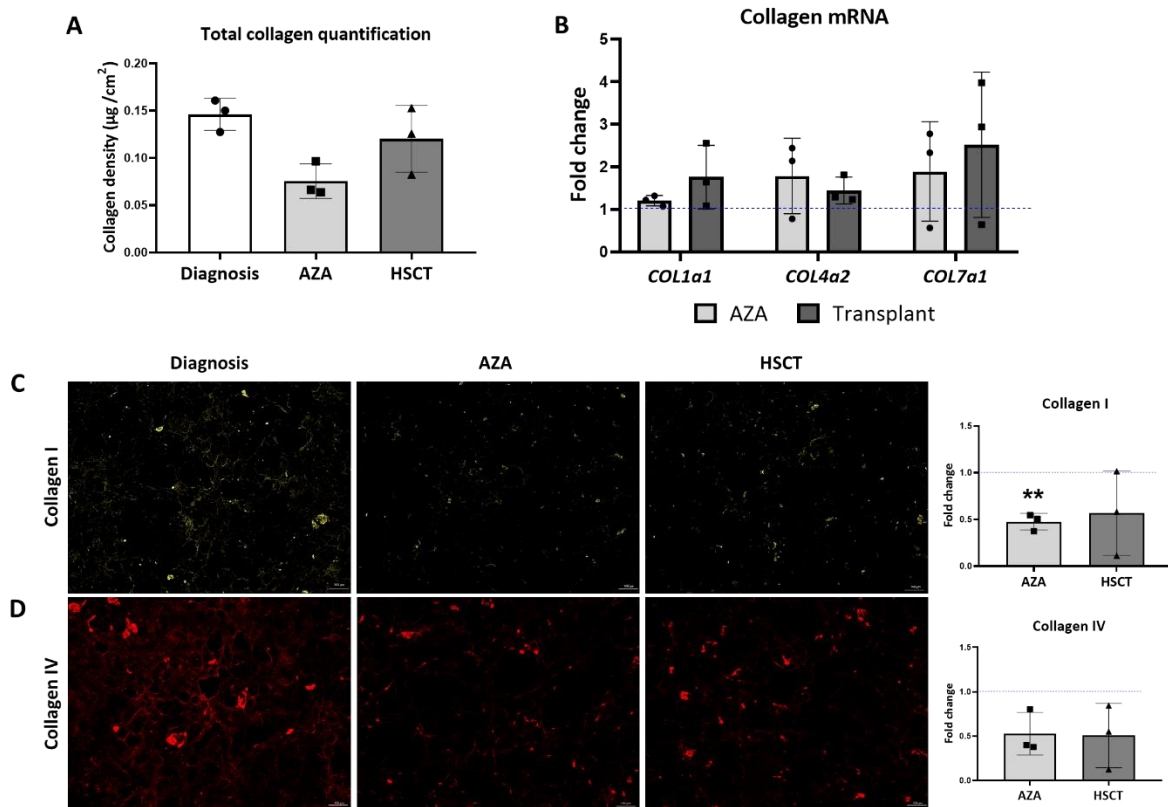


**Figure 22** Changes in the collagens in MDS MSC derived ECM post AZA therapy. A) Total collagen quantification of the ECM from MDS MSC from patients at diagnosis, after receiving 3-4 cycles of AZA therapy and post-HSCT using sircol assay. B) Relative mRNA levels of COL1a1, COL4a2 and COL7a1 measured via RT-qPCR. C, D) Left: Representative images of collagen I (yellow) and collagen IV (red) immunostaining respectively. Right: Bars represent mean  $\pm$  SD of  $n = 3$ , each measured in an independent experiment and expressed as fold change relative to ECM from MDS MSC of patients at diagnosis as control, shown by the dotted line with the ordinate value of 1. An asterisk above the bar indicates significant differences to the control:  $**p < 0.01$ .

#### 4.4.4. AZA treatment does not improve the GAG profile of MDS MSCs

Further, the impact of AZA treatment and HSCT on the GAG composition of the MDS ECM was analysed by lectin staining. There was no apparent difference in either wheat germ agglutinin or peanut agglutinin staining in the ECM from MSCs isolated following AZA treatment (Figure 23A, B). Similar to the collagens, the variability between samples from patients post-HSCT was particularly high (Figure 23 A, B). The same was true for CS level determined by immune histochemical staining (Figure 23C) and for GAGs separated by gel electrophoresis and stained with stains-all (Figure 23D). The high variability in the HSCT sample group may be due to differences between patients in terms of treatment response, residual MDS cells and the intensity of graft versus host disease (GvHD), which occurred to some extent in all cases.

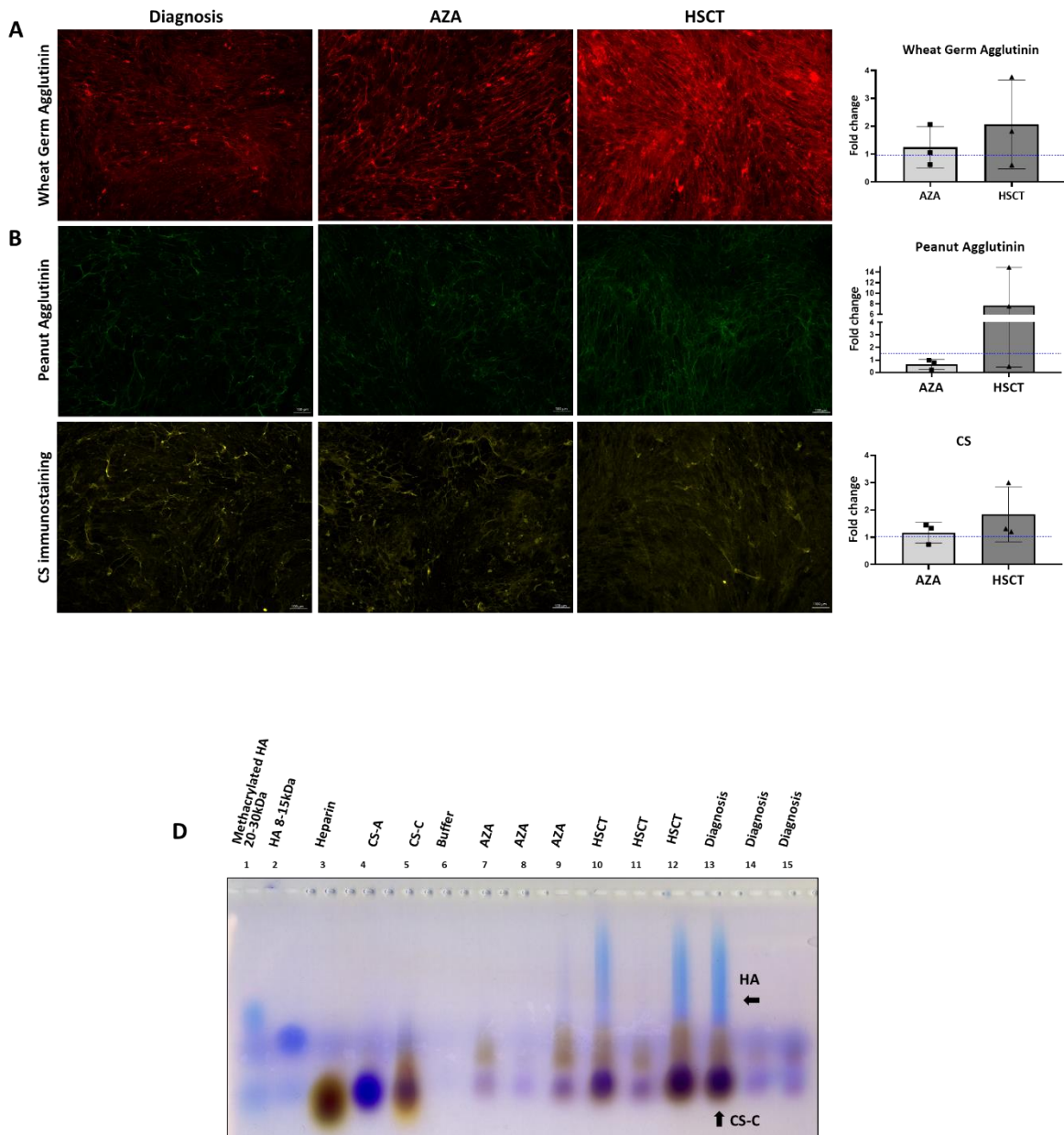


**Figure 23 GAG composition of MDS MSC-derived ECM does not change after AZA therapy or post HSCT.** A, B) Left: Representative images from the lectin staining using wheat germ agglutinin (red) which binds to N-acetyl-glucosamine GAGs (HA, HS and KS) and peanut agglutinin (green) binds to N-acetyl-galactosamine and terminal  $\beta$ -galactose containing GAGs (CS, DS and KS) from each sample group. Right: Semi-quantitative analysis of relative fluorescence intensity in the immunofluorescence images by ImageJ. C) Left: Representative images of CS (yellow) immunostaining of ECM samples. Right: Semi-quantitative analysis of relative fluorescence intensity in the immunofluorescence images by ImageJ analysis. Bars represent mean  $\pm$  SD of  $n = 3$  for each group, each measured in an independent experiment and expressed as fold change relative to the ECM from MDS MSC of patients at diagnosis as control, shown by the dotted line with the ordinate value of 1. D) Gel images of stains all gel staining to characterise the GAGs in the ECM samples from MDS MSCs of patients at diagnosis, and after receiving AZA therapy and post-HSCT. HA: Hyaluronic acid, HMW-HA: High molecular weight-hyaluronic acid, CS-A: Chondroitin sulphate-A, CS-C: Chondroitin sulphate-C.

#### 4.4.5. AZA treatment improves ECM-mediated haematopoietic support

To further investigate the potential functional impact of AZA treatment and HSCT on MDS ECM, healthy donor HSPCs were cultured on the various ECM samples (HR-MDS MSC at diagnosis, post-AZA treatment and post-HSCT) for 7 days and then were analysed for proliferation, colony formation ability, and cell morphology. No difference was detected in the proliferation of the HSPCs on different ECMs (Figure 24A). However, transfer of cultured cells to colony assays revealed an increased colony forming capacity of HSPCs that has been cultured on ECM from treated compared to untreated MDS patients (Figure 24B). Moreover, the HSPCs on HR-MDS MSC-derived ECM from patients post-AZA treatment and post-HSCT showed a more polarized morphology (Figure 24C), similar to that seen previously when the HSPCs were cultured on healthy donor derived MSC ECM (Figure 18B).

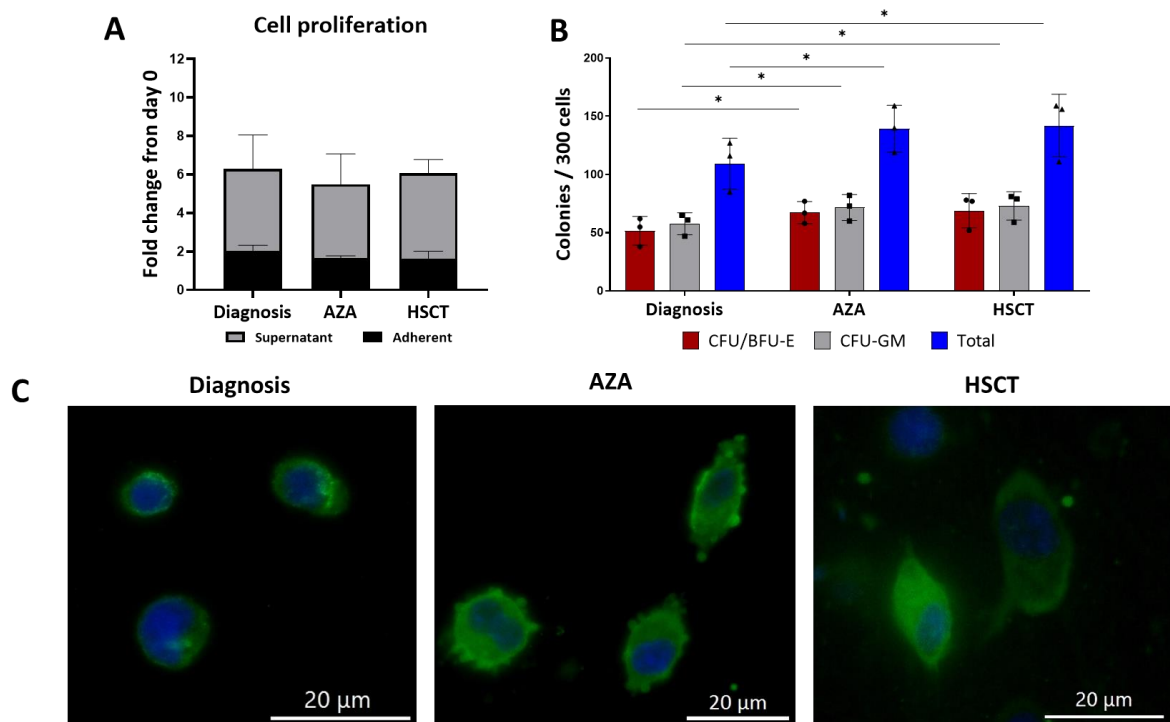


**Figure 24** MDS ECM improves haematopoietic support post-AZA therapy and post-HSCT. A) Proliferation of HSPCs on different ECM as determined using trypan blue. The supernatant fraction denotes the cells that are not attached to the ECM whereas the adherent fraction denotes the cells in contact with the ECM. The cell numbers are normalized to the cell number at day 0. B) CFU assay after culturing of HSPCs on ECM from MDS MSCs of patients at diagnosis, and after receiving AZA therapy and post-HSCT for 7 days. C) Representative images from the immunostaining of HSPCs on ECM using anti-vinculin (green) and DAPI (blue). Bars represent mean  $\pm$  SD for  $n = 3$  samples per group. \* $p < 0.05$ .

#### **4.4.6. *In vitro* AZA treatment does not change the phenotypic characteristics of MDS MSC-derived ECM**

Having shown that AZA therapy of patients leads to stable changes in the biology of bone marrow- MSCs in terms of their subsequent deposition of ECM. It was of interest to compare this long term *in vivo* AZA effect to the possible indirect and direct effects of AZA treatment on MSCs *in vitro*. To address this, the MSCs isolated from untreated patients at the time of diagnosis were cultured *in vitro*, and treated with 10 $\mu$ M AZA. These AZA treated MSCs were compared to both untreated MSC and MSC from treated patients (*in vivo* AZA MSCs). Due to limited availability of the relevant MSC samples at lower passage numbers, these experiments were performed using samples from a patient cohort different to that used in 4.4.2. The MSCs were analysed for their proliferation, cell surface markers, adipogenic, and osteogenic differentiation ability. Structurally the MSCs from all the groups displayed a similar fibroid, disorganised morphology similar to that of HR-MDS MSCs in 4.1.1 and 4.4.2 (Figure 25A). The proliferation rate of untreated MDS MSCs was slightly but not significantly higher than that of treated MSCs (Figure 25B, C). *In vitro* AZA treatment had no effect on the expression of standard MSC surface markers CD73, CD90, CD105, CD44, CD166 or CD146 (Figure 25D). Nor was there any significant difference detected in the osteogenic or adipogenic differentiation capacity between untreated MDS MSCs and *in vitro* and *in vivo* AZA treated MDS MSCs (Figure 25E, F).



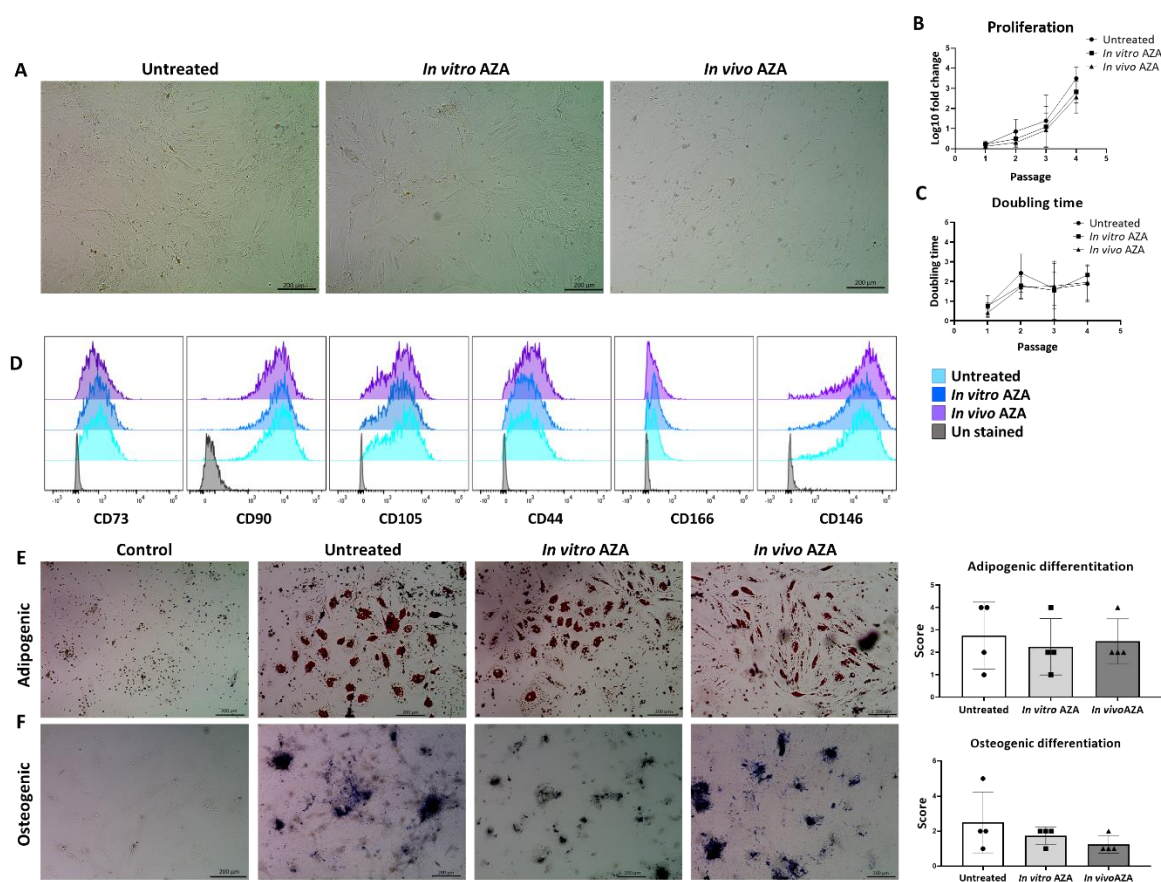


**Figure 25 Phenotypic characteristics does not differ after in vitro and in vivo AZA therapy.** A) Representative bright field images of MSC morphology from untreated MDS MSCs as well as after in vitro or in vivo AZA treatment. B) Cell counts represented as log<sub>10</sub> fold change from the starting number and C) Doubling time of different MSCs determined by trypan-blue staining at indicated passages. Values represent mean ± SD of n = 4 for each group. D) Flow cytometry analysis of MSC surface markers before the start of generation of the ECM. E, F) Right: Representative images of the staining of MSCs with Oil Red O and Van kossa stains for adipogenic and osteogenic differentiation respectively. Left: Scoring of the differentiation potential of the MSCs using ImageJ. Bars represent mean ± SD in triplicate of n = 4 for each group.

#### 4.4.7. AZA has direct and acute effects on ECM deposition by MSCs, as well as long-term effects that may be indirect

To examine the effects of *in vitro* AZA treatment of MSCs on the physical properties of deposited ECM, the MDS MSCs isolated from untreated patients at diagnosis were cultured *in vitro* and treated with 10 $\mu$ M AZA during the ECM generation process. Bright field images revealed a decrease in ECM density following either *in vivo* or *in vitro* AZA treatment, compared to ECM from untreated cells (Figure 26A). At the same time, the rigidity of the ECM was increased both in the MSC from AZA treated patients and, to a lesser extent, by *in vitro* AZA treatment of MSCs from untreated patients (Figure 26B). This suggests that AZA treatment can induce direct and acute changes on MSCs themselves, as well as longer lasting effects that may require interaction with other cells of the BMME.

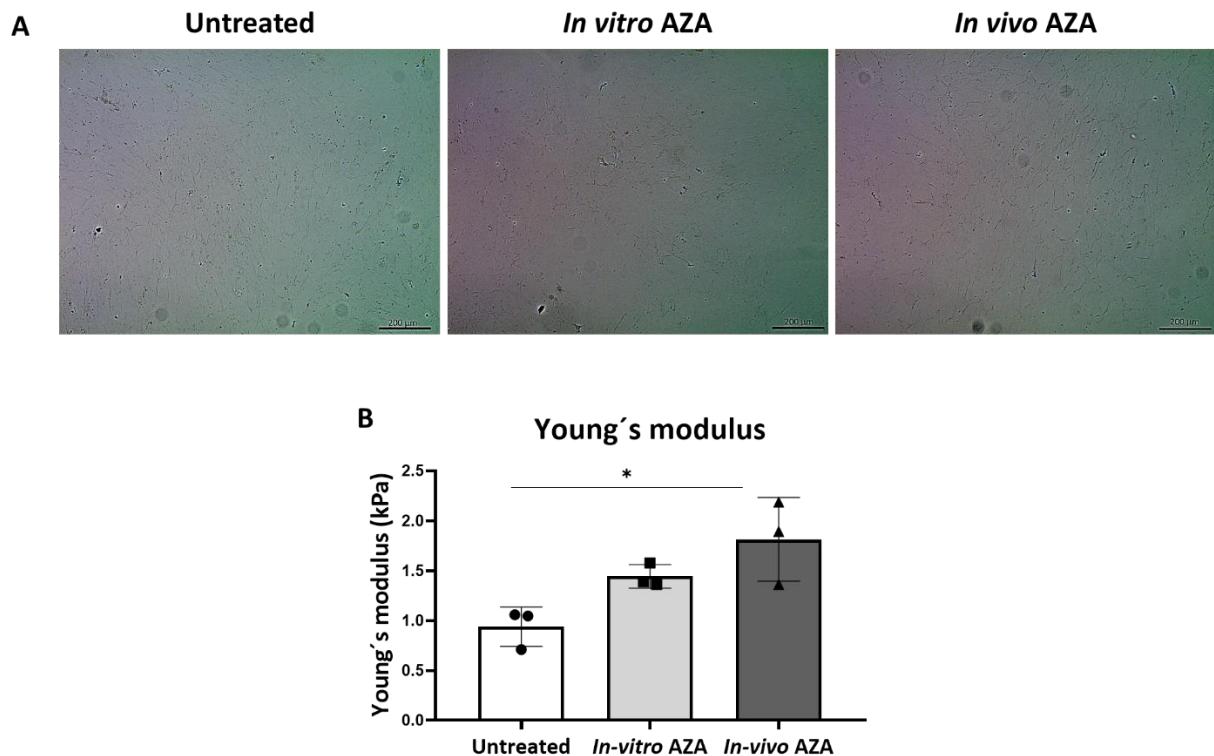


**Figure 26** *In vitro* AZA treatment has a tendency to revert the changes in the biophysical properties of the ECM from MDS MSCs. A) Representative phase contrast images of the ECM from untreated MDS MSCs as well as after *in vitro* or *in vivo* AZA treatment. B) Elastic modulus measurements of the different ECMs as analysed by AFM. Bars represent mean  $\pm$  SD in duplicates for  $n = 3$  samples per group. \* $p < 0.05$ .

#### 4.4.8. Collagen incorporation into ECM is affected differentially by *in vivo* and *in vitro* AZA treatment

Analysis of collagen levels in ECM showed that there was no significant effect of either short-term *in vitro* AZA treatment of isolated MSCs or protracted *in vivo* AZA treatment of patients on the overall collagen content. However, there was a tendency of lower collagen levels in both cases (Figure 27A). Deposition of the major collagens I and IV into ECM was reduced to half in MSCs isolated following AZA therapy *in vivo*, but not in therapy-naïve MSCs exposed to AZA *in vitro* (Figure 27C, D). Focusing on the major collagens I and IV once again revealed distinctly different consequences of *in vivo* vs *in vitro* treatment. *In vitro* exposure to AZA tended to decrease mRNA levels in the MSCs, but not the levels of the corresponding protein in ECM, while *in vivo* treatment of patients yielded MSCs with unchanged levels of collagen I and IV mRNA but significantly lower incorporation of the corresponding proteins into the ECM (Figure 27B, C, D). This suggests multiple effects of AZA on collagen deposition by MSCs that include acute and direct modulation of gene expression in MSCs as well as long term reprogramming of MSCs by extended *in vivo* treatments that are likely to be affecting multiple cell types in the BMME.

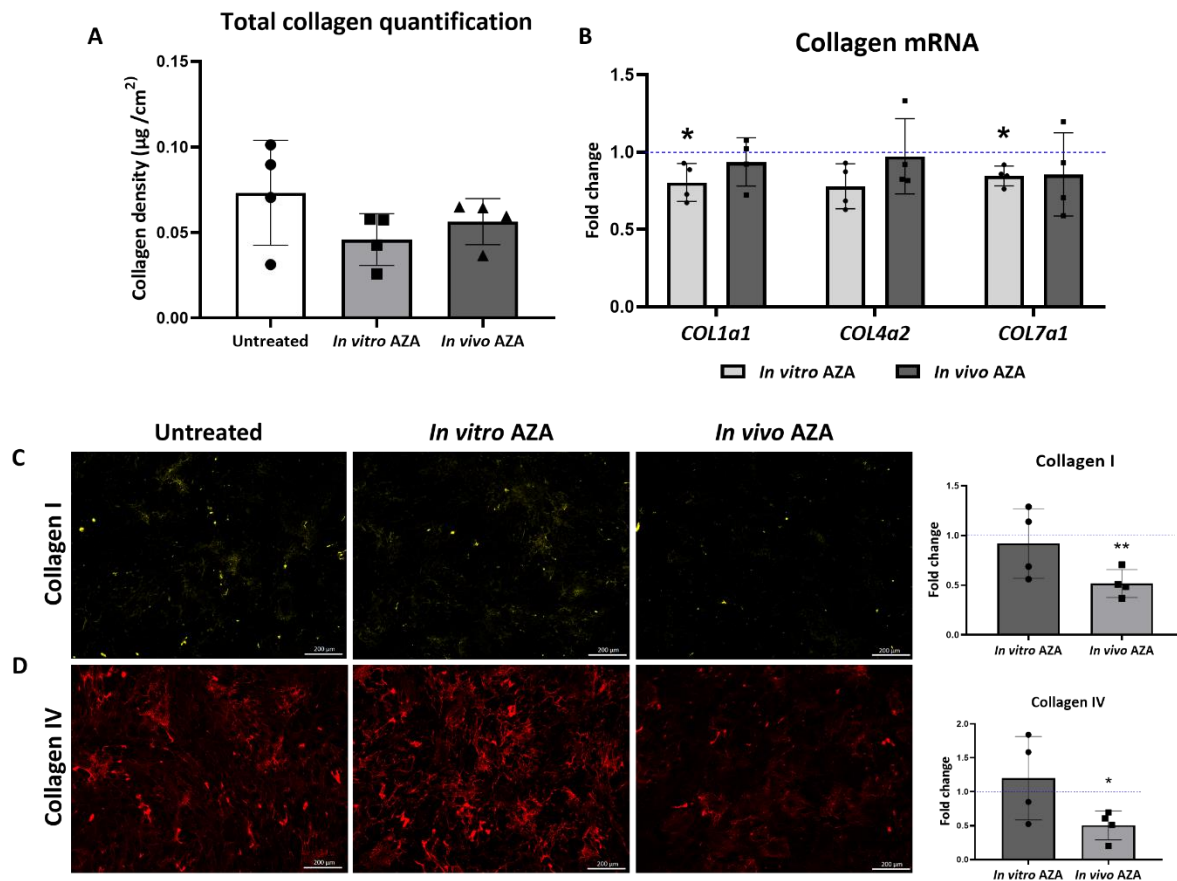


**Figure 27** *In vivo* but not *in vitro* AZA treatment changes the collagen I and IV content of MDS MSC derived ECM. A) Total collagen quantification of the ECM from untreated MDS MSCs as well as after *in vitro* or *in vivo* AZA using sircol assay. B) Gene expression of COL1a1, COL4a2 and COL7a1 analysed by RT-qPCR analysis. C, D) Left: Representative images of collagen I (yellow) and collagen IV (red) immunostaining respectively. Right: Bars represent mean  $\pm$  SD of  $n=4$ , each measured in an independent experiment and expressed as fold change relative to the accompanying untreated MDS MSC ECM control, shown by the dotted line with the ordinate value of 1. An asterisk above the bar indicates significant differences to the control: \* $p < 0.05$  \*\* $p < 0.01$ .

#### 4.4.9. *In vitro* AZA treatment partially alter haematopoietic behaviour of HSPCs on MDS MSC-derived ECM

The functional effect of *in vitro* AZA treatment on MDS MSC-derived ECM on HSPCs was examined. Healthy HSPCs were cultured on different ECM (MDS MSCs at diagnosis and after *in vitro* and *in vivo* AZA treatment) for 7 days and then were analysed for proliferation, cell morphology and colony formation ability. No significant difference was detected in the proliferation of HSPCs on different ECMs (Figure 28A). Interestingly, contradictory to improved support of HSPCs observed on MDS MSC from patients post-AZA therapy observed in 4.4.5, a variable effect of *in vivo* and *in vitro* AZA therapy was observed on the CFU capacity (Figure 28B). Improved colony formation of HSPCs on the ECM from *in vivo* AZA treated MDS MSCs was observed in only one patient out of the four patients analysed indicating the heterogeneity of the disease. This variability in colony formation capacity of the HSPCs on *in vivo* AZA treated MDS MSC derived ECM did not correlate with the AZA treatment response of the patients. Moreover, no increase in the colony formation unit capacity was observed on *in vitro*

AZA treated MDS MSC-derived ECM (Figure 28B). Moreover, polarized morphology of HSPCs on ECM from *in vitro* and *in vivo* AZA treated MDS MSCs was observed when compared to untreated MDS MSCs (Figure 28C) which was similar to that observed in 4.3.2. These partial changes in the HSPC behaviour on both *in vitro* and *in vivo* AZA treated ECM indicates a synergistic direct and indirect effect of AZA on MDS MSC-derived ECM which is independent of the collagen composition of the ECM.

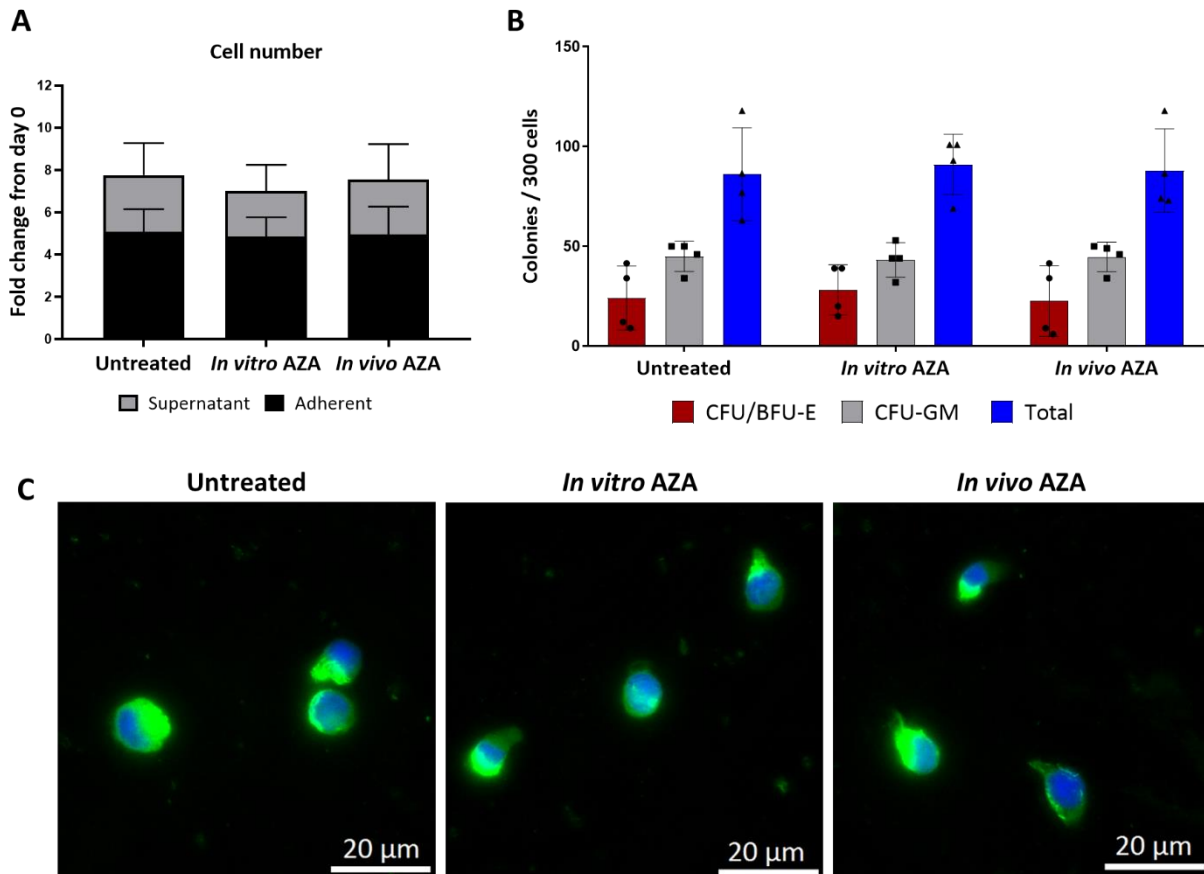


**Figure 28** *In vitro* AZA treatment partially modulated the haematopoietic behaviour of MDS MSC-derived ECM. A) Proliferation of HSPCs on different ECM as determined using trypan blue. The supernatant fraction denotes the cells that were not attached to the ECM whereas the adherent fraction denotes the cells in contact with the ECM. The cell numbers were normalized to the cell number at day 0. B) CFU assay after culturing of HSPCs on ECM from untreated MDS MSCs as well as after *in vitro* or *in vivo* AZA treatment for 7 days. C) Representative images from the immunostaining of HSPCs on ECM substrates using anti-vinculin (green) and DAPI (blue). Bars represent mean  $\pm$  SD for  $n = 4$  samples per group. \* $p < 0.05$

## 5. Discussion

The importance of the BMME and especially of MSC-HSPC interactions in MDS has become increasingly evident in the past decade<sup>16,17,22</sup>. However, the role of MSC-derived ECM is still underexplored. To address this, the reported study investigates the biophysical and biochemical composition of the ECM derived from cultured bone marrow MSCs from MDS patients compared to those from healthy donors. This study also analyses the associated ECM changes in their ability to support HSPCs. This work revealed MDS-associated alterations in the ECM formation by MSCs that were maintained through subsequent culture. These alterations also affected HSPC support.

Moreover, the changes were also investigated in ECM from MSC isolated before and after treatment of MDS patients with AZA and also after subsequent HSCT. This revealed the two stages of therapy to be associated with varying degrees of reversion of ECM phenotype, with a potential to resemble more closely the healthy ECM. This study is one of the first to provide evidence that HMA therapy *in vivo* results in stable changes at the level of MSC-derived ECM that may have functional consequences for support of haematopoiesis.

### 5.1. Phenotypic and transcriptional characteristics of MDS MSCs

The surface marker phenotypes of MSCs cultured from healthy donor and MDS bone marrow were analysed alongside the characterisation of their respective ECMs. Consistent with the results of previous studies<sup>135,136,154</sup>, no difference was observed between the healthy donor and the MDS MSCs for any of the markers CD73, CD90, CD105, CD44, CD146 or CD166 (Figure 7D). Although, this surface marker phenotype is clearly robust, there have been conflicting reports of MDS-associated changes in the properties of bone marrow MSC in terms of both proliferation and differentiation capacity, with accelerated senescence being reported in some studies<sup>15,21,155</sup>. In the experiments described here, no change was observed in the proliferation of MSCs from either LR- or HR-MDS compared to those from healthy donors (Figure 7B, C). Similarly, a number of studies have reported a bias towards adipogenic and away from osteogenic differentiation capacity MDS MSCs<sup>18,155</sup> while others found no difference<sup>15,136</sup>. Again, the study reported here, revealed no consistent difference in the differentiation profile of MDS MSCs compared to those from healthy donors, with effective differentiation into both lineages being retained in all cases (Figure 7E, F). Similarly, the analysis of surface phenotype, growth and differentiation characteristics of MSC isolated from MDS patients before and after treatment with AZA (*in vitro* and *in vivo*) and subsequent HSCT revealed no consistent differences (Figure 20 E, F, and Figure 25E, F). This supports a previous report in which MDS-derived MSC were exposed to AZA *in vitro*<sup>135</sup>. The reason for the apparent inconsistencies in the properties of cultured MSCs reported in

different studies is unclear. Given the heterogeneity of the disease, it is possible that some of the inconsistency between studies is a consequence of differences between the patient groups studied and the relatively small sample numbers available. Indeed, the variation within groups in our studies was often quite large, as may be expected from a heterogeneous disease group. However, it is also likely that the precise culture conditions and particularly the medium and serum used also vary between studies and affects the phenotypes observed. In this respect, it is interesting that the non-targeted RNA Seq analysis of the cultured MSCs in this study identified a decrease in the levels of mRNA for genes in the “osteoblastic differentiation” or “ossification” pathways in LR-MDS and HR-MDS respectively (Figure 14). This suggests that, at the RNA level at least, there may well be a latent tendency for less osteoblastic differentiation in MDS-derived MSC. It is possible that the extent to which these underlying differences in gene expression lead to consistent changes in cell behaviour and may well depend on the precise growth conditions used. The experiments reported here used consistent conditions and a single batch of pre-tested serum in an attempt to minimise such variation.

Gene expression in the cultured MSCs was studied using two approaches: a targeted analysis of ECM associated genes by RT-qPCR to be discussed below and a non-targeted RNA Seq to identify pathways most affected in a non-biased manner. The RNA Seq approach identified a number of processes at the mRNA levels depending on disease status (Figure 14). LR-MDS MSCs were observed to have increased expression of genes involved in inflammation, as well as regulatory transcription factors and a decreased expression of genes involved in osteoblastic differentiation, while HR-MDS MSCs have decreased levels of genes affecting ECM production and cartilage/bone formation. The predicted increase in the expression of inflammatory pathways in LR-MDS MSCs is of high interest, since inflammatory processes are thought to play a decisive role at this stage, with specific changes in inflammatory gene expression in the haematopoietic cells being associated with specific MDS mutations<sup>133,156</sup>. It will be interesting to investigate further the relationship between the haematopoietic and stromal cells in this context. The decreased expression of genes associated with osteoblastic differentiation and osteogenic processes in MDS is interesting, since these processes are generally thought to be negatively affected in MDS. Moreover, in contrast to the ECM proteins analysed in this study, there was a suppression of genes involved in ECM pathways in HR-MDS MSCs. Here, it will be necessary to analyse and validate these findings in more detail in order to identify firstly the specific positive and negative regulators affected in each pathway. Secondly, to identify the extent to which changes at the mRNA level of certain genes are reflected by the corresponding proteins and the concerned pathways. The targeted analysis of ECM related genes at both the mRNA and protein level discussed below suggests that alterations in mRNA often fail to result in changes in the amount or activity of the corresponding protein.

## 5.2. Biophysical alteration in MDS MSC-derived ECM

Next, using a previously developed approach<sup>147</sup>, *in vitro* ECMs were generated by culturing MSC monolayers on POMA-fibronectin coverslips followed by decellularization using NH<sub>4</sub>OH and DNase-1 solution. The ECM generated by healthy donor, LR- and HR-MDS MSCs were then subjected to biophysical, biochemical and functional characterisation.

Alterations were found in the structure and rigidity of the ECM associated with both LR- and HR-MDS MSCs (Figure 8). The ECM deposited by the MDS MSCs was denser and softer (decreased rigidity) than that of the healthy donor derived ECM (Figure 8). These changes were progressive, beginning in LR-MDS and becoming more prominent in HR-MDS, suggesting that they may reflect the quantitative MDS cell load within the marrow. This is not necessarily intuitive, since inflammatory processes tend to reach a peak in LR-MDS and to subside again in the later stages of HR-MDS, presumably reacting to a shift in MDS cell phenotype resulting from clonal selection. Recently, *Xu, Q. et al* observed increased expression and activity of MSC-mediated LOX and LOXL2 in MDS marrow<sup>54</sup>. LOX and LOXL enzymes catalyses the cross-linking of collagen and elastin fibres in the ECM<sup>157</sup>. Increased expression of LOX and LOXL proteins would be expected to lead to an increase in the degree of crosslinking and therefore in the rigidity of the ECM. The MDS-associated increase in LOX/LOXL expression would therefore be expected to increase the rigidity of ECM rather than to lead to a decrease, as was observed in the reported study. Since the rigidity of the ECM can also be modulated by the concentration of ECM proteins, nano-scale fibre deposition, fibre topology and hydration of the ECM<sup>109,158–160</sup>, it seems likely that one or more of these factors more than compensates for any increase in LOX /LOXL expression in the cultured MSCs.

The decreased rigidity of the ECM in MDS was reversed in MSCs isolated from the patients post-AZA therapy (Figure 21B). Similarly, direct exposure of cultured MDS MSCs to AZA also resulted in a corresponding increase in the rigidity of the ECM, although this still remained lower than that observed from MDS MSCs isolated from patients post-AZA therapy (Figure 26B). It therefore seems likely that the AZA-mediated restoration of ECM rigidity is a result of the effect of AZA, both directly on the MSCs and indirectly via effects on the haematopoietic MDS clone.

Modulation of the rigidity of MDS ECM was also observed in MDS MSCs from patients post-HSCT. There was an increased rigidity of the ECM produced by MSCs from patients post-HSCT but it remained lower to that observed in the ECM from the MDS MSCs of the patients post-AZA therapy (Figure 21B). This may be due to the presence of the residual clones in the marrow and post-HSCT related GvHD.

### 5.3. MDS associated changes in the composition of MSC-derived ECM

Alongside the biophysical cues, the ECM also provides biochemical cues governing homing, engraftment, proliferation and differentiation of the cells in a given microenvironment<sup>47,51,52</sup>. Using targeted approaches, a selection of biochemical ECM components including glycoprotein (fibronectin), collagens and GAGs were analysed in the various ECMs generated from the different MSC samples. An immunostaining approach revealed no detectable differences in the fibronectin composition of the ECM from healthy donor and MDS-derived MSCs. However, consistent differences were seen in both collagens and GAGs.

#### 5.3.1. Alterations in collagens

The overall collagen content of ECM was analysed by sircol assay and the specific content of collagens I and IV by immunostaining. Both an increase in total collagen and a specific increase in collagens I and IV were observed in ECM from both LR- and HR-MDS MSCs compared to healthy donor-derived ECM (Figure 10). Interestingly, HR-MDS MSC derived ECM contained a higher level of overall collagen than LR-MDS MSC-derived ECM, but lower amounts of collagens I and IV, which are expected to be among the most prevalent. This firstly suggests that HR-MDS MSCs deposit an increased amount of a collagen species other than I and IV. Secondly, the expression of collagens I and IV peaks at the stage of LR-MDS, together with sterile inflammation. Since collagen gene expression can be affected both positively and negatively by a range of cytokines<sup>161-164</sup>, it is possible that the peak in collagens I and IV is a result of a response to the inflammatory environment of LR-MDS bone marrow. MDS MSCs have previously been reported to have an increased level of in TGFB/ SMAD (mothers against decapentaplegic) signalling<sup>112-114</sup>, which is known to be a potent stimulator of collagen expression<sup>165-167</sup>. Although the inhibition of TGFB signalling in the MDS MSC following treatment with a TGFB-ligand trap has been shown to improve the haematopoietic support of healthy HSPCs by MDS MSCs<sup>112</sup>, the effects on collagen gene expression or collagen deposition have not yet been determined.

While the effects of ligand traps were not analysed here, those of the commonly used HMA, AZA was analysed. Here the effects on the expression and incorporation of collagens into ECM appear to depend strongly on the context. AZA treatment of MDS patients changed the bone marrow MSCs such that they subsequently incorporated less collagen I and IV protein into the ECM, even though, there was no decrease in the corresponding mRNAs in the MSCs (Figure 22B, 27B). This suggests a shift in post-transcriptional regulation that decreases the translation, stability or incorporation into ECM or possibly increases the degradation rate of collagen once incorporated. In contrast, direct exposure of cultured MSCs to AZA for a period of 10 days led to a decrease in mRNA levels of collagen I (*Col1a1*) and IV (*Col4a2*), but not to a reduction in collagen I and IV protein in the ECM (Figure 27B). This suggests



that the isolated MSCs respond to AZA exposure with a reduction in collagen I and IV gene expression combined with a compensatory increase in stability, incorporation or durability of the collagen proteins in the ECM. Furthermore, it would appear that the response to AZA may also depend on the duration of treatment, since a short term 48 hour exposure of healthy donor MSCs to AZA has previously been reported to increase the mRNA levels of *Col1a1* and *Col4a2*<sup>135</sup>, rather than to decrease them, as was seen in the reported study, following the longer 10 day exposure (Figure 27B). These contrasting effects of different treatments demonstrate the multiple levels at which AZA can act both directly on MSCs and indirectly *via* effects on interacting cells in the BMME. This also highlights potential differences between short and long term responses. For this reason, while the potential of AZA to impact the ECM is clear, the complexity of the response is likely to make detailed characterisation of the relevant mechanisms challenging.

### 5.3.2. Alterations in GAGs

No significant changes in the total sulphated GAG content were observed when comparing healthy donor MSC-derived ECM with those from either LR or HR-MDS (Figure 11A). However, significant differences were found between LR- and HR-MDS MSC derived ECM in the content of specific GAG species. Specifically peanut agglutinin, which binds to N-acetyl-galactosamine or terminal  $\beta$ -galactose residues in GAGs such as CS, DS and KS, revealed significantly higher levels in LR- than in HR-MDS samples (Figure 11C). While this was partly due to an increase in LR-MDS, the dominant feature was a strong decrease in the signal in HR-MDS MSC samples. Immunostaining and “stains all” staining of electrophoresed matrix proteins confirmed a significant reduction in CS in HR-MDS derived ECM (Figure 12B). Although the precise relevance of this reduction to the disease state remains unclear, a mouse knockout model of *CSGALNACT1*, reported delayed short-term reconstitution and increased LSK HSPCs in the bone marrow<sup>90</sup>. This suggested that CS is required for controlled haematopoietic differentiation and that a reduction in CS may therefore be involved in the over proliferation of progenitor cells seen in HR-MDS.

Those GAGs that are stained by wheat germ agglutinin, which binds to N-acetyl-glucosamine residues in HA, HS, KS and to sialic acid residues, were also increased as a group in LR-MDS and reduced significantly in HR-MDS (Figure 11B). Here, though, the final levels of these GAGs in the HR-MDS MSC derived ECM were similar to those of ECM from healthy donor MSCs. Specific analysis of HA confirmed that this GAG species was actually significantly higher in both LR and HR-MDS relative to healthy donor. Although increased levels of HA have previously been noted in serum of the HR-MDS patients<sup>168</sup>, both the source and the relevance remain unclear. It is interesting that the gel-electrophoretic analysis of HA revealed a relatively large amount of low molecular weight HA species in one of the LR-MDS

samples (Figure 12D), since LMW-HA tends to be pro-inflammatory, while HMW-HA has the opposite effect<sup>92,94,97</sup>. It is therefore possible that LMW-HA contributes to the inflammatory characteristic of the LR-MDS marrow environment. The significant increase in *IL6* expression induced by the exposure of bone marrow MNCs to LMW-HA together with increases in a range of other inflammation genes that did not reach significance (Figure 15), suggests that this could, at least in principle, contribute to the inflammatory microenvironment in LR-MDS.

Furthermore, AZA treatment, had no effect on the GAG content of ECM as revealed by lectin- and “stains all” gel- staining (Figure 23). This does not rule out potential effects on the sulphation pattern, which can also be decisive for function<sup>169,170</sup>. However, it cannot be detected by agglutinin staining, but it does suggest that AZA primarily effects collagen rather than GAG deposition.

#### **5.4. Functional impact of MDS MSCs-derived ECM on healthy HSPCs**

Characterisation of the interaction of HSPCs with ECM was limited to healthy donor derived HSPCs, since those from MDS patients were not maintained on any of the ECM tested, regardless of source. It is therefore not possible to judge whether or not MDS-derived ECMs may offer a surface particularly supportive of MDS cells. The preferential interaction of HSPCs with the ECM appeared to be comparable, with a similar degree of enrichment of both CD34+ and CD34+/CD117+ cells on all ECM tested. Despite of this, there were clear indications of a compromised interaction between healthy donor HSPCs and MDS-derived ECM, since under these conditions the healthy donor HSPC lost their typical polar morphology as well as a proportion of their colony forming potential, while both were retained on healthy donor derived ECM (Figure 18). This study is among the first to describe an impact of MDS-derived ECM on HSPC behaviour. Although the increase in colony forming potential on MSC-derived ECM from AZA treated patients was not observed in all cases (Figure 24B and Figure 28B) this most likely reflects the heterogeneity of disease. This is similar to the observations of *Xu, Q. et al* where *in vitro* AZA treatment resulted in improved erythroid differentiation in only 25 % of the AZA-treated MDS MSCs samples tested<sup>54</sup>.

The changes in cell morphology of HSPCs cultured on the different ECM (Figure 18A) are in line with previous studies that have already shown the properties of haematopoietic cells to be responsive to changes in substrate rigidity as well as to various ligand and ECM protein coatings<sup>43,46</sup>. Specifically, HSPCs displayed polarized morphology on the stiffer ECM produced by healthy donor MSCs or by MDS MSCs from patient’s post-HSCT, or following *in vitro* or *in vivo* AZA treatment. The non-polarized round morphology was seen on the softer ECM produced by LR- and HR-MDS MSCs. A previous study reported that the polarization of myosin II fibres seen during growth on stiffer matrix resulted in increased asymmetric division<sup>50</sup>. This suggests that there may be a bias towards symmetric division on

softer matrix. Hence, the softer ECM observed in the MDS MSC-derived ECM may drive the symmetric division of the MDS clone, contributing to accumulation of the blasts in the MDS marrow.

The observed changes in cell morphology could also be a result of changes in the ligand density and availability on the denser MDS MSC-derived ECM. CD29 (ITGB1), CD41 (ITGA2), CD51 (ITGAV), CD61 (ITGA3) and hyaluronic receptor CD44 are known to interact with different ECM proteins to regulate maintenance, homing and proliferation of HSPCs<sup>43,147,171,172</sup>. Specifically, Kräter *et.al* observed increase in CD51/61 expression of HSPCs cultured on a decellularized ECM, while other studies have shown a role of CD51/61 in the fate specification of HSPCs<sup>171</sup>. Furthermore, an anti-CD51/61 antibody has been reported both to decrease the CFU potential of HSPCs cultured on fibronectin coated surface<sup>43</sup>, and to reduce the erythroid differentiation potential of HSPCs cultured on decellularized ECM<sup>54</sup>. In contrast to these previous reports, the current study identified no change in the CD51/61 expression of HSPCs cultured on ECM from the various sources. These conflicting observations may be a consequence of differences in the methods employed: integrins bind to ECM target ligands as an active heterodimer complex comprising of an alpha and beta subunit. CD51 can form heterodimers with CD29, CD61, and ITGB5<sup>173</sup>. The antibody used by Kräter *et.al* was raised to a CD51/61 heterodimer. While, two different flow cytometry antibodies for the alpha and beta subunits were used in the current study. This may therefore detect the two integrins regardless of its active stage or its proximity to each other. Moreover, interactions between integrins and non-integrin receptors such as DDR, LAIR-1, and RHAMM within the different ECM cannot be ruled out.

One possible explanation for the altered support provided by MDS ECM for HSPCs could be a change in the ability of the ECM to present growth factors involved in the regulation of cell proliferation and differentiation<sup>51</sup>. However, while pre-loading of ECM with growth factors improved their subsequent support of HSPCs, there was no difference in this respect between ECM derived from healthy donor MSC and that from MDS patient MSCs (Figure 19).

In summary, this study has demonstrated changes in ECM structure, collagen content, and GAG composition between the ECM of MDS and healthy MSCs. This is one of the first to show an impact of MDS-derived ECM on both the morphology and function of HSPCs. The focus on MSC-derived ECM is a clear limitation, since MSCs may highly contribute to the ECM environment of the haematopoietic niche, but are certainly not the only cell type to do so. Future studies should be extended to consider the ECM contributions from other cell types, particularly those of endothelial and osteoblastic lineages. The study presented here provide a starting point for more comprehensive analyses of this nature. Finally, the partial revision of the MDS ECM phenotype following *in vivo* AZA treatment suggests that the ECM itself may be a potential therapeutic target. A more detailed understanding of

the contribution of ECM to disease processes will probably enable us to find novel therapeutic targets to improve drug response in MDS.

## 6. Summary

Dissertation to fulfil the requirements for the academic degree Dr. rer. nat.

“Functional characterisation of the mesenchymal cell derived extracellular matrix in myelodysplastic neoplasms”

Submitted by Amanpreet Kaur Bains

Completed at the University of Leipzig, Medical faculty, Department of Haematology, Cell Therapy and Hemostaseology.

Supervised by Prof. Dr. med. Uwe Platzbecker, Dr. phil. habil. Michael Cross and Dr. rer. nat. Manja Wobus

July 2023

Myelodysplastic neoplasms (MDS) are a group of heterogeneous, clonal disorders characterised by ineffective haematopoiesis and peripheral blood cytopenia. MDS is highly progressive, difficult to treat, and is one of the most common blood cancers, affecting 4-5/100.000 people below the age of 70 and many more thereafter. Single or multiple driver gene mutations and chromosomal abnormalities in the haematopoietic compartment lead to MDS. These somatic gene mutations account for the dysregulation of epigenetic, DNA repair, cohesion complex, and spliceosome pathways. The International prognostic scoring system (IPSS) that was developed in 1997, revised (IPSS-R) in 2016 and updated in 2022 (IPSS-M) classifies MDS into low risk (LR-), intermediate (Int-), and high risk (HR-) groups. The haematopoietic disorder is accompanied by changes in the bone marrow microenvironment (BMME) and especially in mesenchymal cells (MSCs). BMME provides a supportive milieu for haematopoiesis and can be targeted by clinically available drugs such as AZA. The non-cellular component of the BMME, the extracellular matrix (ECM), is a framework providing structural and biochemical support via cell-ECM interactions and the maintenance of growth factor gradients. To date, studies of bone marrow interactions in homeostasis and disease have focused largely on soluble and membrane-associated factors, while the involvement of the ECM in MDS and its response to therapy is underexplored. Therefore, this study aimed to characterise the MDS MSC-derived ECM of both LR- and HR-MDS in comparison to that from healthy age matched donors in terms of composition, biophysical properties and functional haematopoietic support. This study also aimed to evaluate the impact of *in vivo* and *in vitro* AZA treatment on MDS MSC-derived ECM. To investigate this, *in vitro* ECMs were generated by culturing of MSC monolayers on chemically prepared coverslips followed by decellularization using NH<sub>4</sub>OH and DNase-1 solution. The biophysical properties of the ECM were analysed using atomic force microscopy (AFM). Using targeted approaches, a

selection of biochemical ECM components including glycoprotein (fibronectin), collagens and glycosaminoglycans (GAGs) were analysed in the various ECMs generated from the different MSC samples.

AFM analysis revealed that MDS MSCs produce a softer ECM than the healthy donor MSCs, and that this difference becomes more prominent as the disorder progresses from LR- to HR- MDS. An increase in overall collagen content and a specific increase in collagens I and IV was observed in the ECM deposited by both LR- and HR-MDS MSCs when compared to healthy donor MSCs. Lectin staining revealed disease stage-specific differences in GAG composition: The levels of GAGs carrying N-acetyl-glucosamine and those carrying N-acetyl-galactosamine sugars were both increased in ECM from LR-MDS, while ECM from HR-MDS retained high levels of N-acetyl-glucosamine but contained only low levels of N-acetyl-galactosamine GAGs. The changes in N-acetyl-galactosamine and N-acetyl-glucosamine GAGs were further confirmed by chondroitin sulphate (CS) immunostaining, and hyaluronic acid (HA) ELISA respectively. Electrophoretic analysis revealed the presence of low molecular weight (LMW)-HA in one of the LR-MDS MSC-derived ECM. Furthermore, the stimulation of MNCs with LMW-HA showed an increase in gene expression of pro-inflammatory cytokines like *IL6* suggesting the possible involvement of LMW-HA in the inflammatory bone marrow state of LR-MDS. ECM derived from both LR- and HR-MDS MSCs had a reduced ability to support HSPC, as revealed by a loss of both polar morphology and subsequent colony-forming potential.

The decreased rigidity of the ECM produced by MSCs from MDS patients was reversed in MSCs isolated from the patients post-AZA therapy. Similarly, direct exposure of cultured MDS MSCs to AZA also resulted in a corresponding increase in the rigidity of the ECM, although this remained lower than that observed from MDS MSCs isolated post-AZA therapy. A reduction in the collagen content of the ECM was only observed when using MSC from AZA-treated patients, but not following *in vitro* AZA treatment of MSCs from untreated patients. This indicated that the AZA-mediated restoration of ECM rigidity is an indirect result of effects in the context of the BMME and not on the MSCs alone. Interestingly, a few ECMs derived from MDS patients after AZA therapy had an improved ability to maintain functional HSPCs, as assessed by subsequent colony formation assay. Moreover, a polarized morphology of HSPCs cultured on the ECM derived from both *in vivo* and *in vitro* AZA-treated MDS MSCs, suggests a partial restoration of the HSPC behaviour on the AZA-treated MDS ECM.

In conclusion, this study has demonstrated changes in the structure, collagen content, and GAG composition of ECM derived from MSCs from MDS patients compared to healthy donors. This study is one of the first to demonstrate an impact of MDS-derived ECM on both the morphology and function of HSPCs, supporting the relevance of the bone marrow ECM in haematological malignancies. The

partial revision of the MDS ECM phenotype following *in vivo* AZA treatment suggests that the ECM itself may be a potential therapeutic target. An improved, in-depth understanding of the contribution of ECM to disease processes is therefore likely to enable us to find novel therapeutic targets to improve drug response in MDS in the future.

## 7. Zusammenfassung der Arbeit

Dissertation zur Erlangung des akademischen Grades Dr. rer. nat.

“Functional characterisation of the mesenchymal cell derived extracellular matrix in myelodysplastic neoplasms”

eingereicht von: Amanpreet Kaur Bains

angefertigt an der Medizinischen Fakultät der Universität Leipzig, Forschungslabor Hämatologie und Zelltherapie, Arbeitsgruppe Platzbecker/ Cross

betreut von Prof. Dr. med. Uwe Platzbecker, Dr. phil. habil. Michael Cross und Dr. rer. nat. Manja Wobus

Juli 2023

Myelodysplastische Neoplasien (MDS) sind eine Gruppe heterogener, klonaler Erkrankungen, die durch ineffektive Hämatopoese und Zytopenie des peripheren Blutes gekennzeichnet sind. MDS sind hochgradig progressiv, schwer zu behandeln und gehören zu den häufigsten Blutkrebserkrankungen, von denen 4-5/100.000 Menschen unter 70 Jahren betroffen sind. Die Inzidenz steigt mit zunehmendem Alter deutlich an. MDS wird durch einzelne oder mehrfache Mutationen von Treibergenen und Chromosomenanomalien im hämatopoetischen Kompartiment verursacht. Diese somatischen Genmutationen sind für die Dysregulation von epigenetischen, DNA-Reparatur-, Kohäsionskomplex- und Spleißosomen-Signalwegen verantwortlich. Das Internationale Prognosesystem (IPSS) wurde 1997 entwickelt, 2016 überarbeitet (IPSS-R) und 2022 aktualisiert (IPSS-M), um MDS in Gruppen mit niedrigem Risiko (LR-), mittlerem (Int-) und hohem Risiko (HR-) einzuteilen. Die hämatopoetische Erkrankung geht mit Veränderungen in der Mikroumgebung des Knochenmarks (BMME) einher, insbesondere bei mesenchymalen Zellen (MSCs). Das BMME bietet ein unterstützendes Milieu für die Hämatopoese und kann durch klinisch verfügbare Medikamente wie AZA beeinflusst werden. Die nichtzelluläre Komponente der BMME, die extrazelluläre Matrix (ECM), ist ein Gerüst, das durch Zell-ECM-Interaktionen und die Aufrechterhaltung von Wachstumsfaktorgradienten strukturelle und biochemische Unterstützung bietet. Bislang haben sich Studien über die Interaktionen im Knochenmark bei Homöostase und Krankheit hauptsächlich auf lösliche und membranassoziierte Faktoren konzentriert, während die Beteiligung der ECM an MDS und ihre Reaktion auf die Therapie noch nicht ausreichend erforscht ist. Daher zielte diese Studie darauf



ab, die aus MDS-MSCs abgeleitete ECM sowohl bei LR- als auch bei HR-MDS im Vergleich zu der von gesunden, altersgleichen Spendern zu charakterisieren, und zwar hinsichtlich der Zusammensetzung, der biophysikalischen Eigenschaften und der funktionellen hämatopoetischen Unterstützung. Ziel dieser Studie war es auch, die Auswirkungen einer *in vivo* und *in vitro* AZA-Therapie auf die aus MDS-MSCs stammende ECM zu untersuchen. Hierfür wurden *in vitro* ECMs durch Kultivierung von MSC-*Monolayern* auf chemisch-präparierten-Deckgläsern und anschließender Dezellularisierung mit NH<sub>4</sub>OH und DNase-1-Lösung erzeugt. Die biophysikalischen Eigenschaften der ECM wurden mittels Rasterkraftmikroskopie (AFM) analysiert. Mit gezielten Ansätzen wurde eine Auswahl biochemischer ECM-Komponenten, darunter Glykoproteine (Fibronektin), Kollagene und Glykosaminoglykane (GAGs), in den ECMs analysiert.

Die AFM-Analyse ergab eine weichere ECM, die von MDS-MSCs im Vergleich zu gesunden Spender-MSCs gebildet wurde, was mit dem Fortschreiten der Erkrankung von LR- zu HR-MDS noch deutlicher wurde. Sowohl in LR-MDS- als auch in HR-MDS-ECMs wurde im Vergleich zu gesunden Spender-ECMs ein Anstieg des Gesamtkollagengehalts und eine spezifische Zunahme der Kollagene I und IV beobachtet. Darüber hinaus zeigte die Lektinfärbung krankheitsspezifische Unterschiede in der GAG-Zusammensetzung: Der Gehalt an N-Acetylglucosamin-tragenden GAGs und an N-Acetylgalactosamin-tragenden GAGs war in der ECM von LR-MDS erhöht, während die ECM von HR-MDS einen hohen Gehalt an N-Acetylglucosamin, aber nur einen geringen Gehalt an N-Acetylgalactosamin-GAGs aufwies. Die Veränderungen bei den N-Acetyl-Galactosamin- und N-Acetyl-Glucosamin-GAGs wurden durch Chondroitinsulfat (CS)-Immunfärbung bzw. Hyaluronsäure (HA) ELISA weiter bestätigt. Eine Elektrophoretische Analyse zeigte das Vorhandensein von niedermolekularem (LMW)-HA in einer der von LR-MDS-MSCs stammenden ECM. Darüber hinaus zeigte die Stimulierung von mononuklearen Zellen mit LMW-HA einen Anstieg der Genexpression von pro-inflammatorischen Zytokinen wie IL6, was auf eine Rolle von LMW-HA im entzündlichen Zustand des Knochenmarks von LR-MDS hindeutet. Darüber hinaus wies die ECM von LR- und von HR-MDS, eine verminderte Fähigkeit, hämatopoetische Stammvorläuferzellen (HSPCs) zu unterstützen, auf. Dies zeigte sich in einem Verlust sowohl der polaren Morphologie von HSPCs als auch des anschließenden koloniebildenden Potenzials selbiger.

Darüber hinaus wurde die verringerte Steifigkeit der ECM von MDS-MSCs, die nach der AZA-Therapie aus den Patienten isoliert wurden, umgekehrt. In ähnlicher Weise führte die direkte Exposition von kultivierten MDS-MSCs mit AZA zu einer entsprechenden Erhöhung der Steifigkeit der ECM. Diese war jedoch geringer als bei den nach der AZA-Therapie isolierten MDS-MSCs. Die Verringerung des Kollagengehalts der ECM wurde nur in der *in vivo* mit AZA behandelten MSC-ECM beobachtet, nicht aber in den *in vitro* mit AZA behandelten Proben. Dies deutet darauf hin, dass die AZA-vermittelte Wiederherstellung der ECM-Steifigkeit ein Ergebnis der indirekten Wirkung von AZA im Knochenmark

ist und eventuell vom MDS-Klon ausgeht. Interessanterweise wurde bei einigen ECMs von MDS-Patienten nach der AZA-Therapie eine Verbesserung der Koloniebildung hierauf- kultivierter HSPCs beobachtet. Darüber hinaus deutet eine polarisierte Morphologie von HSPCs, die auf der ECM von *in vivo* und *in vitro* AZA-behandelten MDS-MSCs vorkultiviert wurden, auf eine teilweise Wiederherstellung des Verhaltens von HSPCs auf der AZA-behandelten MDS-ECM hin.

Zusammenfassend lässt sich sagen, dass diese Studie Veränderungen in der Struktur, im Kollagengehalt und in der GAG-Zusammensetzung zwischen der ECM von MDS-MSCs und der ECM von gesunden MSCs nachgewiesen hat. Dies ist auch eine der ersten Studien, die einen Einfluss der aus MDS-MSCs stammenden ECM auf die Morphologie und Funktion von HSPCs zeigt. Dies weist auf die Rolle der ECM bei der Entstehung hämatologischer Malignome hin. Darüber hinaus deutet die teilweise Korrektur des MDS-ECM-Phänotyps nach einer *in vivo* AZA-Behandlung darauf hin, dass die ECM selbst ein potenzielles therapeutisches Ziel sein könnte. Ein besseres und tieferes Verständnis des Beitrags der ECM zu MDS-Krankheitsprozessen wird es uns daher ermöglichen, neue therapeutische Ziele zu finden, um das Ansprechen auf Medikamente verbessern zu können.

## 8. Bibliography

1. Seita, J. & Weissman, I. L. Hematopoietic stem cell: self-renewal versus differentiation. *Wiley interdisciplinary reviews. Systems biology and medicine* **2**, 640–653; 10.1002/wsbm.86 (2010).
2. Eaves, C. J. Hematopoietic stem cells: concepts, definitions, and the new reality. *Blood* **125**, 2605–2613; 10.1182/blood-2014-12-570200 (2015).
3. Loeffler, D. & Schroeder, T. Symmetric and asymmetric activation of hematopoietic stem cells. *Current opinion in hematology* **28**, 262–268; 10.1097/MOH.0000000000000644 (2021).
4. Scientific Image and Illustration Software | BioRender. Available at <https://www.biorender.com/> (2023).
5. SanMiguel, J. M., Young, K. & Trowbridge, J. J. Hand in hand: intrinsic and extrinsic drivers of aging and clonal hematopoiesis. *Experimental hematology* **91**, 1–9; 10.1016/j.exphem.2020.09.197 (2020).
6. Jacobs, K. B. *et al.* Detectable clonal mosaicism and its relationship to aging and cancer. *Nature genetics* **44**, 651–658; 10.1038/ng.2270 (2012).
7. Chen, J. *et al.* Myelodysplastic syndrome progression to acute myeloid leukemia at the stem cell level. *Nature Medicine*, 25(1), 103-110. *Nature medicine* **25**; 10.1038/s41591-018-0267-4 (2018).
8. Cypris, O., Božić, T. & Wagner, W. Chicken or Egg: Is Clonal Hematopoiesis Primarily Caused by Genetic or Epigenetic Aberrations? *Front. Genet.* **10**, 785; 10.3389/fgene.2019.00785 (2019).
9. Steensma, D. P. *et al.* Clonal hematopoiesis of indeterminate potential and its distinction from myelodysplastic syndromes. *Blood* **126**, 9–16; 10.1182/blood-2015-03-631747 (2015).
10. Schepers, K., Campbell, T. B. & Passegué, E. Normal and Leukemic Stem Cell Niches: Insights and Therapeutic Opportunities. *Cell Stem Cell*, 16(3), 254-267. *Cell Stem Cell* **16**, 254–267; 10.1016/j.stem.2015.02.014 (2015).
11. Boulais, P. E. & Frenette, P. S. Making sense of hematopoietic stem cell niches. *Blood* **125**, 2621–2629; 10.1182/blood-2014-09-570192 (2015).
12. Morrison, S. J. & Scadden, D. T. The bone marrow niche for haematopoietic stem cells. *Nature* **505**, 327–334; 10.1038/nature12984 (2014).
13. Zhang, P. *et al.* The physical microenvironment of hematopoietic stem cells and its emerging roles in engineering applications. *Stem Cell Res Ther* **10**, 327; 10.1186/s13287-019-1422-7 (2019).
14. Itkin, T. *et al.* Distinct bone marrow blood vessels differentially regulate haematopoiesis. *Nature* **532**, 323–328; 10.1038/nature17624 (2016).
15. Ferrer, R. A. *et al.* Mesenchymal stromal cells from patients with myelodysplastic syndrome display distinct functional alterations that are modulated by lenalidomide. *Haematologica* **98**, 1677–1685; 10.3324/haematol.2013.083972 (2013).
16. Poon, Z. *et al.* Bone marrow MSCs in MDS: contribution towards dysfunctional hematopoiesis and potential targets for disease response to hypomethylating therapy. *Leukemia* **33**, 1487–1500; 10.1038/s41375-018-0310-y (2019).
17. Medyouf, H. *et al.* Myelodysplastic Cells in Patients Reprogram Mesenchymal Stromal Cells to Establish a Transplantable Stem Cell Niche Disease Unit. *Cell Stem Cell*, 14(6), 824-837. *Cell Stem Cell* **14**, 824–837; 10.1016/j.stem.2014.02.014 (2014).

18. Weickert, M.-T. *et al.* Bone marrow stromal cells from MDS and AML patients show increased adipogenic potential with reduced Delta-like-1 expression. *Sci Rep* **11**, 5944; 10.1038/s41598-021-85122-8 (2021).
19. Weidner, H. *et al.* Myelodysplastic syndromes and bone loss in mice and men. *Leukemia* **31**, 1003–1007; 10.1038/leu.2017.7 (2017).
20. Asada, N., Takeishi, S. & Frenette, P. S. Complexity of bone marrow hematopoietic stem cell niche. *International journal of hematology* **106**, 45–54; 10.1007/s12185-017-2262-9 (2017).
21. Zhao, Y. *et al.* Down-regulation of Dicer1 promotes cellular senescence and decreases the differentiation and stem cell-supporting capacities of mesenchymal stromal cells in patients with myelodysplastic syndrome. *1* **100**, 194–204; 10.3324/haematol.2014.109769 (2015).
22. Pleyer, L., Valent, P. & Greil, R. Mesenchymal Stem and Progenitor Cells in Normal and Dysplastic Hematopoiesis—Masters of Survival and Clonality? *International Journal of Molecular Sciences*, 17(7), 1009. *International Journal of Molecular Sciences* **17**; 10.3390/ijms17071009 (2016).
23. Dominici, M. *et al.* Minimal criteria for defining multipotent mesenchymal stromal cells. The International Society for Cellular Therapy position statement. *Cytotherapy* **8**, 315–317; 10.1080/14653240600855905 (2006).
24. Bianco, P., Robey, P. G. & Simmons, P. J. Mesenchymal stem cells: revisiting history, concepts, and assays. *Cell Stem Cell* **2**, 313–319; 10.1016/j.stem.2008.03.002 (2008).
25. Huang, G. T.-J., Gronthos, S. & Shi, S. Mesenchymal stem cells derived from dental tissues vs. those from other sources: their biology and role in regenerative medicine. *Journal of Dental Research* **88**, 792–806; 10.1177/0022034509340867 (2009).
26. Zuk, P. A. *et al.* Multilineage cells from human adipose tissue: implications for cell-based therapies. *Tissue engineering* **7**, 211–228; 10.1089/107632701300062859 (2001).
27. Pinho, S. *et al.* PDGFR $\alpha$  and CD51 mark human nestin+ sphere-forming mesenchymal stem cells capable of hematopoietic progenitor cell expansion. *J Exp Med* **210**, 1351–1367; 10.1084/jem.20122252 (2013).
28. Pinho, S. & Frenette, P. S. Haematopoietic stem cell activity and interactions with the niche. *Nature reviews. Molecular cell biology* **20**, 303–320; 10.1038/s41580-019-0103-9 (2019).
29. Bernardo, M. E., Locatelli, F. & Fibbe, W. E. Mesenchymal stromal cells. *Annals of the New York Academy of Sciences* **1176**, 101–117; 10.1111/j.1749-6632.2009.04607.x (2009).
30. Klein, G. The extracellular matrix of the hematopoietic microenvironment. *Experientia* **51**, 914–926; 10.1007/BF01921741 (1995).
31. Weber, J. M. & Calvi, L. M. Notch signaling and the bone marrow hematopoietic stem cell niche. *Bone* **46**, 281–285; 10.1016/j.bone.2009.08.007 (2010).
32. Ciuculescu, M. F. *et al.* Perivascular deletion of murine Rac reverses the ratio of marrow arterioles and sinusoid vessels and alters hematopoiesis in vivo. *Blood* **125**, 3105–3113; 10.1182/blood-2014-10-604892 (2015).
33. Banerjee, T., Calvi, L. M., Becker, M. W. & Liesveld, J. L. Flaming and fanning: The Spectrum of inflammatory influences in myelodysplastic syndromes. *Blood Reviews* **36**, 57–69; 10.1016/j.blre.2019.04.004 (2019).
34. Flores-Figueroa, E., Varma, S., Montgomery, K., Greenberg, P. L. & Gratzinger, D. Distinctive contact between CD34+ hematopoietic progenitors and CXCL12+ CD271+ mesenchymal stromal

- cells in benign and myelodysplastic bone marrow. *Laboratory investigation; a journal of technical methods and pathology* **92**, 1330–1341; 10.1038/labinvest.2012.93 (2012).
35. Muth, C. A., Steinl, C., Klein, G. & Lee-Thedieck, C. Regulation of hematopoietic stem cell behavior by the nanostructured presentation of extracellular matrix components. *PLOS ONE* **8**, e54778; 10.1371/journal.pone.0054778 (2013).
36. Ding, L., Saunders, T. L., Enikolopov, G. & Morrison, S. J. Endothelial and perivascular cells maintain haematopoietic stem cells. *Nature* **481**, 457–462; 10.1038/nature10783 (2012).
37. Netelenbos, T. *et al.* Proteoglycans on bone marrow endothelial cells bind and present SDF-1 towards hematopoietic progenitor cells. *Leukemia* **17**, 175–184; 10.1038/sj.leu.2402738 (2003).
38. Ricard-Blum, S. Protein–glycosaminoglycan interaction networks: Focus on heparan sulfate. *Perspectives in Science* **11**, 62–69; 10.1016/j.pisc.2016.10.004 (2017).
39. Smock, R. G. & Meijers, R. Roles of glycosaminoglycans as regulators of ligand/receptor complexes. *Open biology* **8**; 10.1098/rsob.180026 (2018).
40. Lee-Thedieck, C., Schertl, P. & Klein, G. The extracellular matrix of hematopoietic stem cell niches. *Advanced Drug Delivery Reviews* **181**, 114069; 10.1016/j.addr.2021.114069 (2022).
41. Gupta, P. *et al.* Human LTC-IC can be maintained for at least 5 weeks in vitro when interleukin-3 and a single chemokine are combined with O-sulfated heparan sulfates: requirement for optimal binding interactions of heparan sulfate with early-acting cytokines and matrix proteins. *Blood* **95**, 147–155; 10.1182/blood.V95.1.147 (2000).
42. Zanetti, C. & Krause, D. S. "Caught in the net": the extracellular matrix of the bone marrow in normal hematopoiesis and leukemia. *Experimental hematology* **89**, 13–25; 10.1016/j.exphem.2020.07.010 (2020).
43. Choi, J. S. & Harley, B. A. C. Marrow-inspired matrix cues rapidly affect early fate decisions of hematopoietic stem and progenitor cells. *Science Advances* **3**, e1600455; 10.1126/sciadv.1600455 (2017).
44. Lee-Thedieck, C. & Spatz, J. P. Biophysical regulation of hematopoietic stem cells. *Biomater. Sci.* **2**, 1548–1561; 10.1039/C4BM00128A (2014).
45. Gvaramia, D. *et al.* Combined influence of biophysical and biochemical cues on maintenance and proliferation of hematopoietic stem cells. *Biomaterials* **138**, 108–117; 10.1016/j.biomaterials.2017.05.023 (2017).
46. Li, W. *et al.* Biophysical cues of bone marrow-inspired scaffolds regulate hematopoiesis of hematopoietic stem and progenitor cells. *Biomaterials* **298**, 122111; 10.1016/j.biomaterials.2023.122111 (2023).
47. Choi, J. S. & Harley, B. A. C. The combined influence of substrate elasticity and ligand density on the viability and biophysical properties of hematopoietic stem and progenitor cells. *Biomaterials* **33**, 4460–4468; 10.1016/j.biomaterials.2012.03.010 (2012).
48. Jansen, L. E., Birch, N. P., Schiffman, J. D., Crosby, A. J. & Peyton, S. R. Mechanics of intact bone marrow. *Journal of the mechanical behavior of biomedical materials* **50**, 299–307; 10.1016/j.jmbbm.2015.06.023 (2015).
49. Holst, J. *et al.* Substrate elasticity provides mechanical signals for the expansion of hemopoietic stem and progenitor cells. *Nat Biotechnol* **28**, 1123–1128; 10.1038/nbt.1687 (2010).

50. Shin, J.-W. *et al.* Contractile forces sustain and polarize hematopoiesis from stem and progenitor cells. *Cell Stem Cell* **14**, 81–93; 10.1016/j.stem.2013.10.009 (2014).
51. Hynes, R. O. The extracellular matrix: not just pretty fibrils. *Science* **326**, 1216–1219; 10.1126/science.1176009 (2009).
52. Silver, I. A., Murrills, R. J. & Etherington, D. J. Microelectrode studies on the acid microenvironment beneath adherent macrophages and osteoclasts. *Experimental Cell Research* **175**, 266–276; 10.1016/0014-4827(88)90191-7 (1988).
53. Glavey, S. V. *et al.* Proteomic characterization of human multiple myeloma bone marrow extracellular matrix. *Leukemia* **31**, 2426–2434; 10.1038/leu.2017.102 (2017).
54. Xu, Q. *et al.* Inhibition of lysyl oxidases synergizes with 5-azacytidine to restore erythropoiesis in myelodysplastic and myeloid malignancies. *Nature communications* **14**, 1497; 10.1038/s41467-023-37175-8 (2023).
55. Slany, A. *et al.* Extracellular matrix remodeling by bone marrow fibroblast-like cells correlates with disease progression in multiple myeloma. *Journal of proteome research* **13**, 844–854; 10.1021/pr400881p (2014).
56. Ehninger, A. *et al.* Loss of SPARC protects hematopoietic stem cells from chemotherapy toxicity by accelerating their return to quiescence. *Blood* **123**, 4054–4063; 10.1182/blood-2013-10-533711 (2014).
57. Nakamura-Ishizu, A. *et al.* Extracellular matrix protein tenascin-C is required in the bone marrow microenvironment primed for hematopoietic regeneration. *Blood* **119**, 5429–5437; 10.1182/blood-2011-11-393645 (2012).
58. Bhatia, R. Contact with fibronectin enhances preservation of normal but not chronic myelogenous leukemia primitive hematopoietic progenitors. *Experimental Hematology* **30**, 324–332; 10.1016/S0301-472X(01)00799-8 (2002).
59. Susek, K. H. *et al.* Bone marrow laminins influence hematopoietic stem and progenitor cell cycling and homing to the bone marrow. *Matrix biology : journal of the International Society for Matrix Biology* **67**, 47–62; 10.1016/j.matbio.2018.01.007 (2018).
60. Dao, M. A., Hashino, K., Kato, I. & Nolte, J. A. Adhesion to fibronectin maintains regenerative capacity during ex vivo culture and transduction of human hematopoietic stem and progenitor cells. *Blood* **92**, 4612–4621 (1998).
61. Kerst, J. M. *et al.* Alpha 4 beta 1 and alpha 5 beta 1 are differentially expressed during myelopoiesis and mediate the adherence of human CD34+ cells to fibronectin in an activation-dependent way. *Blood* **81**, 344–351; 10.1182/blood.V81.2.344.344 (1993).
62. Mao, Y. & Schwarzbauer, J. E. Fibronectin fibrillogenesis, a cell-mediated matrix assembly process. *Matrix Biology* **24**, 389–399; 10.1016/j.matbio.2005.06.008 (2005).
63. Nilsson, S. K. *et al.* Immunofluorescence Characterization of Key Extracellular Matrix Proteins in Murine Bone Marrow In Situ. *J Histochem Cytochem.* **46**, 371–377; 10.1177/002215549804600311 (1998).
64. Schneider, R. K. *et al.* Activated fibronectin-secretory phenotype of mesenchymal stromal cells in pre-fibrotic myeloproliferative neoplasms. *J Hematol Oncol* **7**, 92; 10.1186/s13045-014-0092-2 (2014).

65. Kibler, C. *et al.* Adhesive interactions of human multiple myeloma cell lines with different extracellular matrix molecules. *Cell adhesion and communication* **5**, 307–323; 10.3109/15419069809040300 (1998).
66. Ellis, S. L. *et al.* The role of Tenascin C in the lymphoid progenitor cell niche. *Experimental hematology* **41**, 1050–1061; 10.1016/j.exphem.2013.09.009 (2013).
67. Sakai, T., Ohta, M., Kawakatsu, H., Furukawa, Y. & Saito, M. Tenascin-C induction in Whitlock-Witte culture: a relevant role of the thiol moiety in lymphoid-lineage differentiation. *Experimental Cell Research* **217**, 395–403; 10.1006/excr.1995.1102 (1995).
68. Klein, G., Beck, S. & Müller, C. A. Tenascin is a cytoadhesive extracellular matrix component of the human hematopoietic microenvironment. *The Journal of cell biology* **123**, 1027–1035; 10.1083/jcb.123.4.1027 (1993).
69. Soini, Y., Kamel, D., Apaja-Sarkkinen, M., Virtanen, I. & Lehto, V. P. Tenascin immunoreactivity in normal and pathological bone marrow. *Journal of Clinical Pathology* **46**, 218–221; 10.1136/jcp.46.3.218 (1993).
70. Seiffert, M. *et al.* Mitogenic and adhesive effects of tenascin-C on human hematopoietic cells are mediated by various functional domains. *Matrix Biology* **17**, 47–63; 10.1016/S0945-053X(98)90124-X (1998).
71. Luo, Z. *et al.* SPARC promotes the development of erythroid progenitors. *Experimental hematology* **40**, 828–836; 10.1016/j.exphem.2012.06.002 (2012).
72. Park, M. *et al.* Reduced expression of osteonectin and increased natural killer cells may contribute to the pathophysiology of aplastic anemia. *Applied immunohistochemistry & molecular morphology : AIMM* **23**, 139–145; 10.1097/PAI.0000000000000023 (2015).
73. Aumailley, M. *et al.* A simplified laminin nomenclature. *Matrix biology : journal of the International Society for Matrix Biology* **24**, 326–332; 10.1016/j.matbio.2005.05.006 (2005).
74. Gu, Y.-C. *et al.* Laminin isoform-specific promotion of adhesion and migration of human bone marrow progenitor cells. *Blood* **101**, 877–885; 10.1182/blood-2002-03-0796 (2003).
75. Siler, U. *et al.* Characterization and functional analysis of laminin isoforms in human bone marrow. *Blood* **96**, 4194–4203 (2000).
76. Montuori, N. *et al.* Expression of the 67-kDa laminin receptor in acute myeloid leukemia cells mediates adhesion to laminin and is frequently associated with monocytic differentiation. *Clinical cancer research : an official journal of the American Association for Cancer Research* **5**, 1465–1472 (1999).
77. Couchman, J. R. & Pataki, C. A. An introduction to proteoglycans and their localization. *The journal of histochemistry and cytochemistry : official journal of the Histochemistry Society* **60**, 885–897; 10.1369/0022155412464638 (2012).
78. Kjellén, L. & Lindahl, U. Proteoglycans: structures and interactions. *Annual review of biochemistry* **60**, 443–475; 10.1146/annurev.bi.60.070191.002303 (1991).
79. Zhang, L. Glycosaminoglycan (GAG) Biosynthesis and GAG-Binding Proteins. *Progress in molecular biology and translational science* **93**, 1–17; 10.1016/S1877-1173(10)93001-9 (2010).
80. Salbach-Hirsch, J., Rauner, M., Hofbauer, C. & Hofbauer, L. C. New insights into the role of glycosaminoglycans in the endosteal bone microenvironment. *Biological Chemistry* **402**, 1415–1425; 10.1515/hsz-2021-0174 (2021).

81. Gupta, P. *et al.* Structurally Specific Heparan Sulfates Support Primitive Human Hematopoiesis by Formation of a Multimolecular Stem Cell Niche. *Blood* **92**, 4641–4651; 10.1182/blood.V92.12.4641 (1998).
82. Ichii, M., Frank, M. B., Iozzo, R. V. & Kincade, P. W. The canonical Wnt pathway shapes niches supportive of hematopoietic stem/progenitor cells. *Blood* **119**, 1683–1692; 10.1182/blood-2011-07-369199 (2012).
83. Papy-Garcia, D. & Albanese, P. Heparan sulfate proteoglycans as key regulators of the mesenchymal niche of hematopoietic stem cells. *Glycoconjugate journal* **34**, 377–391; 10.1007/s10719-017-9773-8 (2017).
84. Mansouri, R. *et al.* Osteoblastic heparan sulfate glycosaminoglycans control bone remodeling by regulating Wnt signaling and the crosstalk between bone surface and marrow cells. *Cell death & disease* **8**, e2902; 10.1038/cddis.2017.287 (2017).
85. Shekels, L. L., Buelt-Gebhardt, M. & Gupta, P. Effect of systemic heparan sulfate haploinsufficiency on steady state hematopoiesis and engraftment of hematopoietic stem cells. *Blood cells, molecules & diseases* **55**, 3–9; 10.1016/j.bcmed.2015.03.001 (2015).
86. Wight, T. N., Kinsella, M. G., Keating, A. & Singer, J. W. Proteoglycans in human long-term bone marrow cultures: biochemical and ultrastructural analyses. *Blood* **67**, 1333–1343 (1986).
87. Evanko, S. P., Potter-Perigo, S., Bollyky, P. L., Nepom, G. T. & Wight, T. N. Hyaluronan and versican in the control of human T-lymphocyte adhesion and migration. *Matrix biology : journal of the International Society for Matrix Biology* **31**, 90–100; 10.1016/j.matbio.2011.10.004 (2012).
88. Wight, T. N. *et al.* Versican-A Critical Extracellular Matrix Regulator of Immunity and Inflammation. *Frontiers in immunology* **11**, 512; 10.3389/fimmu.2020.00512 (2020).
89. Ustyuzhanina, N. E. *et al.* Chondroitin Sulfate and Fucosylated Chondroitin Sulfate as Stimulators of Hematopoiesis in Cyclophosphamide-Induced Mice. *Pharmaceuticals* **14**; 10.3390/ph14111074 (2021).
90. Katagiri, T. *et al.* Distinct effects of chondroitin sulfate on hematopoietic cells and the stromal microenvironment in bone marrow hematopoiesis. *Experimental hematology* **96**, 52-62.e5; 10.1016/j.exphem.2021.02.003 (2021).
91. Goncharova, V. *et al.* Hyaluronan expressed by the hematopoietic microenvironment is required for bone marrow hematopoiesis. *The Journal of biological chemistry* **287**, 25419–25433; 10.1074/jbc.M112.376699 (2012).
92. Lee, B. M., Park, S. J., Noh, I. & Kim, C.-H. The effects of the molecular weights of hyaluronic acid on the immune responses. *Biomater Res* **25**, 27; 10.1186/s40824-021-00228-4 (2021).
93. Schraufstatter, I. U., Seroby, N., Loring, J. & Khaldoyanidi, S. K. Hyaluronan is required for generation of hematopoietic cells during differentiation of human embryonic stem cells. *Journal of stem cells* **5**, 9–21 (2010).
94. Rayahin, J. E., Buhrman, J. S., Zhang, Y., Koh, T. J. & Gemeinhart, R. A. High and low molecular weight hyaluronic acid differentially influence macrophage activation. *ACS biomaterials science & engineering* **1**, 481–493; 10.1021/acsbiomaterials.5b00181 (2015).
95. Khaldoyanidi, S. K., Goncharova, V., Mueller, B. & Schraufstatter, I. U. Hyaluronan in the healthy and malignant hematopoietic microenvironment. In *Advances in Cancer Research : Hyaluronan Signaling and Turnover*, edited by M. A. Simpson & P. Heldin (Academic Press 2014), Vol. 123, pp. 149–189.



96. Zhang, Y. W. *et al.* Hyaluronic acid-GPRC5C signalling promotes dormancy in haematopoietic stem cells. *Nat Cell Biol* **24**, 1038–1048; 10.1038/s41556-022-00931-x (2022).
97. Cyphert, J. M., Trempus, C. S. & Garantzotis, S. Size Matters: Molecular Weight Specificity of Hyaluronan Effects in Cell Biology. *International Journal of Cell Biology* **2015**, 563818; 10.1155/2015/563818 (2015).
98. Anagnostopoulou, E. *et al.* Serum Hyaluronic Acid Levels Are Altered in Acute Leukemia Patients: Potential Prognostic Implications. *Acta haematologica* **138**, 44–51; 10.1159/000477574 (2017).
99. Lomparđía, S. *et al.* Hyaluronan abrogates imatinib-induced senescence in chronic myeloid leukemia cell lines. *Scientific reports* **9**, 10930; 10.1038/s41598-019-47248-8 (2019).
100. Krause, D. S., Lazarides, K., Andrian, U. H. von & van Etten, R. A. Requirement for CD44 in homing and engraftment of BCR-ABL-expressing leukemic stem cells. *Nature medicine* **12**, 1175–1180; 10.1038/nm1489 (2006).
101. Fedorchenko, O. *et al.* CD44 regulates the apoptotic response and promotes disease development in chronic lymphocytic leukemia. *Blood* **121**, 4126–4136; 10.1182/blood-2012-11-466250 (2013).
102. Onoda, M., Nakaseko, C., Yokota, A. & Saito, Y. Ligation of CD44 with low-molecular-weight hyaluronan and a monoclonal antibody leads to inhibition of drug-induced apoptosis in a human myeloid cell line. *Hematology* **14**, 213–219; 10.1179/102453309X426236 (2009).
103. Viola, M. *et al.* Biology and biotechnology of hyaluronan. *Glycoconj J* **32**, 93–103; 10.1007/s10719-015-9586-6 (2015).
104. Mikami, T. & Kitagawa, H. Biosynthesis and function of chondroitin sulfate. *Biochimica et Biophysica Acta* **1830**, 4719–4733; 10.1016/j.bbagen.2013.06.006 (2013).
105. Jedrzejewski, M. J. & Stern, R. Structures of vertebrate hyaluronidases and their unique enzymatic mechanism of hydrolysis. *Proteins: Structure, Function, and Bioinformatics* **61**, 227–238; 10.1002/prot.20592 (2005).
106. Sasisekharan, R., Bulmer, M., Moremen, K. W., Cooney, C. L. & Langer, R. Cloning and expression of heparinase I gene from *Flavobacterium heparinum*. *Proceedings of the National Academy of Sciences of the United States of America* **90**, 3660–3664; 10.1073/pnas.90.8.3660 (1993).
107. Ricard-Blum, S. The collagen family. *Cold Spring Harbor perspectives in biology* **3**, a004978; 10.1101/cshperspect.a004978 (2011).
108. Leitinger, B. Transmembrane collagen receptors. *Annual review of cell and developmental biology* **27**, 265–290; 10.1146/annurev-cellbio-092910-154013 (2011).
109. Asgari, M., Latifi, N., Heris, H. K., Vali, H. & Mongeau, L. In vitro fibrillogenesis of tropocollagen type III in collagen type I affects its relative fibrillar topology and mechanics. *Sci Rep* **7**, 1392; 10.1038/s41598-017-01476-y (2017).
110. Çelebi, B., Pineault, N. & Mantovani, D. The Role of Collagen Type I on Hematopoietic and Mesenchymal Stem Cells Expansion and Differentiation. *AMR* **409**, 111–116; 10.4028/www.scientific.net/AMR.409.111 (2011).
111. Malara, A. *et al.* Megakaryocytes contribute to the bone marrow-matrix environment by expressing fibronectin, type IV collagen, and laminin. *Stem cells (Dayton, Ohio)* **32**, 926–937; 10.1002/stem.1626 (2014).

112. Wobus, M. *et al.* Luspatercept restores SDF-1-mediated hematopoietic support by MDS-derived mesenchymal stromal cells. *Leukemia*, 1–12; 10.1038/s41375-021-01275-5 (2021).
113. Sarhan, D. *et al.* Mesenchymal stromal cells shape the MDS microenvironment by inducing suppressive monocytes that dampen NK cell function. *JCI Insight* **5**; 10.1172/jci.insight.130155 (2020).
114. Geyh, S. *et al.* Transforming growth factor  $\beta$ 1-mediated functional inhibition of mesenchymal stromal cells in myelodysplastic syndromes and acute myeloid leukemia. *1* **103**, 1462–1471; 10.3324/haematol.2017.186734 (2018).
115. Koenigsman, M., Griffin, J. D., DiCarlo, J. & Cannistra, S. A. Myeloid and erythroid progenitor cells from normal bone marrow adhere to collagen type I. *Blood* **79**, 657–665 (1992).
116. Oswald, J. *et al.* Gene-expression profiling of CD34+ hematopoietic cells expanded in a collagen I matrix. *STEM CELLS* **24**, 494–500; 10.1634/stemcells.2005-0276 (2006).
117. Balduini, A. *et al.* Adhesive receptors, extracellular proteins and myosin IIA orchestrate proplatelet formation by human megakaryocytes. *Journal of thrombosis and haemostasis : JTH* **6**, 1900–1907; 10.1111/j.1538-7836.2008.03132.x (2008).
118. Semeniak, D. *et al.* Proplatelet formation is selectively inhibited by collagen type I through Syk-independent GPVI signaling. *J Cell Sci* **129**, 3473–3484; 10.1242/jcs.187971 (2016).
119. Naci, D., Berrazouane, S., Barabé, F. & Aoudjit, F. Cell adhesion to collagen promotes leukemia resistance to doxorubicin by reducing DNA damage through the inhibition of Rac1 activation. *Sci Rep* **9**, 19455; 10.1038/s41598-019-55934-w (2019).
120. Naci, D. *et al.*  $\alpha$ 2 $\beta$ 1 integrin promotes chemoresistance against doxorubicin in cancer cells through extracellular signal-regulated kinase (ERK). *Journal of Biological Chemistry* **287**, 17065–17076; 10.1074/jbc.M112.349365 (2012).
121. Ogana, H. *et al.* The Role of Integrin Beta-1 in the Chemoresistance of Acute Myeloid Leukemia. *Blood* **140**, 8799–8800; 10.1182/blood-2022-167902 (2022).
122. Aref, S. *et al.* Elevated serum endostatin levels are associated with favorable outcome in acute myeloid leukemia. *Hematology* **13**, 95–100; 10.1179/102453308X315898 (2008).
123. Litwin, C. *et al.* Role of the microenvironment in promoting angiogenesis in acute myeloid leukemia. *American journal of hematology* **70**, 22–30; 10.1002/ajh.10092 (2002).
124. Cazzola, M. Myelodysplastic Syndromes. *The New England journal of medicine* **383**, 1358–1374; 10.1056/NEJMra1904794 (2020).
125. Adès, L., Itzykson, R. & Fenaux, P. Myelodysplastic syndromes. *The Lancet*, 383(9936), 2239–2252. *The Lancet* **383**, 2239–2252; 10.1016/S0140-6736(13)61901-7 (2014).
126. Elias, H. K. *et al.* Stem cell origin of myelodysplastic syndromes. *Oncogene* **33**, 5139–5150; 10.1038/onc.2013.520 (2014).
127. Bernard, E. *et al.* Molecular International Prognostic Scoring System for Myelodysplastic Syndromes. *NEJM Evidence* **1**; 10.1056/EVIDoa2200008 (2022).
128. Arber, D. A. *et al.* The 2016 revision to the World Health Organization classification of myeloid neoplasms and acute leukemia. *Blood* **127**, 2391–2405; 10.1182/blood-2016-03-643544 (2016).

129. Pfeilstöcker, M. *et al.* Time-dependent changes in mortality and transformation risk in MDS. *Blood* **128**, 902–910; 10.1182/blood-2016-02-700054 (2016).
130. Geyh, S. *et al.* Insufficient stromal support in MDS results from molecular and functional deficits of mesenchymal stromal cells. *Leukemia* **27**, 1841–1851; 10.1038/leu.2013.193 (2013).
131. Platzbecker, U. Treatment of MDS. *Blood* **133**, 1096–1107; 10.1182/blood-2018-10-844696 (2019).
132. Platzbecker, U., Kubasch, A. S., Homer-Bouthiette, C. & Prebet, T. Current challenges and unmet medical needs in myelodysplastic syndromes. *Leukemia* **35**, 2182–2198; 10.1038/s41375-021-01265-7 (2021).
133. Schneider, M. *et al.* Activation of distinct inflammatory pathways in subgroups of LR-MDS. *Leukemia*, 1–10; 10.1038/s41375-023-01949-2 (2023).
134. University of Leipzig & Novartis Pharmaceuticals. A Phase II, Single-Arm, Open-Label Study to Assess the Efficacy and Safety of Canakinumab for the Treatment of Anemia in Patients With IPSS-R Very Low, Low, or Intermediate Risk Myelodysplastic Syndromes or MDS/MPN. NCT05237713, CANFIRE. Available at <https://clinicaltrials.gov/ct2/show/NCT05237713> (2022).
135. Wenk, C. *et al.* Direct modulation of the bone marrow mesenchymal stromal cell compartment by azacitidine enhances healthy hematopoiesis. *Blood Adv* **2**, 3447–3461; 10.1182/bloodadvances.2018022053 (2018).
136. Zhao, Z.-G. *et al.* Functional characteristics of mesenchymal stem cells derived from bone marrow of patients with myelodysplastic syndromes. *Cancer Letters* **317**, 136–143; 10.1016/j.canlet.2011.08.030 (2012).
137. Pronk, E. & Raaijmakers, M. H. G. P. The mesenchymal niche in MDS. *Blood* **133**, 1031–1038; 10.1182/blood-2018-10-844639 (2019).
138. Wang, L. *et al.* Notch-dependent repression of miR-155 in the bone marrow niche regulates hematopoiesis in an NF- $\kappa$ B-dependent manner. *Cell Stem Cell* **15**, 51–65; 10.1016/j.stem.2014.04.021 (2014).
139. Stoddart, A. *et al.* Inhibition of WNT signaling in the bone marrow niche prevents the development of MDS in the *Apc<sup>del/+</sup>* MDS mouse model. *Blood* **129**, 2959–2970; 10.1182/blood-2016-08-736454 (2017).
140. Vallée, A. & Lecarpentier, Y. Crosstalk Between Peroxisome Proliferator-Activated Receptor Gamma and the Canonical WNT/ $\beta$ -Catenin Pathway in Chronic Inflammation and Oxidative Stress During Carcinogenesis. *Front. Immunol.* **9**, 745; 10.3389/fimmu.2018.00745 (2018).
141. Wang, J. & Xiao, Z. Mesenchymal stem cells in pathogenesis of myelodysplastic syndromes. *Stem Cell Investigation* **1**, 16; 10.3978/j.issn.2306-9759.2014.08.02 (2014).
142. Raaijmakers, M. H. G. P. *et al.* Bone progenitor dysfunction induces myelodysplasia and secondary leukaemia. *Nature* **464**, 852–857; 10.1038/nature08851 (2010).
143. Blau, O. *et al.* Mesenchymal stromal cells of myelodysplastic syndrome and acute myeloid leukemia patients have distinct genetic abnormalities compared with leukemic blasts. *Blood* **118**, 5583–5592; 10.1182/blood-2011-03-343467 (2011).
144. Chen, S. *et al.* Massive parallel RNA sequencing of highly purified mesenchymal elements in low-risk MDS reveals tissue-context-dependent activation of inflammatory programs. *Leukemia* **30**, 1938–1942; 10.1038/leu.2016.91 (2016).

145. Winter, S., Shoaie, S., Kordasti, S. & Platzbecker, U. Integrating the "Immunome" in the Stratification of Myelodysplastic Syndromes and Future Clinical Trial Design. *Journal of clinical oncology : official journal of the American Society of Clinical Oncology* **38**, 1723–1735; 10.1200/JCO.19.01823 (2020).
146. Hempel, U. *et al.* Human Bone Marrow Stromal Cells: A Reliable, Challenging Tool for In Vitro Osteogenesis and Bone Tissue Engineering Approaches. *Stem cells international* **2016**, 7842191; 10.1155/2016/7842191 (2016).
147. Prewitz, M. C. *et al.* Tightly anchored tissue-mimetic matrices as instructive stem cell microenvironments. *Nat Methods* **10**, 788–794; 10.1038/nmeth.2523 (2013).
148. Rother, S. *et al.* Bioinspired Collagen/Glycosaminoglycan-Based Cellular Microenvironments for Tuning Osteoclastogenesis. *ACS applied materials & interfaces* **7**, 23787–23797; 10.1021/acsami.5b08419 (2015).
149. Stokowy, T. *et al.* Analysis options for high-throughput sequencing in miRNA expression profiling. *BMC research notes* **7**, 144; 10.1186/1756-0500-7-144 (2014).
150. Kim, D., Langmead, B. & Salzberg, S. L. HISAT: a fast spliced aligner with low memory requirements. *Nature methods* **12**, 357–360; 10.1038/nmeth.3317 (2015).
151. Pertea, M., Kim, D., Pertea, G. M., Leek, J. T. & Salzberg, S. L. Transcript-level expression analysis of RNA-seq experiments with HISAT, StringTie and Ballgown. *Nature protocols* **11**, 1650–1667; 10.1038/nprot.2016.095 (2016).
152. Love, M. I., Huber, W. & Anders, S. Moderated estimation of fold change and dispersion for RNA-seq data with DESeq2. *Genome biology* **15**, 550; 10.1186/s13059-014-0550-8 (2014).
153. Wu, T. *et al.* clusterProfiler 4.0: A universal enrichment tool for interpreting omics data. *Innovation (Cambridge (Mass.))* **2**, 100141; 10.1016/j.xinn.2021.100141 (2021).
154. Aanei, C. M. *et al.* Intrinsic growth deficiencies of mesenchymal stromal cells in myelodysplastic syndromes. *Stem cells and development* **21**, 1604–1615; 10.1089/scd.2011.0390 (2012).
155. Corradi, G. *et al.* Mesenchymal stromal cells from myelodysplastic and acute myeloid leukemia patients display in vitro reduced proliferative potential and similar capacity to support leukemia cell survival. *Stem Cell Res Ther* **9**, 271; 10.1186/s13287-018-1013-z (2018).
156. Basiorka, A. A. *et al.* The NLRP3 inflammasome functions as a driver of the myelodysplastic syndrome phenotype. *Blood* **128**, 2960–2975; 10.1182/blood-2016-07-730556 (2016).
157. Lucero, H. A. & Kagan, H. M. Lysyl oxidase: an oxidative enzyme and effector of cell function. *Cellular and molecular life sciences : CMLS* **63**, 2304–2316; 10.1007/s00018-006-6149-9 (2006).
158. Jones, M. G. *et al.* Nanoscale dysregulation of collagen structure-function disrupts mechano-homeostasis and mediates pulmonary fibrosis. *eLife Sciences Publications, Ltd* (2018).
159. Velling, T., Risteli, J., Wennerberg, K., Mosher, D. F. & Johansson, S. Polymerization of type I and III collagens is dependent on fibronectin and enhanced by integrins alpha 11beta 1 and alpha 2beta 1. *The Journal of biological chemistry* **277**, 37377–37381; 10.1074/jbc.M206286200 (2002).
160. Kerch, G. Role of Changes in State of Bound Water and Tissue Stiffness in Development of Age-Related Diseases. *Polymers* **12**; 10.3390/polym12061362 (2020).

161. Duncan, M. R. & Berman, B. Stimulation of collagen and glycosaminoglycan production in cultured human adult dermal fibroblasts by recombinant human interleukin 6. *Journal of Investigative Dermatology* **97**, 686–692; 10.1111/1523-1747.ep12483971 (1991).
162. Theiss, A. L., Simmons, J. G., Jobin, C. & Lund, P. K. Tumor necrosis factor (TNF) alpha increases collagen accumulation and proliferation in intestinal myofibroblasts via TNF receptor 2. *Journal of Biological Chemistry* **280**, 36099–36109; 10.1074/jbc.M505291200 (2005).
163. Lertchirakarn, V., Birner, R. & Messer, H. H. Effects of interleukin-1 beta on human pulpal fibroblast proliferation and collagen synthesis. *Journal of endodontics* **24**, 409–413; 10.1016/S0099-2399(98)80022-8 (1998).
164. Pfisterer, K., Shaw, L. E., Symmank, D. & Weninger, W. The Extracellular Matrix in Skin Inflammation and Infection. *Front. Cell Dev. Biol.* **9**, 682414; 10.3389/fcell.2021.682414 (2021).
165. Chang, N., Xiu, L. & Li, L. Sphingosine 1-phosphate receptors negatively regulate collagen type I/III expression in human bone marrow-derived mesenchymal stem cell. *Journal of cellular biochemistry* **115**, 359–367; 10.1002/jcb.24670 (2014).
166. Ghosh, A. K., Yuan, W., Mori, Y. & Varga, J. Smad-dependent stimulation of type I collagen gene expression in human skin fibroblasts by TGF-beta involves functional cooperation with p300/CBP transcriptional coactivators. *Oncogene* **19**, 3546–3555; 10.1038/sj.onc.1203693 (2000).
167. Inagaki, Y. & Okazaki, I. Emerging insights into Transforming growth factor beta Smad signal in hepatic fibrogenesis. *Gut* **56**, 284–292; 10.1136/gut.2005.088690 (2007).
168. Fei, C.-M. *et al.* Clinical significance of hyaluronan levels and its pro-osteogenic effect on mesenchymal stromal cells in myelodysplastic syndromes. *J Transl Med* **16**, 234; 10.1186/s12967-018-1614-4 (2018).
169. Yu, P., Pearson, C. S. & Geller, H. M. Flexible Roles for Proteoglycan Sulfation and Receptor Signaling. *Trends in neurosciences* **41**, 47–61; 10.1016/j.tins.2017.10.005 (2018).
170. Da Soares Costa, D., Reis, R. L. & Pashkuleva, I. Sulfation of Glycosaminoglycans and Its Implications in Human Health and Disorders. *Annual review of biomedical engineering* **19**, 1–26; 10.1146/annurev-bioeng-071516-044610 (2017).
171. Kräter, M. *et al.* Bone marrow niche-mimetics modulate HSPC function via integrin signaling. *Scientific reports* **7**, 2549; 10.1038/s41598-017-02352-5 (2017).
172. Cao, H. *et al.* The role of CD44 in fetal and adult hematopoietic stem cell regulation. *1* **101**, 26–37; 10.3324/haematol.2015.135921 (2016).
173. Moreno-Layseca, P., Icha, J., Hamidi, H. & Ivaska, J. Integrin trafficking in cells and tissues. *Nat Cell Biol* **21**, 122–132; 10.1038/s41556-018-0223-z (2019).

## 9. Annexes

### 9.1. Annex I

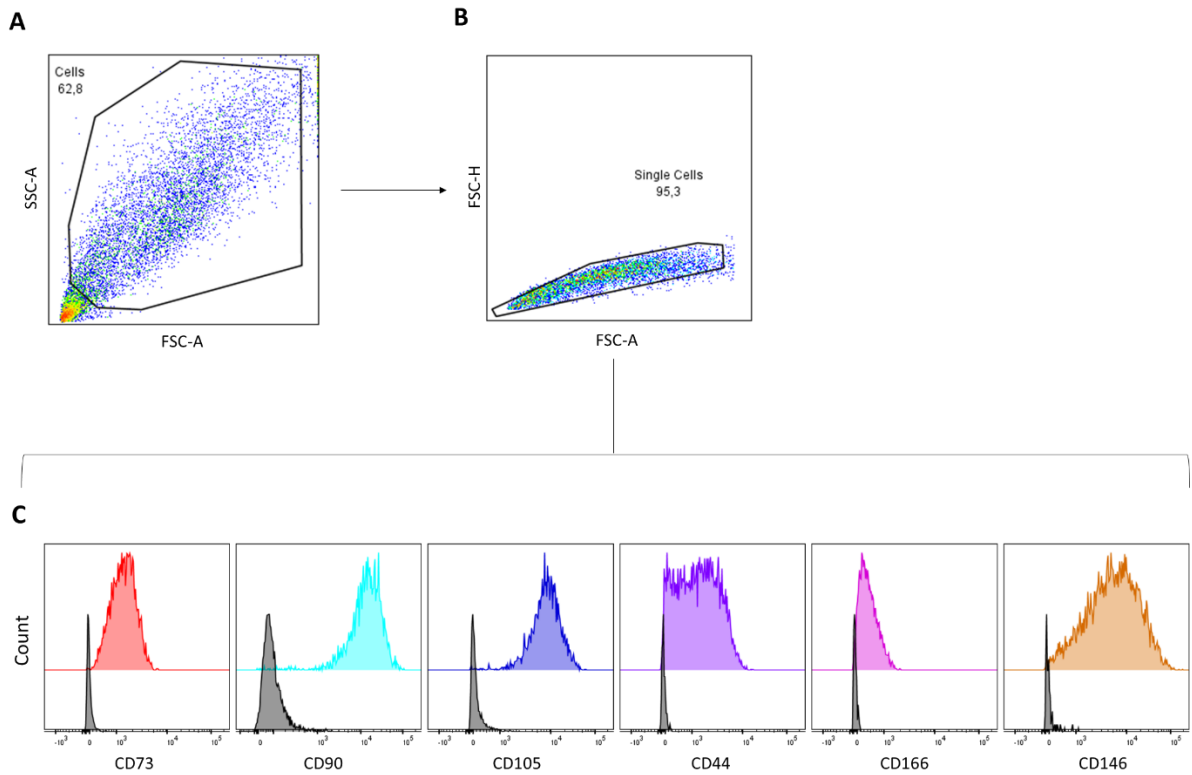


**Figure 29 Gating strategy for flow cytometry analysis of MSCs.** Representative plots of flow cytometry analysis. A) MSCs were gated to exclude cell debris based on the forward and side scatter. B) Single cells were gated based on forwards scatter area and height. C) Single cells were gated for its positive expression of CD73, CD90, CD105, CD44, CD166 and CD146 against an unstained control (grey).

## 9.2. Annex II

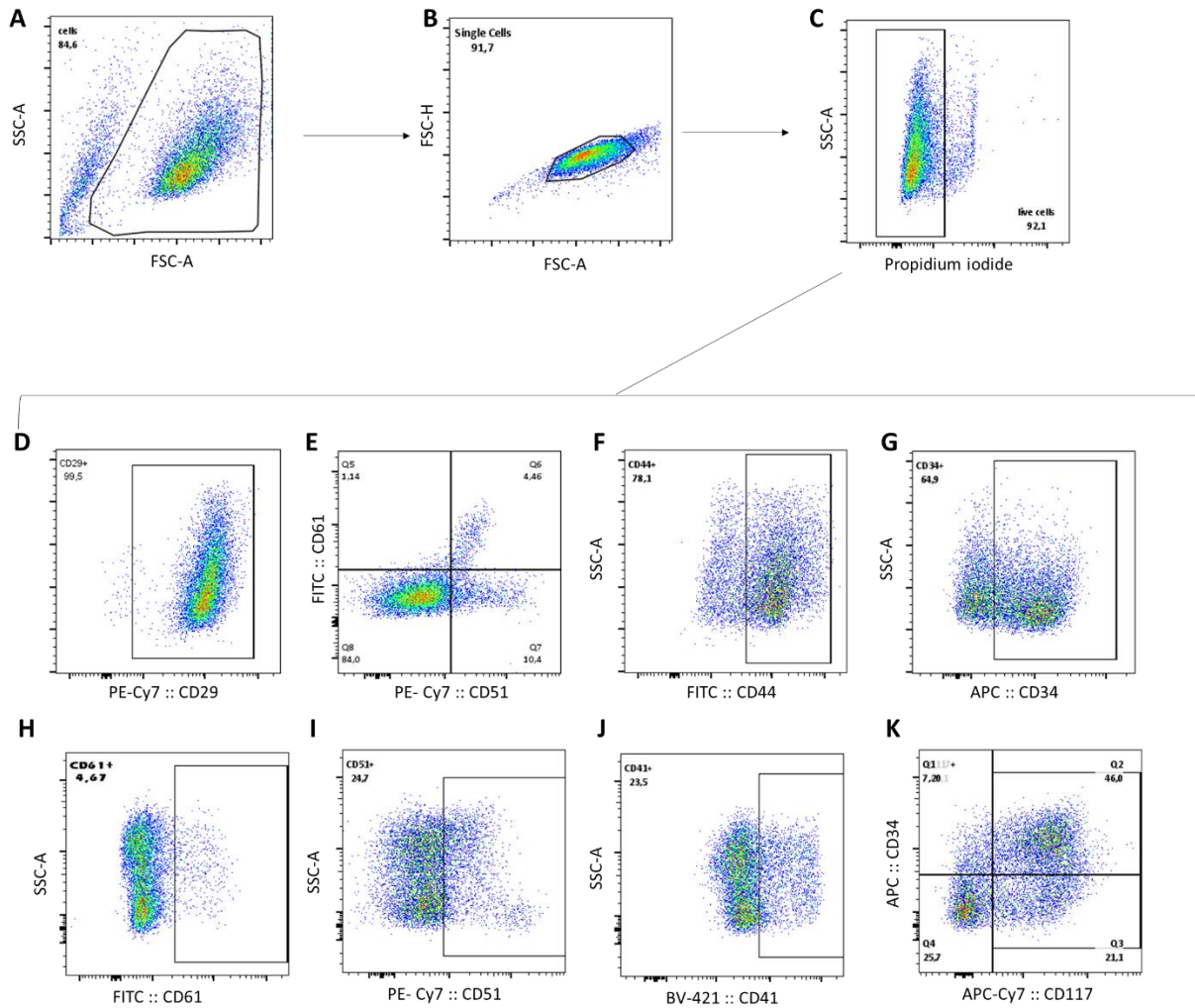


**Figure 30 Gating strategy for flow cytometry analysis of HSPCs on different ECMs.** Representative plots of flow cytometry analysis. A) HSPCs were gated to exclude cell debris based on the forward and side scatter B) Single cells were gated based on forward scatter area and height. C) Live cells were gated using propidium iodide. D-J) Live cells were gated for positive expression of CD29, CD34, CD41, CD44, CD51, CD61, and CD51+CD61+ cells. K) Live cells were gated for CD117 and CD34/CD117+ cells.

### 9.3. Annex III

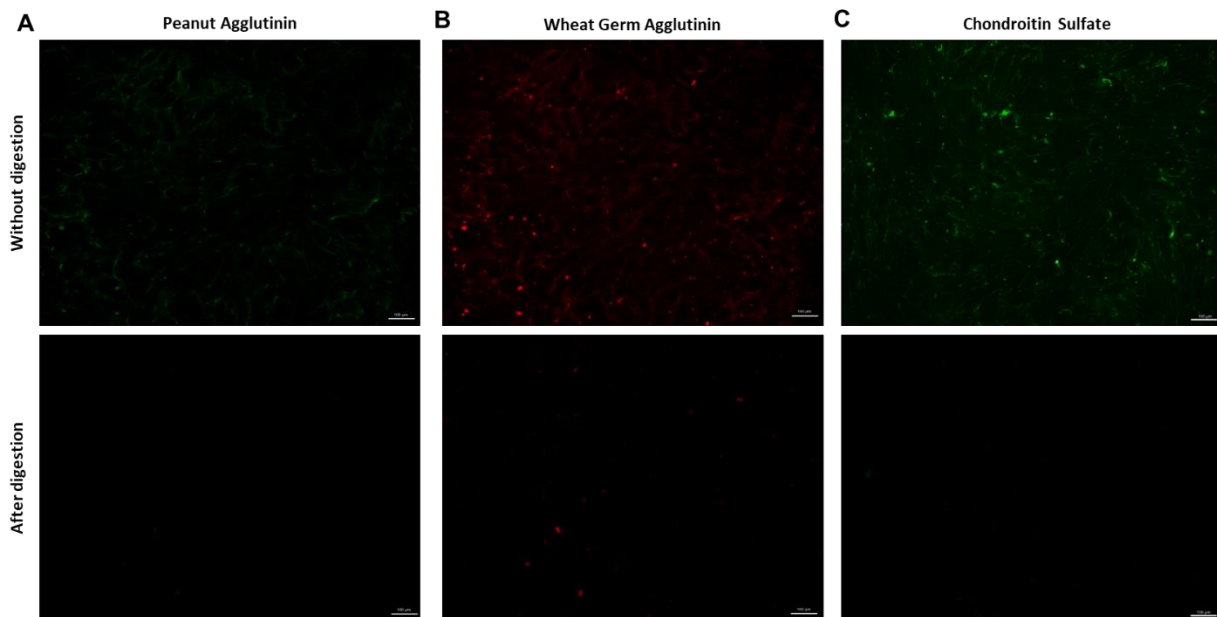


**Figure 31** Analysis of specificity of lectin staining and CS staining after pre-treatment with heparinases-1 and chondroitinase ABC respectively. Representative images of HR-MDS MSC-derived ECM using A) Peanut agglutinin which binds to N-acetyl-galactosamine and terminal  $\beta$ -galactose containing GAGs (CS, DS and KS). B) Wheat germ agglutinin which binds to N-acetyl-glucosamine GAGs (HA, HS and KS) and sialic acid without or with enzymatic pre-treatment with chondroitinase ABC and Heparanase-1. C) Representative CS immunostaining images of HR-MDS MSC-derived ECM after pre-treatment without or with enzymatic pre-treatment with chondroitinase ABC.



## 10. Disclosure

### Declaration on the independent preparation of the dissertation

I hereby declare that I have prepared this dissertation independently and without unauthorized assistance or use of other than the stated aids. I affirm that no third party has received, directly or indirectly, any remuneration or pecuniary benefits from me for work related to the contents of the submitted dissertation, and that the submitted work has not been submitted in the same or similar form to any other examination authority for the purpose of doctoral studies or any other examination procedure in Germany or abroad. All materials derived from other sources and by other persons that have been used in the dissertation or to which direct reference is made are identified as such. In particular, all persons who were directly involved in the preparation of this dissertation are named. The applicable legal provisions for the Approval of Clinical Studies, the provisions of the Animal Protection Act, the provisions of the Genetic Engineering Act and the general provisions of Data Protection Law have been complied with. I assure that I am aware of and have complied with the principles of Leipzig University's Statutes on Safeguarding Good Academic Practice statutes.

### Erklärung über die eigenständige Abfassung der Arbeit Hiermit erkläre

ich, dass ich die vorliegende Arbeit selbstständig und ohne unzulässige Hilfe oder Benutzung anderer als der angegebenen Hilfsmittel angefertigt habe. Ich versichere, dass Dritte von mir weder unmittelbar noch mittelbar eine Vergütung oder geldwerte Leistungen für Arbeiten erhalten haben, die im Zusammenhang mit dem Inhalt der vorgelegten Dissertation stehen, und dass die vorgelegte Arbeit weder im Inland noch im Ausland in gleicher oder ähnlicher Form einer anderen Prüfungsbehörde zum Zweck einer Promotion oder eines anderen Prüfungsverfahrens vorgelegt wurde. Alles aus anderen Quellen und von anderen Personen übernommene Material, das in der Arbeit verwendet wurde oder auf das direkt Bezug genommen wird, wurde als solches kenntlich gemacht. Insbesondere wurden alle Personen genannt, die direkt an der Entstehung der vorliegenden Arbeit beteiligt waren. Die aktuellen gesetzlichen Vorgaben in Bezug auf die Zulassung der klinischen Studien, die Bestimmungen des Tierschutzgesetzes, die Bestimmungen des Gentechnikgesetzes und die allgemeinen Datenschutzbestimmungen wurden eingehalten. Ich versichere, dass ich die Regelungen der Satzung der Universität Leipzig zur Sicherung guter wissenschaftlicher Praxis kenne und eingehalten habe.

.....

Datum

.....

Unterschrift

## 11. Curriculum Vitae

### Personal Data

**Full name**

Amanpreet Kaur Bains

**Contact Details**

[Akaur1996@gmail.com](mailto:Akaur1996@gmail.com)

[Amanpreet.bains@medizin.uni-leipzig.de](mailto:Amanpreet.bains@medizin.uni-leipzig.de)

### Education and Qualifications

<b>August 2019 - Present</b>	<i>PhD studies</i> Experimental haematology, Department of Haematology and Cell Therapy, Faculty of Medicine, University of Leipzig
<b>October 2018</b>	Master's degree, Master of Science Molecular medicine, University of Sheffield
<b>March- August 2018</b>	Master's thesis: Effect of confinement and topographical cues on cell behaviour for therapeutic use in bone regeneration" supervised by Dr Ilida Ortega and Dr. Thomas Paterson
<b>March 2016</b>	Bachelor's degree, Bachelor of Science: Biotechnology, Microbiology, Chemistry Osmania University
<b>September-December 2016</b>	Bachelor's thesis: Isolation, Identification and Characterization of Coliforms from Various Pushkaralu water samples and their Antimicrobial Susceptibility" under the supervision of Dr. Kusuma Dorcas

### Work experience

<b>March 2019 - June 2019</b>	Research assistant, L V Prasad Eye Institute, Kallam Anji Reddy Campus, Hyderabad India
<b>September 2018 - January 2019</b>	Visiting Researcher (Research Trainee) at Department of Clinical dentistry, University of Sheffield, Sheffield, UK
<b>August 2016 - January 2017</b>	Certificate course in Clinical Genetics and Genetic counselling at Institute of Genetics and hospital for genetic diseases, Hyderabad, India

### Awards

<b>April 2023</b>	Travel grant and complimentary registration for the European Haematology Association (EHA) Hybrid Congress 2023
<b>April 2023</b>	People choice award for best image; American society of matrix biology (ASMB) image contest
<b>August 2022</b>	Fazit-stiftung for completion of doctoral studies
<b>July 2022</b>	Deutsche Gesellschaft für Matrixbiologie (DGMB) travel grant to attend Matrix biology Europe: MBE 2022
<b>April 2022</b>	Travel grant and complimentary registration for the European Haematology Association (EHA) Hybrid Congress 2022
<b>September 2017</b>	India Postgraduate Merit scholarship by the University of Sheffield

**Conferences/Presentations**

- Oral presentation at “ASMB Image contest science behind the image E-Symposium” June 2023
- Participated and presented a poster at “The EHA2023 Hybrid Congress” June 2023
- Participated and presented a poster at “10<sup>th</sup> German stem cell network conference (GSCN 2022)” September 2022
- Participated and presented a poster at “Matrix biology Europe (MBE 2022)” September 2022
- Participated and presented a poster at “The EHA2022 Hybrid Congress” June 2022
- Participated and presented a poster at “The Joint Nordic Matrix Biology Meeting ” November 2021
- Participated and presented a poster at “Biomaterials and tissue engineering group 20th Annual White rose progress meeting” (BiTEG 2018) at University of Sheffield

**Publication**

**Bains, Amanpreet Kaur;** Behrens Wu, Lena; Rivière, Jennifer; Rother, Sandra; Magno, Valentina; Friedrichs, Jens et al. (2022): Bone marrow mesenchymal stromal cell-derived extracellular matrix displays altered glycosaminoglycan structure and impaired functionality in Myelodysplastic Syndromes. In *Front. Oncol.* 12, p. 961473. DOI: 10.3389/fonc.2022.961473

Ramos-Rodriguez, David H.; Pashneh-Tala, Samand; **Bains, Amanpreet Kaur;** Moorehead, Robert D.; Kassos, Nikolaos; Kelly, Adrian L. et al. (2022): Demonstrating the Potential of Using Bio-Based Sustainable Polyester Blends for Bone Tissue Engineering Applications. In *Bioengineering (Basel, Switzerland)* 9 (4), p. 163. DOI: 10.3390/bioengineering9040163

**Outreach activities**

<b>August 2022 – Present</b>	DAAD Young Ambassador 2022 for India, Bangladesh, Bhutan, Nepal, Sri Lanka and Germany
<b>October 2017 – January 2019</b>	International Student Ambassador at University of Sheffield.

## 12. Publications

**Bains, Amanpreet Kaur;** Behrens Wu, Lena; Rivière, Jennifer; Rother, Sandra; Magno, Valentina; Friedrichs, Jens et al. (2022): Bone marrow mesenchymal stromal cell-derived extracellular matrix displays altered glycosaminoglycan structure and impaired functionality in Myelodysplastic Syndromes. In *Front. Oncol.* 12, p. 961473. DOI: 10.3389/fonc.2022.961473

Ramos-Rodriguez, David H.; Pashneh-Tala, Samand; **Bains, Amanpreet Kaur;** Moorehead, Robert D.; Kassos, Nikolaos; Kelly, Adrian L. et al. (2022): Demonstrating the Potential of Using Bio-Based Sustainable Polyester Blends for Bone Tissue Engineering Applications. In *Bioengineering (Basel, Switzerland)* 9 (4), p. 163. DOI: 10.3390/bioengineering9040163

## 13. Acknowledgment

I would like to dedicate this thesis to my mentor Mr Rama Rao who lost his life, fighting haemophilia. I would also like to dedicate the thesis to my grandmother who would be very proud of the researcher I have become.

First and foremost, I'd like to thank my supervisors, Dr Michael Cross, Prof Dr Uwe Platzbecker and Dr Manja Wobus, for their guidance and support throughout the project. I especially value Dr Cross's mentoring, both personally and professionally, as well as his patience with my never-ending questions. I would like to express my gratitude to Dr Jens Friedrichs and Dr Valentina Magno at the Leibniz Institute of Polymer Research Dresden, Germany for sharing their technical knowledge of AFM, as well as for providing the POMA slides.

I want to acknowledge the contributions of our collaborators, Xiaofan Xie and Dr Josef Käes who gave me permission to use their AFM facility at the Peter Debye Institute for Soft Matter Physics, University of Leipzig. I also want to thank our collaborators Dr Toni Radanovic and Dr Sandra Rother at the Centre for Molecular Signalling, Saarland University School of Medicine, for sharing their knowledge of GAG detection using ELISA and gel electrophoresis-stains. I also want to thank Dr Knut Krohn, Dr Nora Grieb for her help with RNA sequencing and its analysis. In addition, I want to thank my colleagues for their assistance with my doctoral experimental work and thesis, especially Mandy Richter, Julia Schulz, Simon Krauß, Dr Katharina Zoldan, and Dr Sigrid Uxa.

Additionally, I would like to thank the José Carreras Leukämie-Stiftung for providing funding for the grants given to Manja Wobus, Uwe Platzbecker, and Carsten Werner, as well as the FAZIT Stiftung for providing me with a fellowship to finish my doctoral work.

A special thank you to all the Platzbecker/Cross group lab members, both past and present, as well as my friends outside the lab especially Divyasphoorthi Vardhan and Dr Poonam Naik. They have always been available for discussions and provide a critical assessment of my work. Particularly for helping me out and listening to me during the challenging optimization stage of my doctoral work.

Finally, I want to thank my parents for being a constant source of encouragement and drive for me. Without which, I would not have been able to live far from home and pursue my dream of becoming a researcher.